Addis Ababa University

Addis Ababa Institute of Technology

School of Civil and Environmental Engineering

Geodesy and Geomatics Program

Landslide Hazard, Vulnerability, and Risk Assessment Using GIS and Remote Sensing: The Case of Gozamin District, Northcentral Ethiopia

Niguse Adane

ID No: GSR/9492/11

Advisor

Dr. Worku Zewdie

A Thesis Submitted To

School of Civil And Environmental Engineering Graduate Studies of Addis Ababa Institute of Technology In Partial Fulfillment of The Requirement For The Degree Masters of Science In Geodesy And Geomatics (Specialization In Geomatics)

Addis Ababa University

January, 2022

Addis Ababa University

Addis Ababa Institute of Technology

School of Civil and Environmental Engineering

Geodesy and Geomatics Program

Landslide Hazard, Vulnerability, and Risk Assessment Using GIS and Remote Sensing: The Case of Gozamin District, Northcentral Ethiopia

Niguse Adane

ID No: GSR/9492/11

Advisor

Dr. Worku Zewdie

A Thesis Submitted To

School of Civil And Environmental Engineering Graduate Studies of Addis Ababa Institute of Technology In Partial Fulfillment of The Requirement For The Degree Masters of Science In Geodesy and Geomatics (Specialization In Geomatics)

Addis Ababa University

January, 2022

APPROVAL SHEET

Addis Ababa Institute of Technology

School of Civil and Environmental Engineering

Geodesy and Geomatics

This is to certify that the thesis prepared by **Niguse Adane**, entitled: Landslide Hazard, Vulnerability, and Risk Assessment Using GIS and Remote Sensing: The Case Of Gozamin district, Northcentral Ethiopia and submitted in partial fulfillment of the requirement for the degree of masters of science in geodesy and geomatics (specialization in geomatics) complies with the regulations of the University and meets the accepted standards concerning originality and quality.

Niguse Adane

____

______________________________	____________	________________
Advisor	Signature	Date
______________________________	____________	________________
Internal Examiner	Signature	Date
______________________________	____________	________________
External Examiner	Signature	Date

Acknowledgements

First and foremost, thanks to the almighty God, for His blessings throughout my work to complete the research successfully.

I'd want to convey my heartfelt gratitude to my adviser, Dr. Worku Zewdie, for his invaluable advice, for reviewing and editing my thesis, and for his unwavering support throughout my study.

My appreciation also goes to all staff of the Institute of Land Administration of Debre Markos University, for their kindness, guidance, financial, logistic, and equipment support during field work and for creating a wonderful place for research activities.

I express my thanks to Gozamin district Land Administration and Use office staff, Ethiopian Meteorological Agency, Ethiopian Mapping Agency, Geological Survey of Ethiopia, and Ministry of Agriculture for their providing valuable data and images.

Finally, I want to convey my heartfelt gratitude to my classmates, parents, and friends for their unwavering support, understanding, and encouragement throughout my academic career and the research and writing of this thesis. Without them, this feat would not have been possible. Thank you very much.

Abstract

Landslide is the downslope movement of rock, organic materials, and soil which consists of rock topples, rock falls, earth or debris flows that involve shear displacement along with one or several slip surfaces, which are either visible or may be reasonably inferred under the consequence of gravity. This reason, the study about the hazard, vulnerability, and risk of landslides is very important to reduce the destruction and damages of properties and death of life. This study was mapping the hazard by using the information value method, vulnerability by using weighted linear combination method, and risk zones by the product of vulnerability and hazard of Gozamin district by using ten (10) causative factors which are elevation, slope, aspect, rainfall, land use land cover, soil type, lithology, NDVI, distance from rivers (streams) and distance from the road that trigger a landslide. These causative factors are combined with a landslide inventory map, a map that shows previous landslide distribution. The Landslide hazard zonation (LHZ) shows 17(29.31%) of landslide lies under very highly susceptible region followed by 29(50%) in high, 12(20.69%) of the landslides were in moderate from the total of 58 landslides that occurred in the previous validated by overlaying the hazard map on landslide inventory map. Vulnerability and risk maps also showed that areas that have landslides in previous fall under very high, high, and moderate classes. Furthermore, the study was mapping the surface displacement of the study area due to landslides through using time series analysis of persistent scatterer interferometry (PS-InSAR). The result indicated that there was 16.9 mm displacement along the line of sight of the satellite and -12.2mm in the opposite direction of the satellite line of sight and the result indicates that the landslide is active. Based on the result the concerned governmental organizations and institutions should implement rehabilitation and preventive methods to protect damage.

Keywords: Landslide; Information value model; Landslide hazard zonation; PS-InSAR.

Table of Contents

List of Figures

List of Tables

List of Acronyms

ANN	Artificial Neural Network
CA	Consumers Accuracy
DINSAR	Differential Interferometric Aperture Radar
GIS	Geographic Information System
INSAR	Interferometric Synthetic Aperture Radar
IV	Information Value
IVM	Information Value Method
IW	Interferometric Wide
LD	Landslide Density
LHM	Landslide Hazard Map
LHZ	Landslide Hazard Zonation
LOS	Line of site of satellites
LR	Logistic Regression
PA	Producers Accuracy
RS	Remote Sensing
SLC	Single Look Complex
TOPS	Terrain Observation with Progressive Scan
WLC	Weight Linear Combination
WEM	Weights of Evidence Model

Chapter One

Introduction

1.1. Background of the Study

A natural hazard is the manifestation of a natural condition or phenomenon, which threatens or acts hazardously in a defined space and time (Varnes, 1984). Among the natural hazards, a landslide is the most significant in the world (Crozier & Glade, 2012Crozier & Glade, 2005 Franco Mantovani, Robert Soeters, 1996)). Landslide is the downslope movement of organic materials, soil, and rock which consists of rock topples, rock falls, earth or debris flows that involve shear displacement along one or several slip surfaces, which are either visible or may be reasonably inferred under the consequence of gravity (Wachal & Hudak, 2000; Cruden,1991; Highland & Bobrowsky, 2008).

Whether occurring naturally or triggered by human activity, landslides are among the common geo-environmental hazards in many of the mountainous and hilly terrains of both the developed and developing world. It is responsible for hundreds of billions in property destructions per year, damages transportation networks, buildings & structures, public works projects, agricultural areas, causes deaths and injuries for thousands each year. It often causes long-term economic disruption, population displacement, and negative effects on the natural setting which is becoming severe with the increasing population and poor economics of developing areas (; Dai et al., 2002; Arnous, 2011; Woldearegay, 2013).

Landslide risk is the probable degree of loss due to a landslide (Varnes, 1984). The risk is determined by the product of vulnerability and landslide hazards. Landslide vulnerability and hazard information are essential for the risk assessment of a landslide. Landslide hazard is described as the chance that a specified extent of landslide happens within a specific period & a given area (Ganapathy & Rajawat, 2015). Vulnerability refers to the degree of damage to a given element at risk because of the existence of a specified magnitude of hazard event (Buckle et al., 2000; Papathoma et al., 2011). Specifically, vulnerability is the association between the damage extent of the elements at risk and the concentration of the catastrophe. However, there were limited researches examining vulnerability to landslides. The evaluation of the landslide vulnerability is very complex because of different reasons. Glade, (2003) stated that vulnerability of diverse fundamentals at risk is flexible throughout similar hazard procedures, and the chronological probability of human life being visible to landslide is also flexible. Moreover, the capabilities of different clusters to survive disasters disturb the vulnerability of residents and landslide susceptibility differs.

The landslide study aims to assess the nature of hazards& the losses to human life, agricultural land, roads, buildings, and other properties (Anbalagan & Singh, 1996; Arnous, 2011). Determining landslide-prone areas is important to guarantee the safety of people's lives and avoid negative impacts on the regional and national economy. Landslide hazard map provides treasured information for government agencies, planners, decision-makers, and local landowners to make emergency plans to reduce the negative effects on infrastructure, superstructure, and human life (Ercanoglu et al., 2004; Anbalagan & Singh, 1996).

The previous studies showed that landslide is common in northern, southern, and western highlands and partly rift escarpment of Ethiopia due to different natural & man-made influencing factors (Ayalew & Yamagishi, 2004; Ayalew et al., 2004; Ayenew & Barbieri, 2005; Woldearegay, 2013; Raghuvanshi et al., 2014; Meten et al., 2015). Even though these studies show that there is a landslide hazard they did not try to show the risk and vulnerability of landslide in these areas particularly they did not study the hazard, vulnerability, and risk of the Gozamin district. This study was trying to assess the hazard, risk, and vulnerability of landslides and the surface displacement due to a landslide in the district.

1.2. Statement of the Problem

According to worldwide damage statistics, landslides occurrence was the cause of deaths of about 1,000 people every year, and the estimated property damage was about US $4 billion (Lee & Pradhan, 2007). Landslides are exacerbated by the steep topography of very high mountains and land degradation caused by anthropogenic activities. Deforestation and the construction of highways on steep slopes are examples of anthropogenic activities. Illegal wood cutting, home usage of fuelwood, and agricultural development on sloppy barren fields all contributed to deforestation. Because there was a scarcity of level terrain, farmers grew their crops on sloppy barren fields. Landslides can result in massive casualties and vast economic losses in mountainous areas. According to Ayalew (1999) the Ethiopian highland is a highly populated region, in which more than 60% of the state's population is settled. Due to the settlement of the people and its economic advantages in such areas, it made landslide generated hazard a serious problem to the public, planners, and decision-makers in Ethiopia. Gozamin is among the highly populated areas in Ethiopia and the area has been an economic center because it has suitable soil for agricultural activities and it is not a well-known landslide-prone area but in recent times the problem has occurred in different villages, and because of this both the natural environment and built-up infrastructures are frequently exposed to severe damages. Recently, the local communities living in the problematic areas were resettled to the neighboring villages. To reduce the loss that resulted from landslide hazards, it is needed that the areas which have a potential for such landslide should be identified and mapped (Varnes, 1984; Chau et al., 2004). The evaluation of the factors influencing landslide hazard initiation and occurrence and mapping landslide hazard zonation is important to recognize the spatial probability of landslide for safer strategic planning of future developmental activities and to minimize the upcoming impact. This necessity for studying the landslide process, analyze threatening landslide hazards, and predict future landslides for reducing ongoing and future damage from landslides in the area.

There has been little effort made to date within and around the study area to scientifically assess landslide hazard zonation mapping but vulnerability and risk had not been done yet in Gozamin district even though the area is suffering from a landslide. Investigating by RS and GIS may provide effective information within a short period and with minimum financial inputs when compared to conducting an investigation in this area by ground survey techniques which is practically difficult due to the ruggedness of the topography. Therefore, such surveys should be supported. Thereby, this study was focused on generating LHZ for this area to improve the current spatial plan and to guide local government in managing the future and current land utilization. Before planning and implementing any development activity in high terrain, LHZ is required (Raghuvanshi et al., 2014; Meten et al., 2015; Anbalagan, 1996).

Therefore, the present study was utilized as an appropriate procedure and technique to identify landslide hazard zones, map vulnerability, and risk of landslide and mapping surface displacement due to landslide using optical and microwave remote sensing data. These methods are important to provide landslide-specific information for the extraction of fast and accurate results that will help in decision-making and facilitate the implementation of disaster management strategies.

1.3. Objectives of Study

1.3.1. General Objective

The main objective of this study was to assess landslide hazard, mapping vulnerability, and risk through using GIS and Remote Sensing.

1.3.2. Specific Objectives of Study

Specifically, the study was pointed out the following specific objectives:

- To prepare a landslide inventory map from past and existing landslide records.
- To analyze the effect of causative factors responsible for possible landslides.
- To prepare a landslide potential hazard zone.
- To prepare a landslide risk and vulnerability map of the study area.
- To generate a surface displacement map

1.4. Research Questions

- Which causative factors highly contribute to landslides in the study area?
- Which area is more prone to landslide in the study area?
- Which area is vulnerable and at-risk due to landslides?
- How is the surface displacement in the study area?

1.5. Significance of the Study

The study area landslide hazard map will be used to recognize the spatial likelihoods of landslides for harmless strategic planning of future developmental activities. This may help to select appropriate sites for agriculture, construction, and other development activities, and to minimize the upcoming impact in landslide-prone areas by providing important information for governmental organizations and local government in managing the future and current land utilization. Identification of landslides and production of landslide zonation map is important to planners, local administrations, and decision-makers in disaster planning for reducing the losses of life and property (Anbalagan & Singh, 1996; Ercanoglu et al., 2004).

The study area is placed in the North West Ethiopian highland which is a highly populated region. This shows that people's life & property are exposed to landslide hazards. This study tried to identify landslide hazard zones, map risk, and vulnerability due to landslide of Gozamin district by using remote sensing data to determine landslide features and GIS for the data analysis, landslide susceptibility assessments, and preparation of different maps. The results will use for the expansion of cost-effective investments, support land use planning, serve as a transparent basis for decision making, help people to make informed decisions, and unless people understand the risk they face, it is difficult to inspire actions for risk mitigation.

1.6. Scope of the study

This study was evaluating the landslide causative factors and produced the LHZ map, vulnerability, and risk map of Gozamin district. The study was covering the total area of the district and it uses different causative factors to map landslide hazard zones, vulnerability, the risk of landslides, and surface displacement map due to landslides in the area.

1.7. Organization of the Thesis

This paper is organized into five chapters. Chapter one is the introduction which includes the background, statement of the problem, objectives, scope, and the study significance. The second chapter covers the work of previous researchers about the theoretical background for the landslide, landslide hazard zonation, vulnerability & risk of landslide, application of remote sensing and GIS for landslide studies, and InSAR methods. Chapter three describes the data collection, the methodology of the study work, and data processing and analysis. Chapter four covers the results and discussions the last chapter contains conclusions and recommendations made through the present study.

Chapter Two

Literature Review

2.1. Natural Hazard

Natural hazards comport all injurious geophysical actions, like earthquakes, flooding, and landslides (Pradhan, 2013). Landslides occur worldwide; however, their frequency/intensity is higher in countries with mountainous and hilly environments (Lee & Pradha, 2006).

Landslide hazard is a part of the critical environmental limitations for the growth of both developed and developing countries like Ethiopia, representing a preventive aspect for urbanization and organizations. Landslides can produce huge fatalities and massive economic losses in hilly regions. To alleviate landslide hazards effectively, novel methodologies are essential to grow an improved understanding of landslide hazards and to make balanced decisions on the distribution of funds for the administration of landslide risk (Lan et al., 2004; Chimidi et al., 2017).

2.2. Hazard Assessment

Hazard is defined as “those fundamentals of the physical environment, destructive to man and caused by forces unimportant to him" (Burton et al., 1978).

Standards Australia (2000) described a hazard as ‘a source of potential harm or a condition with a potential to cause damage.’ A natural incident that has a probable origin for injury or damage. Hazard is a threat. A source of danger for the future. It causes harm to persons - death, injury, disease, and stress; Human actions – educational, economic, etc.; Property – damage on the property, economic loss; Environment - pollution, loss of fauna and flora, loss of amenities. Examples of hazards are volcanic eruptions, earthquakes, cyclones, floods, landslides, and other such actions.

There are many diverse ways of categorizing hazards. One is to consider the gradation to which hazards are natural. Natural hazards like earthquakes or floods arise from decently natural processes in the environment; Quasi-natural hazards like smog or desertification arise through the interaction of natural procedures and human actions; Technological hazards like the harmfulness of pesticides to fauna, accidental release of chemicals, or energy from a nuclear plant. These get up directly as an outcome of human actions ((ADPC), 2000).

Hewitt and Burton (1971) itemized a variety of reasons relating to damaging geophysical events, which were not process-specific, including the aerial range of the damaged area, concentration of impact at a point, period of impact at a point, percentage of onset of the incident and predictability of the incident.

A hazard evaluation aims to detect potential hazards and risks in the area, and also to detect suitable safety actions that can be used to alleviate the known hazards. A checklist or an examination of the working area can be a hazard assessment. It should be done day-to-day, even if there were identical work areas. The purpose of finishing hazard assessments daily is to evade becoming complacent or simply not noticing the setting around you. Hazard assessments permit the workers to evaluate the work area every day and fix which safety actions to set in place according to the present risk. Daily evaluations allow employees to view security actions as situational, and modifier the actions as the hazards and environmental variation. They are also recognized as field-level hazard assessments (FLHA), or, simply, risk assessments (https:/www.safeopedia.com/definition/4547/hazard-assessment). The procedure for collecting this information is called hazard assessment. These studies depend heavily on existing scientific information, geomorphic, including geologic, aerial photographs, climate, and hydrological data, satellite imagery, topographic maps, and soil maps; historical evidence, both printed reports and spoken accounts from long-term residents. These may include myths and legends (https:/www.safeopedia.com/definition/4547/hazard-assessment).

For the assessment of most natural phenomena, one cannot expect the complete data required to carry out a comprehensive assessment. Depending on the situation, various methods are used with obvious variations in the degree of accuracy. These methods are the quantitative approach, qualitative approach, deterministic approach, probabilistic approach. By using this technique we can get natural hazards evidence, which signifies the occurrence and effect of expected phenomena (ADPC, 2000).

2.3. Hazard Mapping

It is the process of determining where and to what extent a certain event will represent a hazard to people, property, infrastructure, and economic activity on a regional scale (ADPC, 2000). The likelihood of a hazard occurring varies by location. Plotting data on natural risks and combining it with socio-economic data facilitates analysis. It improves communication between participants in the hazard management process, as well as between decision-makers and planners (ADPC, 2000).

2.4. Landslide

According to Cruden (1991) landslide is defined as the mass movement of debris, rock, or earth down a slope, resulting in a geomorphic transformation of the Earth’s surface. Landslides are a symptom of slope instability, defined as a slope's proclivity for morphologically and structurally damaging landslide processes. It could be manifested in different and combinations of various forms, including rock falls, rockslides, debris flow, soil slips, rock avalanches, and mud-flows (Chau et al., 2004). Individual slope failures are normally not so huge or so high as earthquakes, major floods, hurricanes, or other natural disasters. Other than any geological hazards slope failures are more widespread, and over the years they may be origin more damage to properties. The main triggering aspects of landslides are rugged topography, weakness of geological structure, and variation in bedrock lithology (Varnes, 1978; Abebe et al., 2010). The research of landslides has drawn worldwide consideration mainly due to growing awareness of the socio-economic influence of landslides, as well as the growing pressure of urbanization on the highland environment (Aleott & Chowdhury, 1999).

Due to natural circumstances or manmade activities, landslides have produced multiple economic and human losses (Fleming & Taylor, 1980; Guzzetti et al., 1999). In general, the factors which influence whether a landslide will occur typically include climate, slope angle, weathering, vegetation, water content, and overloading, geology, and slope stability. Understanding how these components interact is crucial to understanding what causes landslides, as well as the impact humans have on these factors by influencing natural processes. A landslide is usually caused by a combination of factors (Aleotti & Chowdhury, 1999).

According to Carrara (1983) and Cruden & Varnes (1996) landslides are triggered by one or a combination of two or more of the following factors; shocks and vibrations, change in slope gradient, change in water content, increasing the load that the land must bear, groundwater movement, weathering of rocks, frost action or wedging, and removal or changing the type of vegetation. The force that is accountable for the occurrence of the landslide is the gravitational force. Gravity is the strength that pulls everything towards the focus of the earth. Therefore, materials that are on the slope are more susceptible to the force of gravity, which causes landslides, than the material which is on relatively flat areas (Nelson, 2013). Generally, the factors which are responsible for causing and triggering slope instability can be grouped as geological factors, geomorphic factors, hydrological factors, land use land cover, manmade activities, and seismicity (Carrara, 1983).

2.5. Landslide Mapping

Landslide mapping can be based on one or a blend of the following activities: aerial- Photo interpretation, ground survey, and a database of historical existences of landslides in an area (Schuster & Highland, 2001). However, in the lack of historical data, one has to rely on field surveys and photo interpretation techniques. The satellite image is generally unsuitable for landslide mapping except where data products can be enlarged to at least 1:50000 scales (Soeters & Westen, 1996). Images are classified by categorizing all pixels into land cover classes or themes as noted by (Lillesand et al., 2004). For any given image, the spectral pattern for every pixel is used as the geometric foundation for the categorization. Different features exhibit different properties like spectral reflectance and emittance. This is the most straightforward approach to landslide hazard zonation because aerial and space images contain a detailed record of features on the ground at the time of data acquisition (Lillesand et al., 2004). An aerial photograph can be the source for data on existing landslides, types of bedrock, and vegetation cover. Typically, large-scale photography is required for mapping existing landslides. The photo scale relies on the size of landslides in the area under study (Sheila, 2006). A map of existing landslides is used as the basic data source for understanding conditions contributing to landslide existence. Normally, such a map is produced by the understanding of aerial photographs which is supported by field verifications (Cruden & Varnes, 1996). The map may be prepared at different levels of detail concerning existing landslides. A simple inventory identifies the definite and probable area of existing landslides and is the minimum level essential for a landslide hazard assessment (Sheila, 2006). There are several considerations to keep in mind when gathering data on existing landslides. First, the time and effort required to conduct an inventory vary with i) geological and topographic complexity,(ii) the size of an area, and (iii) desired level of inventory detail. Second, large map scales to reveal the small features of this added detail are required for more detailed inventories. Third, extra data collecting can add details to an existing inventory. This allows a formerly completed simple inventory to be changed into an intermediate inventory with less time and effort than producing the intermediate inventory only from field work and aerial photography (Varnes, 1984).

Satellite images have the advantage of having a multi-temporal characteristic which makes them useful for change detection. However, updating available data using satellite images requires intensive fieldwork to fill in the missing details. This indicates that satellite images need to be used in combination with other data generation methods (Lillesand et al., 2004). The principles guide landslide hazard assessment. “Landslides in the upcoming will most likely happen under geologic, geomorphic, and topographic circumstances that have produced previous and current landslides’’. The underlying situations and procedures which cause landslides are understood. The comparative importance of situations and progressions contributing to landslide existence can be determined and each assigned some action reflecting its contribution (Varnes,1984; Silva & Pereira, 2014).

2.6. Landslide Hazard Zonation (LHZ) Methods

According to Varnes (1984) LHZ is the procedure of dividing the land surface into zones and ranking these areas according to the degree of definite or possible hazard from landslides. Several landslide susceptibility assessment methods are presented in different works of literature. These methods can be broadly grouped into direct and indirect and qualitative and quantitative (van Westen et al., 1997; van Westen et al., 2006). In the indirect method, the researcher determines the grade of susceptibility based on her/his knowledge and experience. However, in indirect mapping, the researcher uses either deterministic models or statistical models to predict landslide-prone areas, based on the information gained from the interrelationship between landslide controlling factors and landslide distribution (van Westen et al., 2006). The qualitative assessment method evaluates the landslide susceptibility without landslide inventories. This method evaluates the actual landslide based on the spatial distribution of landslide controlling factors. This method is dependent on the experience and skills of the expert preparing the map. It requires prior knowledge of factors controlling landslides. The heuristic method is an example of a qualitative method (Soeters & Westen, 1996). Quantitative methods include statistical and deterministic modeling of landslide susceptibility combining landslide inventory and landslide controlling factors (van Westen & Terlien, 1996).

Landslide inventory also called the frequency method is the modest form of landslide mapping. The susceptibility estimation depends on the quantity of landslide occurrence (Wright et al., 1974). Landslide inventory maps provide a quantitative measure of landslide distribution. They provide a straightforward comparison of different regions. However, landslide inventories assume continuous landslide density in space and cannot provide estimates on future landslides. A catalog of the landslide can be prepared by gathering historical information on individual landslide events and by using satellite images, aerial photographs, and field surveys (Soeters & Westen, 1996).

In physically-based models, the landslide susceptibility is determined through slope stability models resulting in the calculation of factor of safety (Soeters & Westen, 1996). These models provide the best quantitative information on landslide susceptibility that can be directly used in engineering works. In statistical approaches, landslide casual factors or parameters are derived and overlaid with the landslide inventories to forecast the future occurrence of landslides (Carrara et al., 1991; Guzzetti et al., 1999; Dai & Lee, 2001). Statistical methods can be divided into multivariate and bivariate. In a multivariate method, all pertinent landslide casual factors or parameters are treated together (Carrara, 1983; Carrara et al., 1991; Lee & Min, 2001; Su¨zen & Doyuran, 2004). As a result, the interaction effects of different factors are demonstrated by this method. Logistic regression (Dai & Lee, 2001) and determinant analysis are the core types of multivariate statistics used in landslide susceptibility investigation. Artificial neural network (ANN) classifiers are another kind of multivariate method. In the bivariate statistical method, each landslide casual factor map (for example geology, slope, land use, vegetation) is united with the landslide inventory. The weights are derived from either landslide plenty or concentrations in each attribute session within each aspect (Gupta & Josh, 1990; van Westen et al., 1997; Su¨zen

& Doyuran, 2004). Information value method, weight of evidence modeling, and Frequency ratio are types of weight estimation methods employed in the bivariate statistical method. In the present study, the bivariate approach was used based on the landslide inventory data using GIS software to map the landslide hazard zonation.

LHZ is a significant step in landslide examination and landslide risk administration. LHZ can be carried out through several approaches. Fell et al., (2008) classified landslide hazard study methods into expert evaluation, statistical, and mechanical approaches.

2.6.1. Expert Evaluation

Expert evaluation technique includes landslide inventory mapping and heuristic approaches. Landslide inventory maps highlight the location and extent of recorded landslides thus helps in demarcating landslide susceptible areas whereas the heuristic technique includes opinion in classifying the landslide hazard which is based on quasi-static variables (Dai & Lee, 2001). The fundamental critique of the expert assessment approach is that it allows for subjectivity in decision-making, as landslide hazard maps created by various researchers using expert evaluation might differ dramatically (van Westen, 2006; Carrara et al., 1992; van Westen et al., 1997; Dai & Lee, 2001). However, the approach based on expert evaluation will remain the most broadly used and the most versatile. This means it will be essential to rely on more complicated methods for landslide hazard or susceptibility assessment and state of the art terrestrial data management tools, to be combined into the overall methodology of landslide threat or hazards mapping (Fall et al., 2006).

2.6.2. Mechanical Approach

Mechanical approaches include deterministic numerical methods that measure the constancy of the slopes by a safety factor. These methods also facilitate prediction, simulate, and evaluate the steadiness of the condition of slopes by considering diverse instability influences with relatively good accuracy. These mechanical approach methods require exhaustive geological and geotechnical input data which for obvious reasons is time-consuming and requires special skills in data collection. Thus, these deterministic numerical methods cannot be economically applied effectively for large areas. The use of mechanical models (numerical or deterministic models) in landslide hazard evaluation has the advantage of being technically sound. It is possible to calculate the slope stability using these models and a safety factor (van Westen et al., 1997). Mechanical methods should only be used in landslide susceptibility or hazard assessment of vast areas to explore slope constancy, which cannot be assessed with adequate accuracy using conventional landslide hazard assessment approaches. Many factors influence the success of one approach over another, including the size of the study area, the precision of projected results, data availability, and so on (Highland & Bobrowsky, 2008). GIS technology could deliver a powerful instrument to model the landslide hazards for their spatial investigation and forecast. This is because the manipulation, collection, and examination of the conservational data on landslide hazards can be accomplished much more cost-effectively and efficiently (Carrara et al., 1999; Guzzetti et al., 1999). From the start of GIS application in geohazards research in late 1980, many GIS-based investigation models and quantitative forecast models of landslide hazards have been used (Carrara, 1983; van Westen, 2006; Carrara et al., 1991).

2.6.3. Statistical Approach

Statistical methods are based on the statistical determination of the combinations of different variables that were responsible for the instability of slopes in a given area. For this approach, both multivariate and simple statistical methods can be employed to evaluate landslide hazards (Dai & Lee, 2001). The major limitation of statistical methods is gathering large data on landslide distributions and various factors over large areas that require considerable time, resources, and manpower (van Westen et al., 1997). Another constraint is the quantity and quality of data on landslide frequency and various factors on which statistical correlations are established. Thus, the findings are highly influenced by the volume of data gathered and its quality (Fall etal., 2006). Some GIS-based landslide investigation models, like statistical models, are based on the hypothesis that an area where landslides happen is now under disposed to landslide environments and that areas under those environments have a high probability of new landslides existence, or future landslides will happen under conditions similar to those of the previous landslide. Such prone areas are depicted by factors affecting the occurrence of landslides, such as rock and soil types, slope angles and land use that are usually digitized as layers or themes in GIS (Highland & Bobrowsky, 2008). Statistical methods can be divided into multivariate and bivariate.

2.6.3.1. Multivariate statistical analysis

The relative contribution of each thematic data layer to total landslide susceptibility is considered in multivariate statistical analysis for LHZ (Kanungo et al., 2006). These approaches calculate the percentage of landslide areas for each pixel and landslide absence, and then create a presence data layer, which is then used to reclassify the hazard for the given area using a multivariate statistical method. For landslide hazard zonation mapping, logistic regression models, determinant analysis, multiple regression models, conditional analysis, and artificial neural networks (ANN) are regularly employed methodologies.

2.6.3.2. Bivariate statistical analysis

In the bivariate statistical method, each landslide casual factor map (for example geology, slope, land use, aspect) is combined with the landslide inventory. The weights are derived from either landslide densities or abundance in each attribute class within each factor (Gupta & Josh, 1990; van Westen et al., 1997; Süzen & Doyuran, 2004). The frequency analysis approach, weights of evidence model (WEM), weighted overlay model are examples of bivariate statistical methods used in landslide hazard zonation mapping. Another type of bivariate statistical technique for the spatial forecast of landslides based on associations between landslide existence and associated parameters is the known information value model (Sarkar et al., 1995). The information values are decided for each subclass of landslide-associated parameters based on the occurrence of the landslide in a specified mapping unit. The weights of the evidence model (WEM) use diverse combinations of landslide causative factors to define their interrelation with landslide distribution (van Westen et al., 1997). The frequency ratio is based on observed relationships between each causative factor related to landslides and landslide distribution. This method can be used to establish a spatial correlation between the landslide explanatory factors and landslide location (Lee & Min, 2001). The frequency ratio for each subclass of distinct causative factors is calculated based on their association with landslide existence. Landslide susceptibility index (LSI) is calculated by adding the frequency ratio values of each factor. The weighted overlay is based on the relationship of the landslide frequency with landslide causative factors (Sarkar et al., 1995).

2.6.3.2.1. Weights of evidence model

It is a log-linear form of the Bayesian probability technique for landslide susceptibility valuation that uses landslide existence as training points to derive calculation outputs. It computes both the unconditional & conditional probability of landslide hazards. This technique is founded on the computation of positive and negative weights to define the degree of the spatial relationship between landslide existence and each descriptive variable. The Weights of Evidence technique has been functional for landslide susceptibility after the 1990′s (Blahut et al., 2010). It uses various blends of landslide causative factors to define their interrelation with landslide dispersion.

2.6.3.2.2. Weighted overlay method

It is a modest bi-variate statistical technique in which weights are allocated based on the association of the landslide incidence with landslide causative factors. Sarkar et al., (1995) established a procedure of LHZ for Rudrapeayag area in Garhwal Himalayas, India. Numerical weights are allocated to causative factors based on their associations with the landslide incidence. Finally, the data sheets were overlaid to yield the LHZ map.

2.6.3.2.3. Frequency ratio approach

It is one of the bivariate statistical methods of landslide susceptibility evaluation which is based on detected relationships between each causative factor connected to landslides and landslide dispersion. This technique can be used to create a spatial correlation between landslide explanatory factors and landslide location (Lee, 2005). The frequency ratio for each sub-class of individual causative factors is calculated based on their association with landslide incidence. LSI is calculated by adding the frequency ratio values of each factor.

2.6.3.2.4. Information Value Method (IVM)

IVM is a bi-variate statistical technique for geographical landslide forecasting based on connections between related characteristics and the occurrence of landslides (Sarkar et al., 2006). The IVs are calculated based on the occurrence of a landslide in a specific mapping unit for each subclass of landslide-related factors. This technique has been used in several types of research for LHZ mapping.

Akbar & Ha, (2011) has studied landslide hazard zoning along the Himalayan Kaghan Valley of Pakistan by the integration of GPS, GIS, and remote sensing technology. They used many causative factors like elevation, land use, geology, slope aspect, rainfall intensity, soil, distances from the main road, slope inclination, distances from the main river, distances from secondary roads, and those from trunk streams were analyzed for the existence of landslides. To obtain landslide hazard zones these factors were used with an improved form of pixel-based information value model. Finally, the study identifies causative aspects with the maximum effect of landslide existence in the area where distances from the main road, distance from secondary roads, land use, distances from the main river and those from trunk streams, and rainfall intensity. In conclusion, they create that landslide existence was in very high hazard zones, high, moderate, and no landslides were in low or very low hazard zones.

Mokadem, (2018) utilized a GIS-Based statistical model for the evaluation of landslide susceptibility by using lithology, slope, slope exposure, lineament, and hydrographic network as a causative factor. In the study, a probabilistic, technique Informative value was used for landslide hazard evaluation, using a geographic information system. Landslide susceptibility mapping was gained using the combination of spatial distribution maps of various factors. The gained results using this technique are near to reality and could be sometimes similar to the results detected in the field.

Landslide activity is very common mostly in the highlands of Ethiopia and rift margin due to the influencing factors like the rugged topography and high relief, geological, hydrological (surface and groundwater), heavy summer rainfall, land use conditions, manmade activity, and a minor level, with seismicity large variety of landslides can occur. Most landslide types are soil slips or mudflows, rock slides, toppling, and fall in hilly and mountainous terrains of north, south, and western regions of Ethiopia and parts of rift valley escarpments. Human lives, infrastructures, agricultural lands, and the usual environment have been affected by different types and sizes of landslides (Berhanu et al, 1999; Ayalew, 1999; Ayenew & Barbieri, 2005; Ayalew and Yamagishi, 2004; Abebe et al., 2010; Woldearegay, 2013; Raghuvanshi et al., 2014; Meten et al., 2015; Hamza & Raghuvanshi, 2017). Several types of research have been done following various analytical, empirical approaches, and qualitative to evaluate the sources and influences that activate landslides in different portions of the highlands of the country.

Filagot et al., (2018) conducted a study on LHZ and slope instability evaluation by using InSAR and optical remote sensing in Arbaminch-Gidole Road, Southern Ethiopia. The study used an information value bivariate statistical model to map landslide hazard zone and six causative factors namely; aspect, slope angle, slope material, elevation, NDVI, and land-use and land-cover were considered. The landslide hazard zonation map thus prepared indicates that the majority of the study area 78.38km^2 (36.3%) falls within very low hazard (VLH) zone and 72.85km^2 (34.2%) of the area fall within low hazard (LH) zone. A perusal of results further shows that 12.78 km^2 (6.6%), 32.72 km^2 (15.4%), and 15.89 km^2 (7.5%) of the area falls into very high hazard (VHH), high hazard (HH), and moderate hazard (MH), respectively. Further, validation of the LHZ map with past landslide inventory data shows that 92.3% of the existing landslides fall in very high hazard (VHH) and high hazard (VHH) zone. As a result, it can be safely assumed that the hazard zones indicated in this study are consistent with prior landslide data, and the potential zone represented can be used to safely plan the region. The model has good results on the study area that was checked by overlaying the result with the inventory map.

The researches that are discussed above are few of many studies and have good results to identify hazard zones so this study uses the information value method to identify the hazard and non-hazard zones.

2.7. Landslide Vulnerability and Risk

The likelihood of a landslide causing harm is referred to as landslide risk (Varnes, 1984). The product of the landslide hazard and the vulnerability is used to compute the risk. A landslide risk assessment requires vulnerability and landslide hazard information. Landslide hazard is defined as the probability of a specific magnitude of a landslide occurring inside a particular area over a given period (Guzzetti et al., 1999). The literature on landslide risk assessment is extensive (Lee & Pradhan, 2007; Xie et al., 2018). However, there is a scarcity of studies on landslide vulnerability. The quantity of loss to a specific element at risk due to the presence of a specified magnitude of hazard occasion is referred to as vulnerability (Varnes, 1984). Vulnerability is the relationship between the quantity of harm to the elements under danger and the disaster's concentration. Landslide vulnerability assessment is highly difficult for a variety of reasons. Glade (2003) noted that the vulnerability of numerous elements in risk varies across identical hazard methods, as well as the temporal likelihood of humans being visible to the landslide. Furthermore, the ability of various groups to handle disasters disrupts people's sensitivity, and landslide susceptibility varies. In addition, landslide vulnerability is influenced by parameters such as block mass, wall impact point location, velocity, landslide impact angle, material strength, and precise geometry of the wall. Dealing with all of these issues is difficult (Li et al., 2010). Vulnerability is determined by the qualities of the element at danger as well as the magnitude of the landslide.

There is currently no uniform approach for quantitatively evaluating the susceptibility of various elements under the danger of landslides of various magnitudes and types (Dikshit et al., 2020). As a result, the most common technique in real landslide risk evaluation is to set the landslide vulnerability of various elements at risk to a constant 1, i.e., to trust that the elements at risk will be completely lost and damaged, or to allocate the vulnerability based on experience and expert knowledge (van Westen et al., 2006). Several scholars have used vulnerability curves, vulnerability matrices, and vulnerability indicators to study the vulnerability of buildings, roads, and land use to landslides (Clémence, 2016; Catani et al., 2005). They surveyed the harm ratio of land uses such as fruit forest, grassland, forest, and pasture under different landslide dimensions and established vulnerability curves for different land uses (Clémence, 2016; Catani et al., 2005). Remondo et al., (2005)created a landslide inventory in Northern Spain, specifically for the Deva Valley area, surveyed both the relevant loss caused by landslides and the replacement costs of elements at risk in great detail, and established vulnerability pointers for land, roads, and buildings in the area.

To assess the relative socioeconomic vulnerability to landslides of European societies, Eidsvig et al., (2014) developed a semi quantitative indicator-based approach that took into account the inducing factors about a community's ability to deal with, prepare for, and recover from the loss and damage caused by landslides. By analyzing the shape, color, and texture of remote sensing images after and before a landslide, Martha & Vinod Kumar, (2013) assess the susceptibility of buildings, agricultural land, and roadways and determine the damage situation of buildings. Galli

& Guzzetti, (2007) used many parameters to assess the damage proportion of structures in Umbria, and Italy created a vulnerability index. To estimate the differential permanent landslide displacements at the building's foundation level, Fotopoulou & Pitilakis, (2013) used a dynamic non-linear finite-difference slope model. The acquired differential permanent displacements are pushed at the groundwork level to assess the building's response to varying permanent seismic ground displacements using a restricted element code. Finally, the fragility bends were constructed to assess the susceptibility of low-rise reinforced concrete buildings exposed to slow-moving ground slides caused by earthquakes. Mavrouli et al., (2017) employed the particle finite element method to simulate the impact of rock fall (size and velocity) on masonry structure construction. Then, to evaluate the mechanical qualities, model the masonry structure, and compute the internal stresses, the finite element technique was used. Finally, a failure criterion was used to calculate the susceptibility and damage caused by rock falls on masonry structures. Papathoma et al., 2011) also examined existing methodologies for assessing physical vulnerability to mountain hazards, identifying challenges in their implementation as well as discrepancies between them. Finally, six future needs in the field of vulnerability evaluation were identified, including the technique's user-friendliness, the selection of all relevant indications, the technique's transferability, and so on. Silva and Pereira (2014) employed a semi-quantitative approach to assessing the physical vulnerability of structures and the associated potential fatalities in the North of Portugal due to the presence of shallow slides. Totschnig & Fuchs, (2013) and Totschnig et al., (2011) exploited torrent occurrences in the Austrian Alps to develop a quantitative vulnerability curve for residential buildings to torrent. In terms of absolute and relative values, the results suggest that an enhanced Weibull distribution and a modified Frechet distribution fit well to the observed damage pattern. Even additional studies on human vulnerability to landslides are woefully inadequate.

In Pahuatlán, Mexico, Murillo-García et al., (2017) added the spatial method to the vulnerability assessment model to consider the indicators of exposure, sensitivity, and lack of resilience and assessed the population's vulnerability to landslides by multiplying them in each spatial unit. In general, there has been little research on landslide vulnerability due to a non-uniform absence of precise historical landslide inventories and a landslide intensity characteristic index.

2.8. SAR Interferometry

Interferometric Synthetic Aperture Radar (InSAR) is a technique for monitoring millimeter to a centimeter-level displacement of the Earth's surface through repeated imaging of an area over time(Hanssen, 2004). Data obtained through remote sensing, particularly from active sensor systems such as radar, has become increasingly essential in recent years. Since the launch of the ERS satellites in 1991, ERS 1, and ERS 2 in 1995, high-quality SAR images have been constantly recorded, and a large data library exists today. Interferometric Synthetic Aperture Radar (InSAR) technology is a well-established operational instrument for monitoring and quantifying ground motion all over the world (Esa, 2010). InSAR offers the advantage of providing a high concentration of measurement points over large areas, including locations that are difficult or dangerous to access, as compared to other surveying approaches. Advanced In-SAR techniques developed in the previous decade, such as SqueeSAR and PSInSAR, give high precision time series of movement that emphasize typical displacement patterns, such as seasonal uplift/subsidence cycles and changes in ground movement over time (Arroyo, 2020). As a result, numerous factors influence the accuracy of this approach, including atmospheric and ground conditions, wave-band, and backscatter intensity. The techniques are useful for mapping ground deformations generated by mild earthquakes and landslides, as well as identifying building debris and substantial displacements via decor relation between acquisitions, with an accuracy of more than a quarter of the SAR wavelength. The satellite-target relative position, temporal changes in the image and atmospheric oscillations all influence the interferometric phase. The persistent scatterers are natural or man-made objects that maintain a consistent signal phase from one collection to the next, exhibiting excellent coherence across a SAR data stack. Furthermore, there is a historical archive of SAR data dating back to 1992 that can be utilized. The major importance of SAR Interferometry is to derive changes in the earth's surface in the sense of subsidence horizontal displacements or vertical displacements, i.e. post-seismic movements, and to generate DEM (Lu & Weng, 2007).

Differential Interferometric Synthetic Aperture Radar (DinSAR) interferometry is considered one of the best methods for plotting ground deformations. DInSAR calculates the phase difference (interferogram) between images taken at various intervals after and before an incident. Gheorghe & Armaş, (2016) defined phase variance as "an indicator of the degree of change endured by a region between two attainments." The interference fringes arising from phase variations that can be understood as displacements or heights must be produced by the two SAR data attainments, called images or scenes, of the same area. The ground displacement is the sum of the phase information from an interferogram, but it also contains other components that must be retrieved to achieve millimetric accuracy (phase noise related with the scatter quality; atmospheric noise related with the signal distortions due to the propagation through the atmosphere; topographic error related on the difference between real topography and model topography). In the case of the topographic component, a high-quality Digital Elevation Model (DEM) and advanced DInSAR techniques can be used to obtain these three components that are not connected to ground motion (Lanari et al., 2004; Ferretti et al., 2001).

The phase unwrapping procedure, which is the most crucial in the processing chain, is used to estimate displacement in DInSAR approaches. To execute good unwrapping, the gradient of displacement must meet two constraints, one of which is related to time and the other to space. In space, the phase gradient between close pixels cannot be greater than π, otherwise, it is not possible to follow spatially the real displacement. Similarly, the velocity of displacement between acquisitions cannot be larger than a quarter of the wavelength. The latter can be accomplished by taking images at a faster pace over longer periods, which also allows for the capture of redundant information. This information aids in the reduction of noise caused by atmospheric artifacts and the improvement of accuracy (Ferretti et al., 2000). Permanent Scatterers and the Small Baseline Subset were designed to address this later issue in advanced DInSAR approaches (Berardino et al., 2002; Lanari et al., 2004). As indicated by Colesanti et al., (2003) velocity precision can be as low as 1 mm/year in the best-case scenario.

2.9. Application of GIS and Remote Sensing for Landslide Studies

For earth scientists, RS can be described as comprising the recording and measurement of electromagnetic energy emitted by, or reflected from, the earth’s surface and properties of objects and the relating of such measurements to the nature on the earth's surface. The products which are mostly used in earth sciences are aerial photographs, satellite images, and radar images. The use of remote sensing data in landslide research can be divided into three phases: detection and classification of landslides, monitoring the activity of current landslides, and analysis and prediction of slope collapses in space and time (Franco et al., 1996).

The term "detection" refers to the process of recording landslides within the RS image. It has two parts: classification (what type of landslide is it?) and recognition (does it look like a landslide?). In a broad sense, recognition of a landslide refers to the ability to map a landslide with various morphologies and spectral properties inside a remote sensing image. The magnitude of the structures, their contrast (the difference in spectral properties between the landslides and the surrounding areas), and the morphological expression are all important factors in recognizing landslides (Franco et al., 1996). Monitoring refers to comparing landslide conditions over time, such as aerial extent, speed of movement, soil humidity, surface topography, and so on, to assess a landslide's action.

Remote sensing is becoming an important technique for natural disaster management due to its ability to deliver broad and up-to-date geospatial information. Nowadays, geohazard studies benefit from remote sensing data (satellite images and aerial photography) (Pathak et al., 2014; Tehrany et al., 2014; Devanthéry et al., 2018). For hazard evaluation, the extraction of relevant spatial information related to the landslide, as well as its occurrence, is an important aspect of the process. The use of RS data in conjunction with a GIS has been proven to be a useful tool for processing and creating spatial data. The advancement of earth observation techniques makes landslide mapping, identification, monitoring, and hazard assessments more efficient (Psomiadis et al., 2020). Remote sensing data is an important source of information for landslide investigations. Terrain feature extraction, which is a primary source of data for the development of multiple thematic layers and spatial data analysis in GIS, can benefit from satellite imageries with high spatial resolution. Land use, lithology, slope, lineament density, precipitation distribution, altitude, slope aspect, drainages, and roadways are some of the thematic layers (Chau et al., 2004).

In geological research, a remote sensing system is an effective and extensively used analytical method, particularly in difficult areas (Dietz and Kruse, 1996; Lillesand et al., 2004; Schuster & Highland, 2001). Geological surveys and geomorphology applications benefit from aerial imagery obtained from multispectral and hyper spectral imaging sensors such as ASTER, Landsat, AVIRIS, IRS, ALOS, Quickbird, and others. At this time, a large range of satellite imageries from various sensors is available at a reasonable price. Furthermore, limited financial resources are no longer a barrier because satellite images can be obtained for free from a variety of sources, and Google Earth covers a large portion of the country with high-resolution imageries that are continually updated. Changes caused by natural catastrophes such as floods, landslides, and earthquakes are also assessed using satellite images correlated with ground truth data. Satellite imagery can also be a significant resource for updating small-scale geological maps to a larger scale, followed by field verification (Crippen & Bloom, 2001). Similarly, the risk of landslides (or mass wasting) to settlements and infrastructure near large geological features can be adequately assessed using images and photographs (Lan et al., 2004).

If a landslide inventory has to be completed through field observation, it is a challenging task. The use of satellite images and aerial photographs, on the other hand, always makes it possible to perform the task in less time and with more accuracy. The landslide activity can be closely watched using satellite images, allowing for a more accurate assessment of the potential for disaster (Lan et al., 2004; Ganapathy & Rajawat, 2015).

Slope, aspect, geology and structures, land use/land cover, road network, slope curvature, drainage density, lineament density, and other data are necessary for landslide hazard evaluation. These data come from existing maps, digital data, remote sensing, and field observations, and they're all recorded in a GIS database for study (Hamza & Raghuvanshi, 2017; Lan et al., 2004).

The interpretation of RS data (satellite images and aerial photographs) helps to locate and monitor landslides, whether they are caused by rain or earthquakes. RS can also be used to update and extract lineaments from an existing geological map. It's a useful technique for mapping at-risk elements, especially when using high-resolution satellite images. A current GIS database serves as the foundation for subsequent hazard, vulnerability, and risk analysis, which leads to disaster management operations (van Westen et al., 2006).

Chapter three

Materials and Methods

3.1. Background of the Study Area

3.1.1. Geographical Location of the Study Area

Gozamin district is found in Amhara regional state in East Gojjam Zone, northwestern highlands of Ethiopia. The district is the administrative seat of the zone, which is 270 km far from Bahir Dar, the regional capital, and 300 km far from Addis Ababa. The district shares boundary with Baso Liben on the southeast, on the south by the Abay River which separates it from the region of Oromia, on the west by Debre Elias, on the northwest by Machakel, on the north by Sinan, and the east by Aneded; the Chamwaga River defines part of the boundary between the Gozamin and Baso Liben districts. The geographic location is between 10°1′ 46″ and 10° 35′ 12″ N latitudes and 37° 23′ 45″ and 37° 55′ 52″ E longitudes (Figure 3.1) and covers an area of 1,800 km^2. The district is the second largest next to Machakel in areal size from the East Gojjam zone. It hosts altitudinal variation that extends from 1200-3510 meters above sea level.

3.1.2. Soil and Geology

The genesis of the soils in the district is influenced by the interaction of the soil-forming factors of climate, topography, parent material, organisms, and time. According to the FAO soil classification of 1996, there are four major types of soil in the district that include Chromic Luvisols, Humic soils, Eutric Nitosols, and Rendzinas. From these soil types, Eutric Nitosols is the dominant soil type in the district. Most of the Gozamin district is characterized by Termaber Basalts formation (Miocene age) with a lithology of alkaline porphyritic basalts in thin flow and Blue Nile Basalts formation (Maastrichtian to Oligocene age) with a lithology of columnar alkaline flood basalts (Tsegaw, 2007).

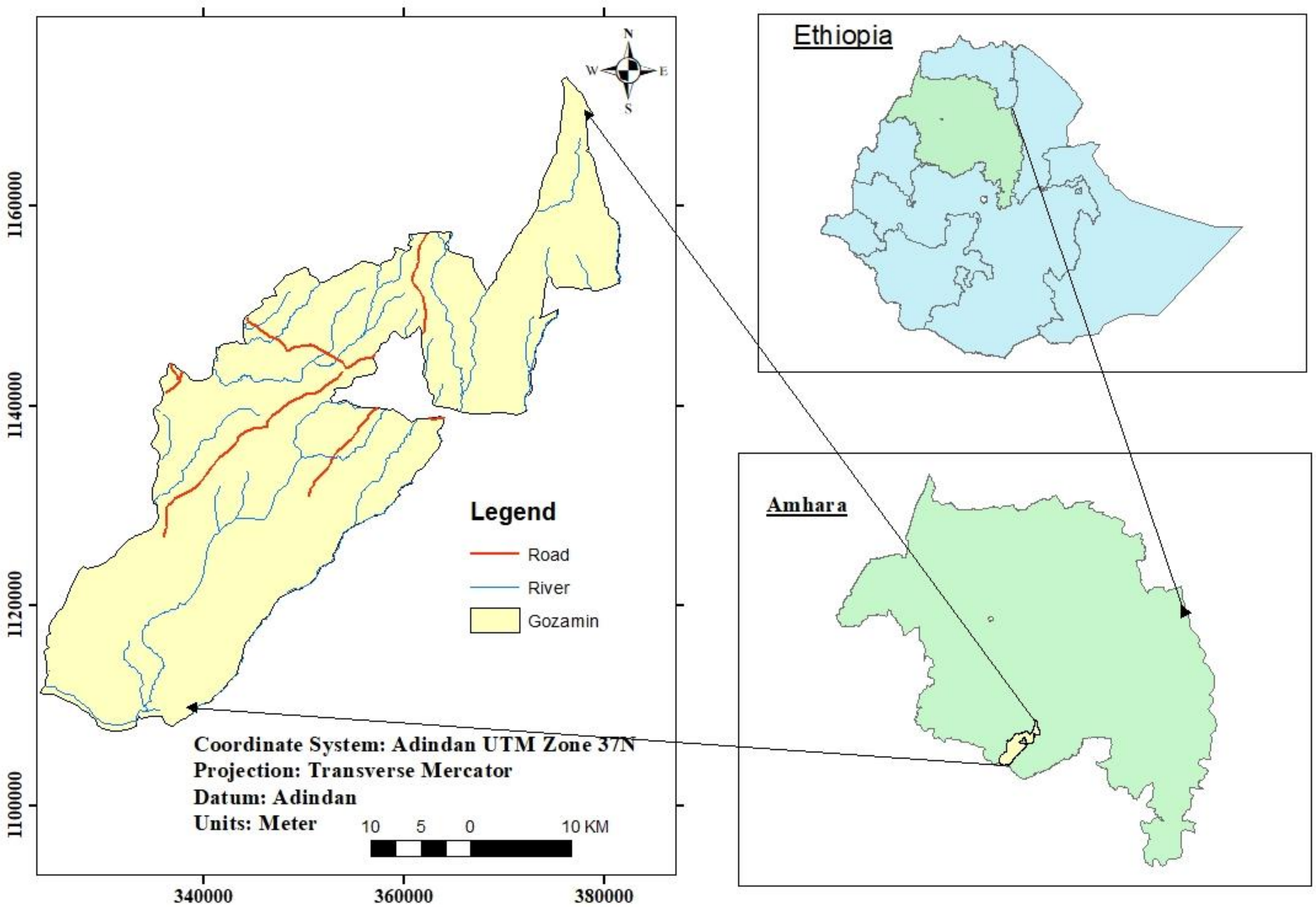

Figure 3.1: Location map of study area

3.1.3. Population

The district's overall population is estimated to be 155,012, with 78,098 females and 76,914 males (Ethiopia Central Statistical Agency, 2013). 4,495 people (2.9 percent) live in cities, which is fewer than the zonal average of 14.24 percent (Ethiopia Central Statistical Agency, 2013). Furthermore, it has an estimated population density of 113.21 people per square kilometer, which is lower than the zonal average of 153.80, according to the East Gojjam Zone Office of Finance and Economic Development (GWAO, 2014). The ethnicity of the district population is Amhara and Amharic is everybody's language.

3.1.4. Socio-Economic Activities

The overwhelming majority of the population in the district depends on farming characterized by a mixed crop-livestock production system. Among the crops grown in the district are cereals such as teff, wheat, maize, oats, and barley. Oilseeds like (Niger seed and linseed), Pulses crops such as (chickpeas and horse beans), fruits like (mango, banana, papaya, lemon, and orange), Vegetables like (potato, onion, tomato, garlic, carrot, and pepper) and rearing of livestock such as cattle, sheep, goats, equines, poultry, and beehives (Gashe, and Kassa, 2017).

3.1.5. Vegetation (Dominant Vegetation)

The vegetation cover of Gozamin District is mainly covered by indigenous trees such as Cheba *(Acacialahail)*, Agam *(Carissa edulis*), Grar *(Acacia Abyssinia*), Atet *(Maytenus spp)*, Zennbaba *(Phooenix reclinate)*, Kega *(Rosa abyssinica)*, Bisana *(Croten macrotachys)*, Embuay *(Solanum spp)*, Shola *(Ficus sycomous)*, Warka *(Ficus alicitolia)*, Wanza *(Cordial abyssinica)*, etc. with different distribution pattern because of its different climatic zones (Kassa A & Gashe A, 2018).

3.1.6. Climate

The district agro-climatic zone constitutes of Kolla, Woina Dega, and Dega. The annual rainfall of Gozamin varies from 1000 –1510 mm per year. The study area's high rainfall season is during Kiremt from June to September and the short rain season is in, Belg, which includes March, April, and May. The mean minimum temperature of Gozamin is 8.5ºC and the mean maximum temperature of 30ºC. The upper part of the Gozamin is known for its minimum temperature which results in the commonness of the Dega kind of climate while the lower portion of the district, which has the maximum temperature, is recognized for its Kolla type of climate (Tsegaw, 2007).

3.2. Data Sources and Software's

3.2.1. Remote Sensing Data

The study was utilized Sentinel-2 MSI remotely sensed satellite data with its fine spatial resolution (10,20, and 60 m), fine temporal resolution (five days), and fine spectral resolution (13 spectral bands), which may be particularly well-suited for land cover classification purposes. It is downloaded from Copernicus Hub (http://scihub.copernicus.eu/) for land use land cover classification and to calculate NDVI values of the study area, and ALOS PALSAR DEM from Alaska satellite family (https://search.asf.alaska.edu/) to produce Slope angle, slope exposure (Aspect), elevation maps of the area by mosaicking three scenes, a Sentinel-1 satellite image from (https://search.asf.alaska.edu/) to map surface displacement due to landslides, and CHIRPS data from(https://data.chc.ucsb.edu/products/CHIRPS-2.0/) to produce rainfall map of the study area (Table 3.1).

Table 3.1: Remotely Sensed Data Used for the Study

Satellite Images	Date of acquisition	Resolution	Applications
Sentinel-1	2017-2020	10m	Surface displacement map
Sentinel-2	12/01/2020	10m	Land use land cover and NDVI
ALOS PALSAR DEM	January 2020	12.5m	Slope angle, slope aspect, elevation
Chirps data	1991-2020	5.849km	Precipitation map

3.2.2. Software's and Instruments

The software's that were used for this study are ERDAS Imagine 2014, IMPACT Tool, ESA Snap, ArcGIS 10.4, Google Earth Pro, and handheld global positioning system (GPS) (Table 3.2).

Table 3.2: Software's and instruments used and their application

Software	Application
ERDAS Imagine	For image classification
Matlab	For stamps visualization
IMPACT Tool	For pre-processing of sentinel-2
ESA Snap	For processing, SAR data to produce surface displacement
Google Earth Pro	For landslide identification and accuracy assessment
GPS (handheld)	Collecting data for landslide inventory map and accuracy assessment of classified data

3.3. Method

3.3.1. Digital Image Preprocessing

Because the information extracted from satellite images should be as close as possible to the true radiant energy and spatial properties at the time of data collection, image preprocessing is required before images are utilized for extracting other information (Hailemariam et al., 2016). Pre-processing is a term used to describe operations on images at the most basic level of abstraction, where both the input and output are intensity images. These iconic images are the same kind as the sensor's original data, with intensity image often represented by a matrix of image pixel values (brightness's). Although geometric transformations of images (e.g. rotation, scaling, and translation) are classified among pre-processing methods here because similar techniques are used, the goal of preprocessing is to improve the image data by suppressing unwanted distortions or enhancing some image features important for further processing. The manipulation and interpretation of digital images using computer application software are known as digital image preprocessing. It is beneficial to improve image quality and preserve image quality for interpretation and classification; interpretation errors can be minimized since the image can be readily managed on a computer (Vision, 1993).

3.3.1.1. Layer Stacking, Resampling, and Reprojection

Layer stacking is a method to build a new multiband file from geo-referenced images of various pixel sizes, extents, and projections (Hailemariam et al., 2016). The original satellite imagery of Sentinel-2 has 13 multispectral bands; which have different resolution band 1, 9, and 10 have 60m and bands 2, 3, 4, and 8 has 10m and bands 5, 6, 7, 8a, 11, and 12 has a resolution of 20m. For this study for land use land cover classification bands 2, 3, 4, 8 which have 10m resolution, and bands, 11, and 12 which have 20m resolution were stacked and resampled to 10m resolution (Nguyen et al., 2020) to make all the bands have similar spatial resolution and pixel number using impact tool (Marangoz et al., 2017). JRC IMPACT tool v1.3b software was used to stack Sentinel-2 bands together which have different resolutions, using nearest neighbor resampling (NO Pan-Sharpening) (https://sentinel. esa. int/web/sentinel/user- guides/ sentinel 2MSI/resolutions/radiometric). Elevation, slope angle, slope aspect, which have 12.5m resolution are resampled to 10m, precipitation which has around 5.8km resolution was resampled to 10m and soil, distance from roads and rivers, and lithology maps which are in the form of vector data are rasterized to 10m resolution to combine the factor maps to landslide inventory map for making landslide hazard map, landslide vulnerability and risk maps. All data used for this study are acquired in Universal Transform Mercator (UTM) coordinate system and World Geodetic System (WGS 84) to make them compatible with local datum and coordinate system, the projection transformation were carried out and assigned to the Adindan UTM zone 37N coordinate system projection for all data sets.

3.3.3. Image Classification

Image classification is the process of extracting unique classes or themes from satellite data or aerial photographs, such as land use and land cover categorization categories (Lillisand & Kieffer, 2000). RS classification is a complicated process that takes into account a variety of characteristics. According to Lu and Weng (2007), the primary steps of image classification include the selection of an appropriate classification system, training sample selection, image preprocessing and feature extraction, post-classification processing, and accuracy assessment.

The unsupervised and supervised classification methods are the two main image classification methods used by image analysts. The maximum likelihood classification method is one of the supervised image classification techniques employed in this paper. It determines the chance that a given pixel belongs to a specific class by assuming that the statistics for each class in each band are normally distributed (Bolstad & Lillesand, 1991). The class with the highest probability is assigned to each pixel (that is, the maximum likelihood). The analyst defines small training sites on the image that are representative of each intended land cover category in supervised image classification. The most successful delineation of training areas typical of a cover type is when an image analyst is familiar with the geography of a region and has experience with the spectral properties of the cover classes. In this sense, I was born in this district, which made image classification easier. The software is subsequently trained to recognize spectral values or signatures associated with the training sites by the picture analyzer. Following the definition of signatures for each land cover type, the software uses those signatures to classify the remaining pixels (ERDAS Field Guide, 2000). There were five land-use Types in this study grazing land, settlement, agricultural land, forest, and water body by using 60 training sample points for all which means in average 12 points for each class.

3.3.4. Accuracy Assessment

Accuracy assessment is the last step in the analysis of RS data, and it helps to ensure that the results are accurate. Once the interpretation/classification is complete, it is carried out. The relationship between the class label and the ‘true' class is what accuracy is all about. During field surveys, a ‘true' class is defined as what is observed on the ground.

The accuracy of image classification is frequently measured in percentages and expressed in terms of consumer (CA) and producer accuracy (PA). The CA is derived by dividing the total number of pixels assigned to each category by the number of appropriately classified pixels. It compensates for the commission's flaws by informing the consumer that a specific ratio is correct for all regions classified as category X. The accuracy assessment producer's accuracy (PA) informs the image expert of the number of pixels correctly identified in a certain category as a percentage of the total number of pixels in the image that actually belong to that group. The correctness of the producer reveals omissions.

The demand for evaluating the accuracy of a map created from any remotely sensed product has become a common criterion and a key component of any classification effort. The user base wants to know if the classified image data being used is correct. Furthermore, different projects demand different levels of precision, and only classified images that are accurate to a certain extent can be used. When a pixel (or feature) from one category is allocated to another, a classification mistake occurs. When a feature is left out of the category being evaluated, it is called an omission error. Errors of commission occur when a feature is incorrectly included in the category being evaluated.

Using handheld GPS, a total of 72 ground truth points were gathered around the prior landslides and randomly selected regions for this investigation. The study used 178 Google earth points out of a total of 250 points for the classification accuracy assessment.

3.3.5. Method for Landslide Hazard Assessment

This study was used one of the bivariate statistical analysis methods which is an information value model that was developed from information theory. The information values of predisposing factors are employed in this model to characterize the likelihood of a landslide occurrence. Based on the occurrence of the landslide in the provided mapping area, the information values for each subclass of landslide-associated parameters are computed. To calculate the weight of each class, the triggering factor maps were integrated with the landslide inventory map. An improved form of the pixel-based information value approach was applied to map landslide susceptibility.

The Model has the advantage of assessing landslide susceptibility objectively. The method allows for the quantified prediction of susceptibility employing a score, even on terrain units not yet affected by landslide occurrence. Each instability influence is crossed with weighting values, and the landslide distribution based on landslide concentrations is calculated for each parameter class, as it occurs with all bivariate statistical methods. Negative values of information values (IV) mean that the presence of the variable is not relevant in landslide occurrence. Positive values of IV indicate a relevant relationship between the presence of the variable and landslide distribution (Yin and Yan, 1988):

According to (Yin & Yan, 1988) weight is mathematically obtained by:

$$\text{Conditional probability} = \frac{\text{Number of landslide pixels with in factor class}}{\text{Number of factor class pixels}} \qquad \text{(Eq.1)}$$

$$\text{Prior probability} = \frac{\text{Sum of landslide pixels of the whole study area}}{\text{Sum of pixels of the whole study area}} \qquad \text{(Eq. 2)}$$

$$\text{Weight of factor class} = \frac{\text{Conditional probability}}{\text{prior Probability}} \qquad \text{(Eq. 3)}$$

$$\text{Information Value} = \log \quad (\text{Weight of factor class}) \qquad \text{(Eq. 4)}$$

Finally, information values were calculated using equation four (Eq. 4) that emanates from the previous three equations of this paper. Weighted factor maps were created by assigning information values to each factor class. The raster calculator then adds all these factor maps to get a landslide susceptibility index value for each pixel (Eq.5).

$$LSI = IV_{Slope} + IV_{Elevation} + IV_{Aspect} + IV_{NDVI} + IV_{Soil} + IV_{Rainfall} + IV_{LULC} + IV_{Geology} + IV_{Drv} + IV_{Drd} \qquad \text{(Eq. 5)}$$

Where LSI represents landslide susceptibility index; IV_{Slope} represents information values of different slopes; $IV_{Elevation}$ represents information values of different elevations; IV_{Aspect} represents information values of different aspect values; IV_{NDVI} represents information values of different NDVI classes; IV_{Soil} represents information values of different soil types $IV_{Rainfall}$

represent information values of different rainfall values; IV_{LULC} represents information values of different land-use types; $IV_{Geology}$ represents information values of different geology types; IV_{Drv} represents information values of distances from river classes; and IV_{Drd} represents information values of distances from road classes.

Standard deviation, natural break, equal interval, and quantile are some of the classification approaches that have been investigated in the GIS Environment (Tehrany et al., 2014b; Tehrany, et al., 2014a). This study was used natural break categorization methods when there was categorization in the GIS environment. It is used to classify unevenly distributed data, and it is capable of classifying LSI maps into different categories considering the inherent data value similarity also, it is suitable when we want to emphasize the relative position of a feature among other features (Zimmer, 2011). LHZ map was classified into five different rank classes like very high, high, moderate, low, and very low hazard zone using the natural break categorization method. The general outline of the methodology is shown in (Figure 3.2).

3.3.6. Method for Risk and Vulnerability Assessment

Vulnerability is the possible overall maximum loss due to a potentially damaging phenomenon throughout a reference period and for a specified area (Lee & Pradhan, 2006; Papathoma et al., 2011)).

Landslide Vulnerability Assessment (LVAs) involves observation information about the types of landslides and how their impact can cause damage at different levels. Landslide vulnerability assessment is often associated with expert judgment because the maximum of the existing information is usually incomplete due to deficiency of data or restraints of data access.

According to a literature assessment, no consensus strategy has been developed that can be used as adequate standards and used effectively for LVAs in Ethiopia.

The WLC approach is widely utilized for landslide vulnerability mapping due to its application flexibility and reliance on expert knowledge. WLC is widely utilized by researchers and landslide experts; although it lacks defined refining processes for producing higher-accuracy probability maps (Irigaray & Hamdouni, 2006). WLC is based on the expert's selection of weighted averages of several parameters. The outcome can differ greatly depending on the expert. Within a GIS overlay environment, each parameter is classified and multiplied with its assigned weight; the weighted averages are added to produce the final output map. For appropriateness or susceptibility assessments, the highest summation scores are chosen for every study aim. How weights are allocated to each component (expert knowledge, experience) and the selection of GIS processes to produce the final output (maps) are essential elements that define the correctness of the WLC technique. For this study, the weights and ranks were given by expert knowledge and reading different literature. The ranks of each class of factor maps were assigned by calculating landslide density (Eq. 6).

$$LD=\frac{L\_pixels}{T\_pixels} \tag{Eq. 6}$$

Where LD denotes landslide density; L_pixels denotes the number of landslide pixels lying within the sub_class of single factor class; and T_pixels denotes the total number of pixels lying within sub_class of a single factor class (Sharma et al., 2011). To obtain the final product, the various elements are merged by adding their weight.

A landslide vulnerability map was created using the weighted linear combination (WLC) Model (Eq.7).

$$\begin{aligned} LVM = {} & (Slope*3)+(rainfall*2)+(elevation)+(LULC)+(aspect)+ \\ & (Proximity\ to\ road)+(proximity\ to\ river*2) + (Soil\ type) + (lithology) \\ & + (NDVI) \end{aligned} \tag{Eq. 7}$$

This study was used adopting the risk definition published by the United Nations Department of Humanitarian Affairs (UNDHA, 1991), landslide risk may be calculated by (Eq. 8).

$$R = H \times V \tag{Eq. 8}$$

Where R is the risk; H is a hazard; V is vulnerability; after the hazard and vulnerability are multiplied the risk map was classified into five (5) different risk levels (very high risk, high risk, moderate risk, low risk, and very low risk) based on the result (Figure 3.2).

3.3.7. Method for Surface Displacement

Differential Interferometric Synthetic Aperture Radar (DInSAR) exploits the phase difference of two SAR images gathered at different times on the same target area (ZEBKER and GOLDSTEIN, 1986; Gabriel et al., 1989). It has widely been applied since the late 1980s to map, detect and quantify surface deformation with sub-cent metric exactness over huge areas (Costantini et al., 2000; Massonnet & Feigl, 1998). Interferometry refers to the technique of combining electromagnetic signals to study their interference patterns. This paper used a technique called the permanent scatterers interferometry (PSI) approach. This paper was used the simplified approach that uses consecutive interferograms to fully exploit the increased coherence of short temporal baseline interferograms. This method is most commonly utilized in non-urban settings, where coherence deteriorates rapidly over time. A stack of N complex SAR images and N-1 successive multi-look interferograms is used to begin the method. The main steps are 2D phase unwrapping of the N-1 multi-look interferograms, using the Minimum Cost Flow method (Mora et al., 2002). Direct integration of the unwrapped interferometric phases, to obtain temporally ordered phases in correspondence to the image acquisition dates; estimation and removal of the atmospheric phase component employing a set of Spatio-temporal filters (Crosetto et al., 2016); using atmosphere-free interferograms, generate the deformation time series and accumulated deformation map, then convert the phases into displacements; Geocoding of the results (Figure 3.2). The slope displacement (Dslope) for the InSAR observation was calculated using the following equation:

$$D_{slope}=D_{los}/(n_{los}.n_{slope})$$

Where D_{los} is the displacement in line-of-sight direction, n_{los} is the LOS unit vector and n_{slope} is the slope unit vector, respectively.

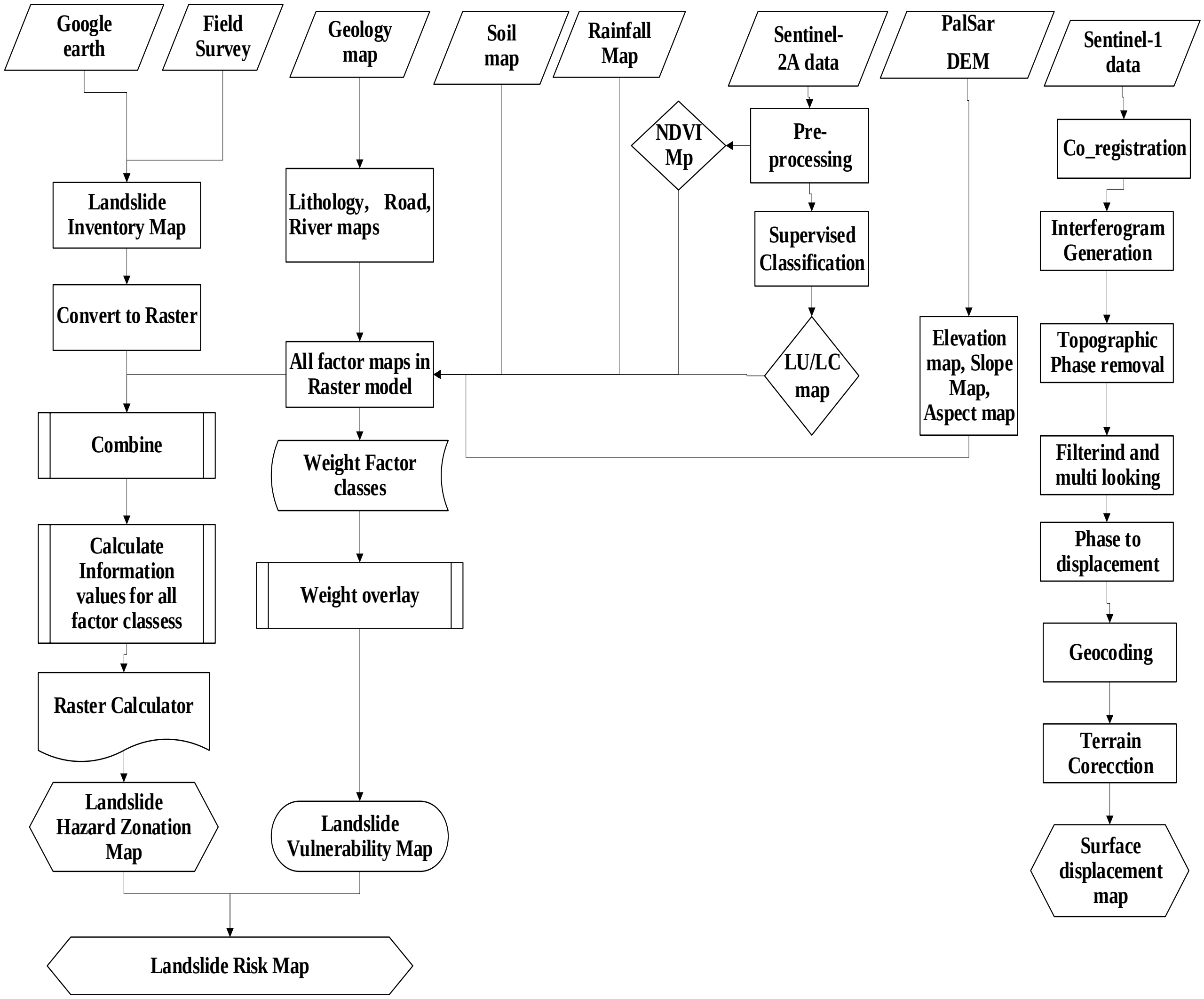

Figure 3.2: General Methodology of the Study

3.4. Landslide Inventory

A landslide inventory map is a map representing the spatial distribution of landslides that occurred in previous times. One of the main processes of landslide hazard mapping and modeling is landslide inventory mapping (Lan et al., 2004; Varnes, 1984; Fall and Noubactep, 2006). The past and the present are the main to the future for landslides zonation. The principle implies that future landslides will be more likely to occur under the conditions which led to past and present instability (Hamza & Raghuvanshi, 2017; Chimidi et al., 2017; Raghuvanshi et al., 2015). Satellite images, aerial photos, GPS observation data, articles, field surveys, internal reports, and reviews provide critical tools to establish a landslide inventory map. The landslide inventory map includes a landslide location that arises in the previous years.

3.5. Conditioning Factors

Generally, landslides are the outcome of the combination of triggers and aggravating factors, particularly the rainfall, structural, and geotechnical characteristics, slope angle, groundwater, surface water… etc. Their distribution overtime is irregular and their frequency is conditioned by extreme natural actions. The conditioning factors used in this study are slope angle, slope exposure (aspect), lithology, land use, NDVI, elevation, distance to the rivers, mean annual precipitations, soil type, and distance to the road generated from different sources. The topographic attributes such as slope angle, slope exposure, and elevation were derived from the 12.5-meter resolution ALOS PALSAR Digital Elevation Model (DEM). The lithology, distance to the road map, and distance from the river were extracted from a 1:250,000 scale geological map, whereas land use map and NDVI were generated from a sentinel-2 satellite image, soil map from soil map of Ethiopia, and precipitation map was extracted from CHIRPS satellite data.

3.5.1. Elevation

Elevation is a substantial landslide conditioning aspect because it is controlled by numerous geomorphological and geological processes (Suman, 2014). The elevation is considered to be an important triggering factor that may affect the slope material by the weathering process (Raghuvanshi et al., 2015; Suman, 2014). Slope movement intensity increases with altitude increasing. But tropical mountainous environments mostly occur 1500 to 1800 m (Nakileza & Nedala, 2020). In this research, ALOS PALSAR DEM with a resolution of 12.5m was used to prepare an altitude map. It ranges from 859 to 3805m and the altitude is classified into 5 classes: 859-1458, 1458-1940, 1940-2336,2336-2807, and 2807-3809 in the GIS environment (Figure 3.3).

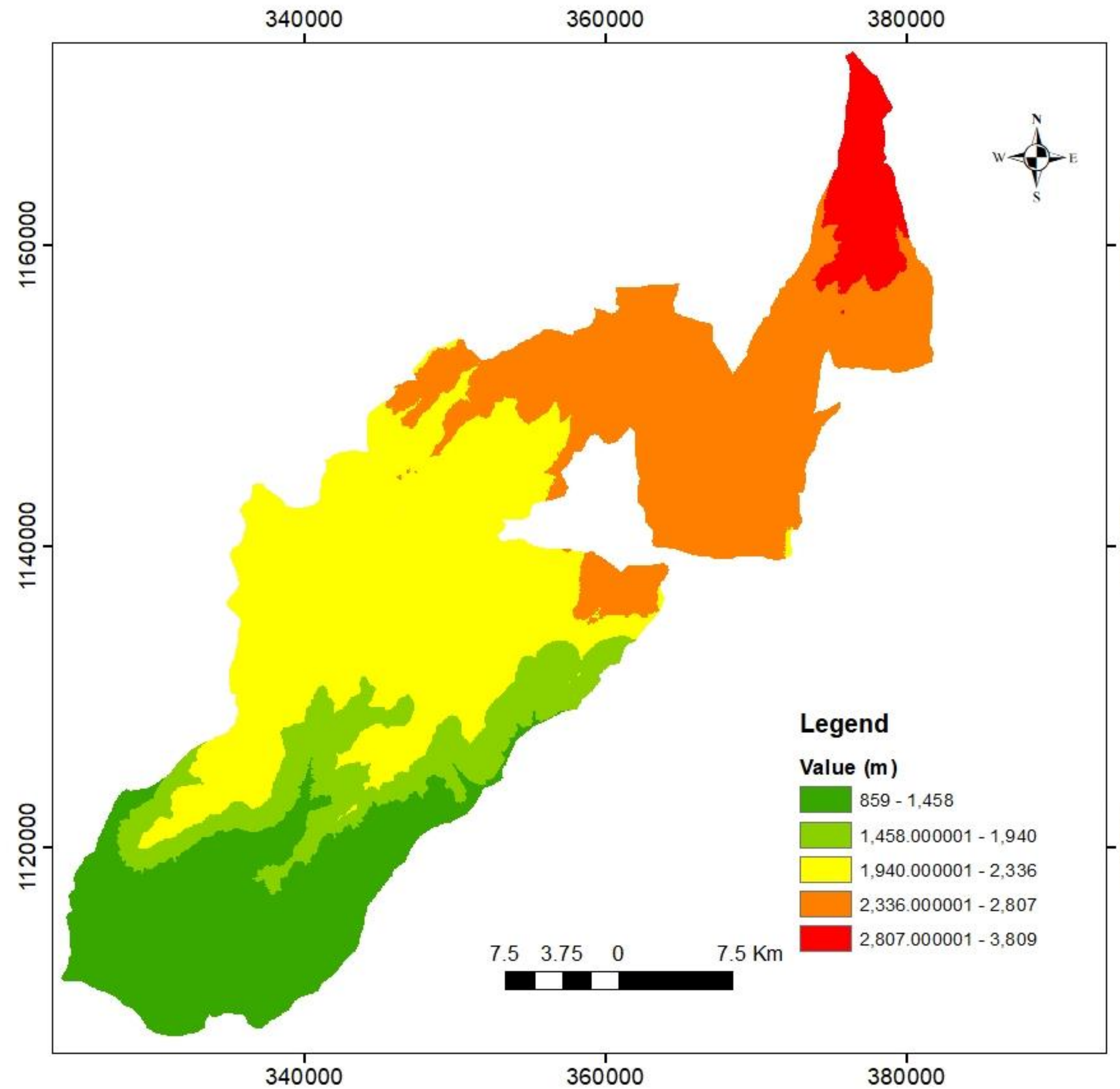

Figure 3.3: Elevation map

3.5.2. Slope Angle

One of the aggravating factors of landslides is slope degrees because it increases the acculturation of the slope movement. Slopes are dynamic systems enabling the movement of material downslope at varying speeds from negligibly slow to fast avalanche. Slopes are dynamic systems that allow material to travel downslope at variable speeds, ranging from negligibly slow to avalanche-like speeds (Michael & Samanta, 2016). Using DEM and GIS functions, slope angle was classified into 5 classes in the GIS environment. The slope inclination map (Figure3.4) shows five slope classes which are 0-5.9°, 6-12.1°, 12.2-21.4°, 21.5-35.3°, and 35.4-79°.

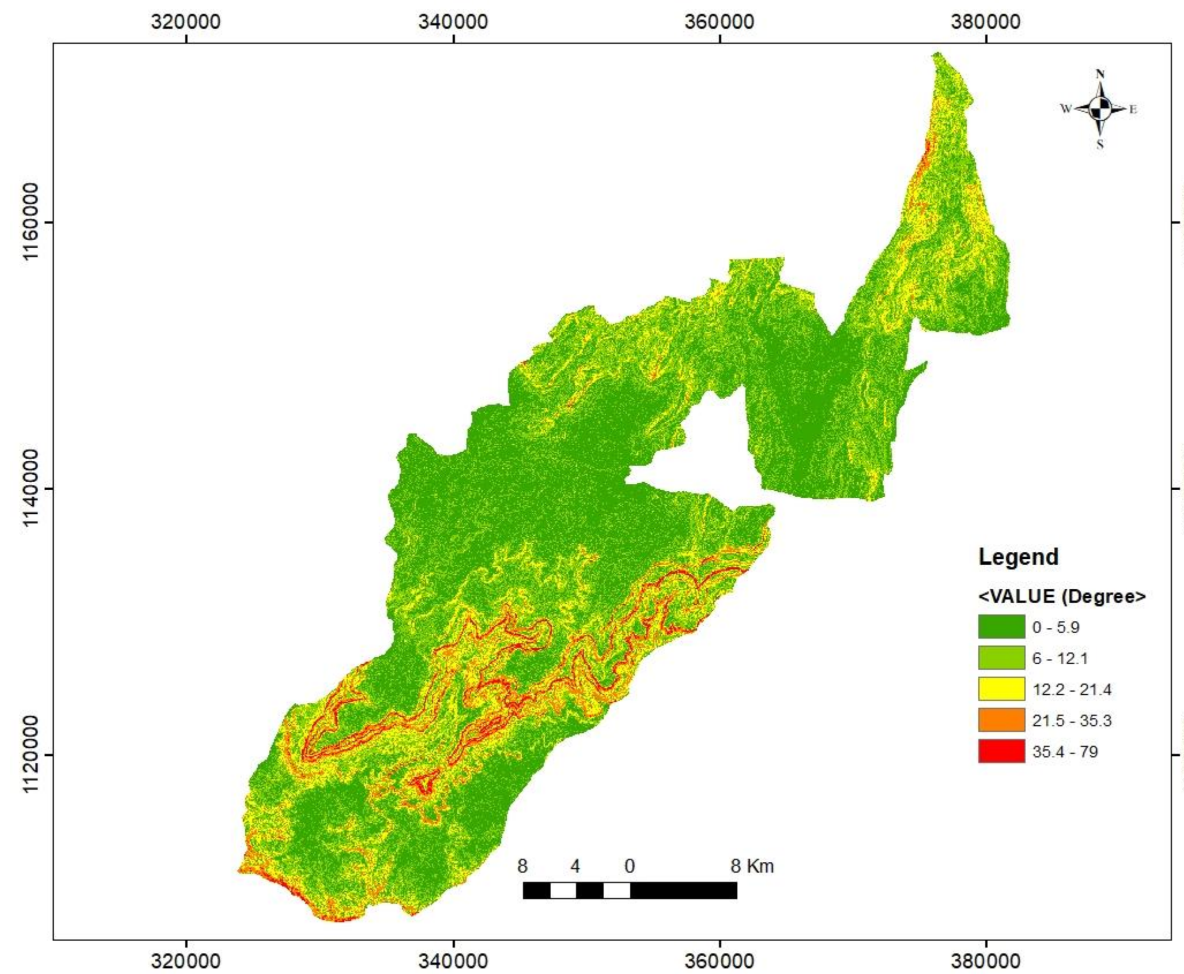

Figure 3.4: Slope map

3.5.3. Slope Exposure (Aspect)

Aspect is considered as the exposition of the slope, it is measured from 0 to 360 in degree clockwise direction with a range of 45 degrees, the values that are less than 1 indicates the flat area. It is a vital conditioning factor in the landslide susceptibility process. The aspect of a slope can influence landslide initiation because it affects vegetation cover and moisture retention and in turn soil strength and susceptibility to landslides (Raghuvanshi *et al*., 2015). In this study, the aspect map was prepared from ALOS PALSAR DEM which has a 12.5m resolution (Figure3.5).

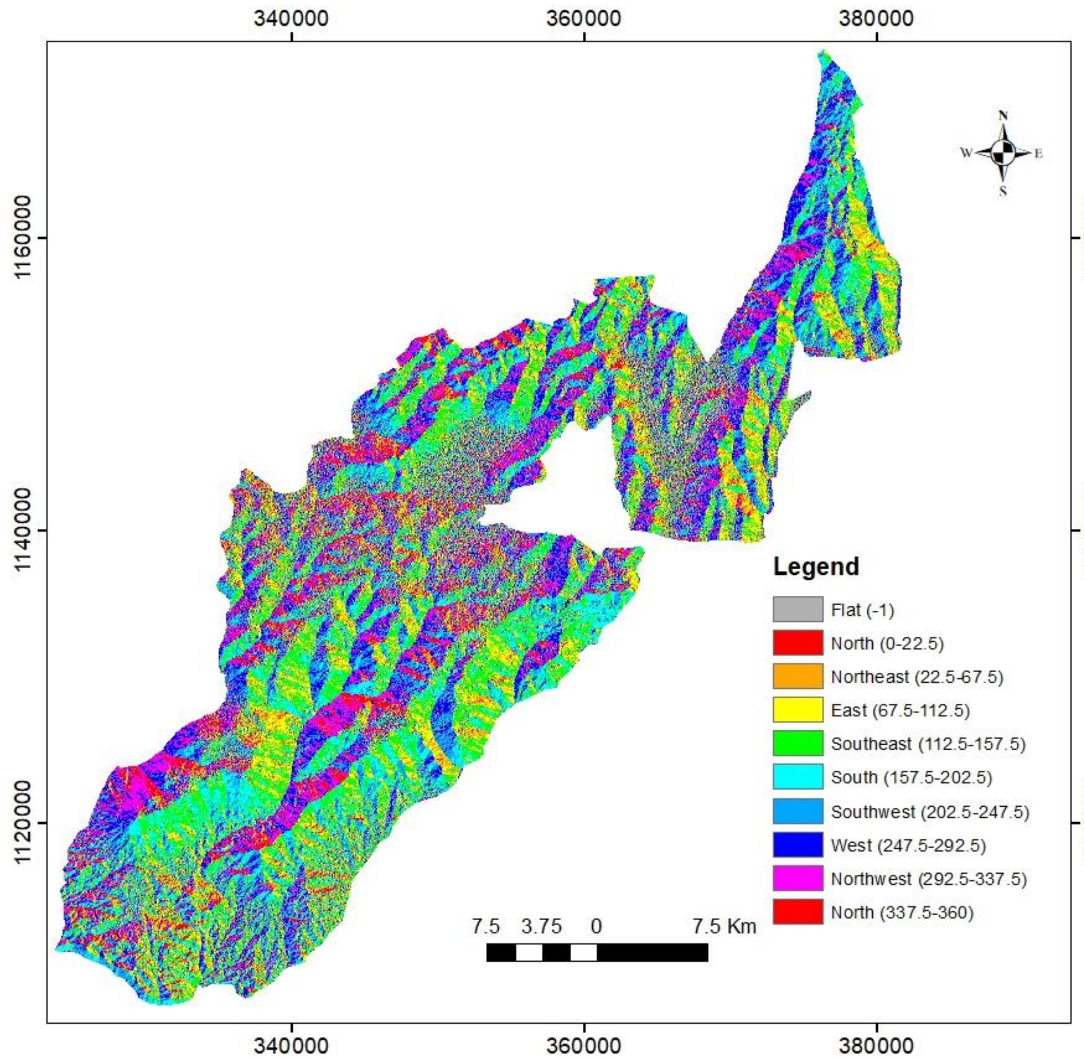

Figure 3.5: Aspect map

3.5.4. Lithology

Lithology is considered as the most important conditioning factor because each lithological unit has a landslide susceptibility level (Yesilnacar & Topal, 2005). In the current study, a lithological map was prepared by the digitization of a 1:250,000 scale geological map. Based on geotechnical and geomorphological characteristics, they were four lithology types in the study area which are Mesozoic, quaternary, paleozoic, and tertiary (Figure 3.6).

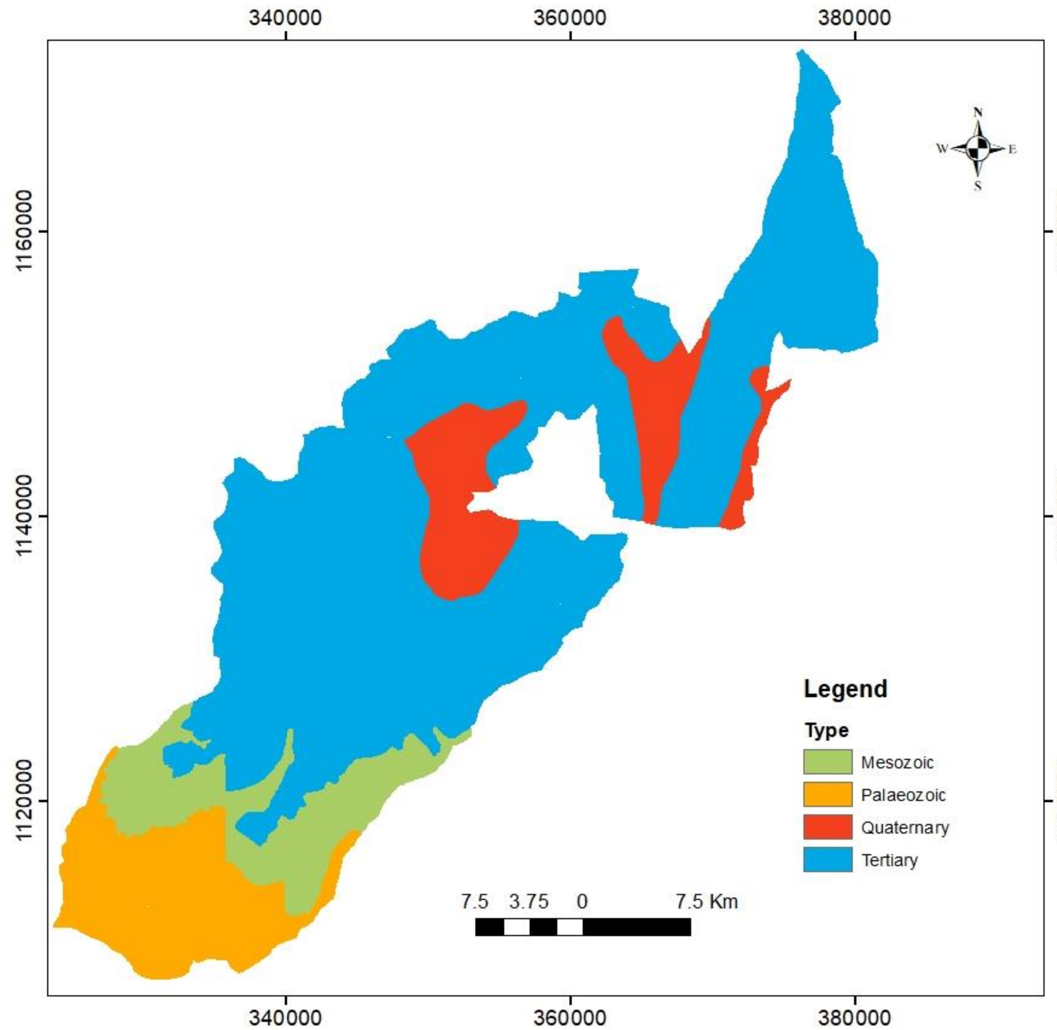

Figure 3.6: Lithology types map

3.5.5. Distance to the Rivers

Generally, landslides developed near rivers where the stream velocity is sufficient to wear away the lower part of the talus. For this distance to the rivers was integrated with landslide susceptibility estimation, using ArcGIS Euclidean distance function, the rivers buffer zone was established and classified into five classes (0-763, 764-1692, 1693-2854,2855-4712, and 4713 - 8461) in the GIS environment (Figure3.7).

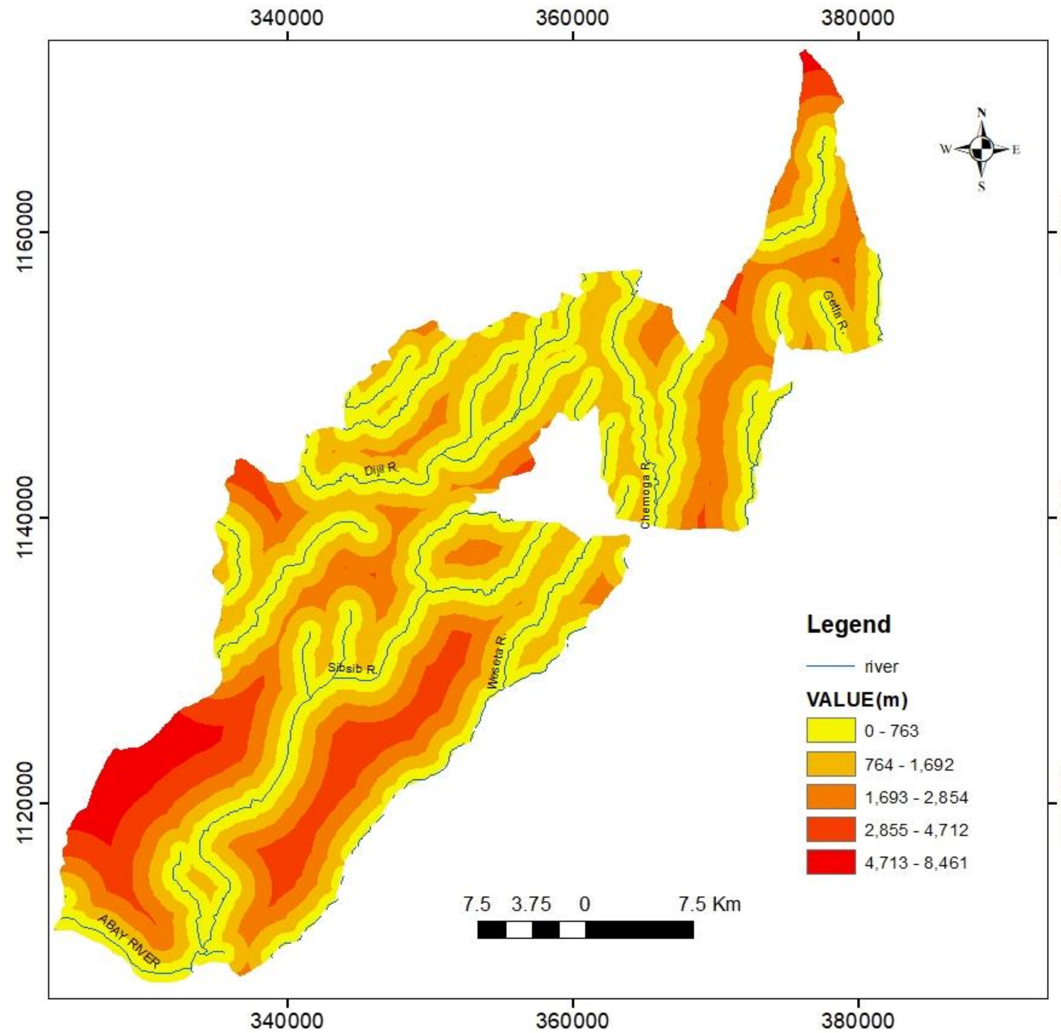

Figure 3.7: Buffer distance from the river

3.5.6. Distance to the Road

The artificial and natural parts of the slopes around a road network are more sensitive to landslide manifestations. During road construction, the human-caused actions influence landslides, and that is through destroying vegetation, application of external loads (Bourenane et al., 2015; Baum et al., 2005). Even if there were no more main roads the distance to the road is considered as a factor in this study. In the current study, the distance to the road is divided into 5 zones in the GIS environment: (0-2870, 2871-6313, 6314-10412, 10413-14758, and 14759-20907) in meter. Because of the rural nature of the study area, there was no sufficient roads infrastructure as a result the buffer zone distances are longer related to other areas especially towns in the country (Figure 3.8).

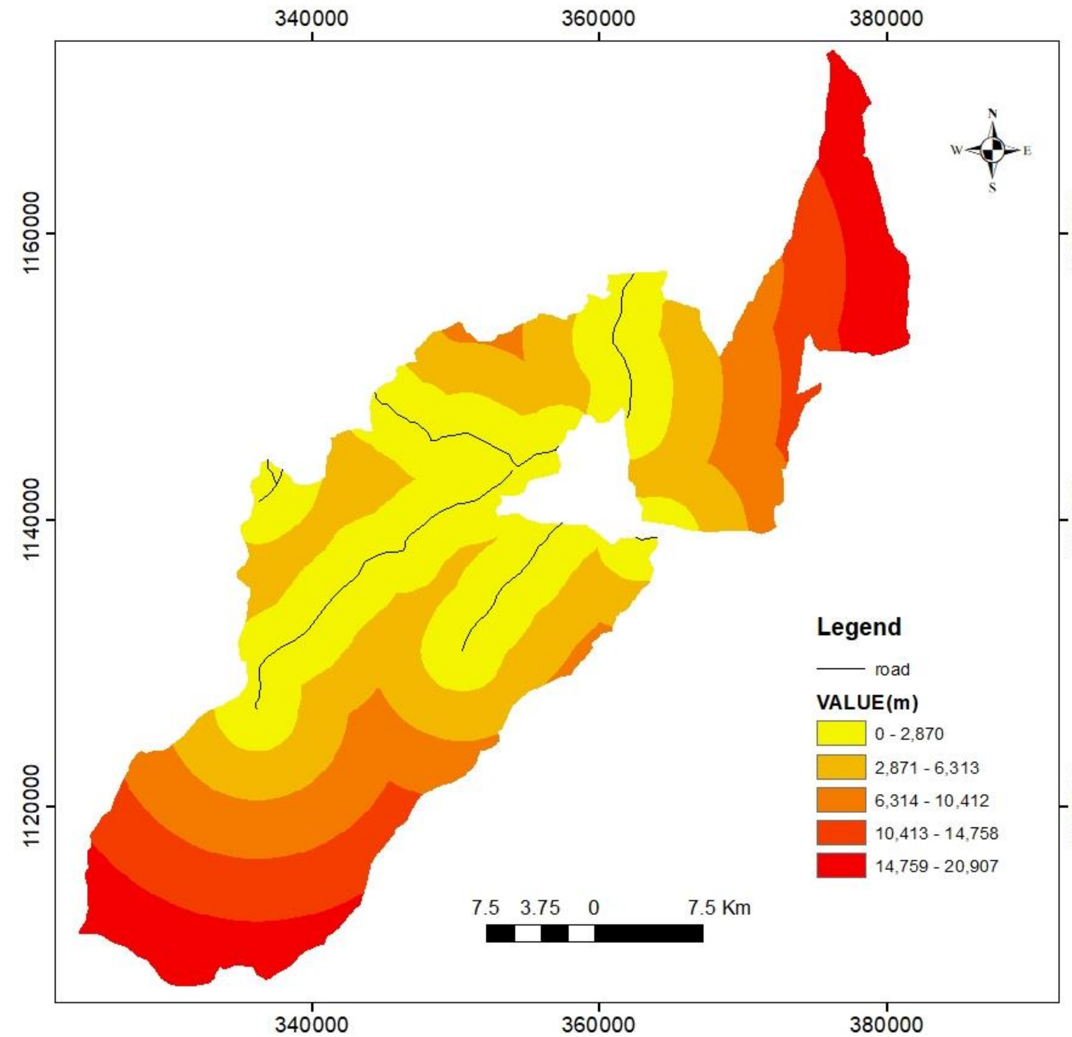

Figure 3.8: Buffer distance from the main road

3.5.7. Land Use Land Cover

LULC plays a substantial role in aggravating landslides since less vegetated areas are disposed to erosion relative to densely vegetated areas. Roots of vegetation strengthen soil capabilities to resist erosion and stabilize slopes. They also control the wetness of slopes through evapotranspiration (Chau et al., 2004; Lee & Pradhan, 2007). The Sentinel 2A level c Multi-spectral (January 2020) satellite image having a spatial resolution of 10 m was used to study the LULC of the study area, which is classified into the agricultural, settlement, grazing land, forest and, water body (Figure 3.9) that was processed by remote sensing software called ERDAS Imagine. The study area is dominated mostly by the grazing and agricultural land class since it is one of the main sources of agricultural results in Ethiopia.

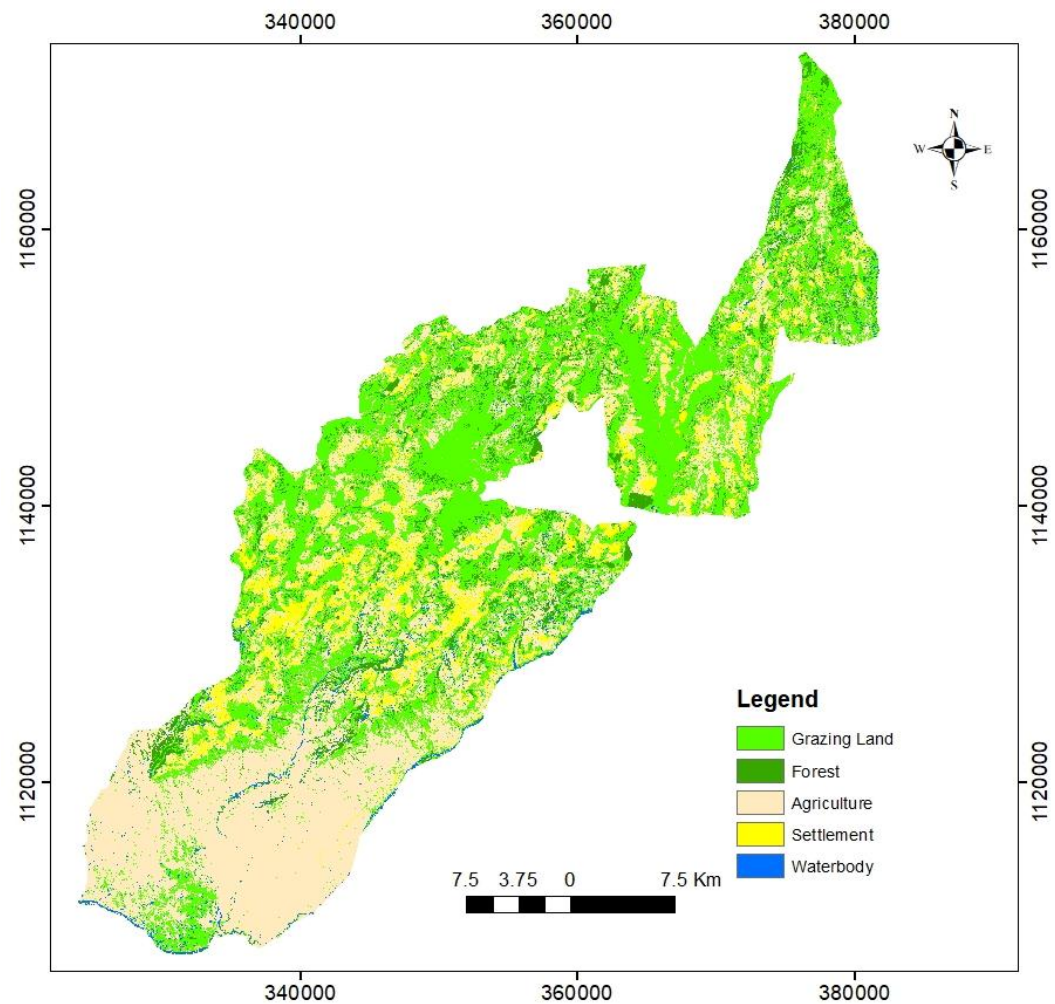

Figure 3.9: Land use and land cover map

3.5.8. Normalized Difference Vegetation Index (NDVI)

In the study, the NDVI value map (Figure 3.10) was extracted from the optical sentinel 2A level c satellite image with a resolution of 10m. NDVI values of high or positive are dense vegetation due to high concentration of chlorophyll resulting in low reflectance in the red band and sparse vegetation has lower values of NDVI and these areas are more prone to landslide than areas where the NDVI value are high. The values of NDVI ranges from -1 to +1 and values closer to +1 indicate that the area is covered by dense vegetation and the values closer to 0 or less imply that there is less or no vegetation in the area (Zhang et al., 2017; Mandanici & Bitelli, 2016). The formula used for calculating NDVI from the sentinel-2 image is the following

$$NDVI = \frac{\text{NIR}-\text{Red}}{\text{NIR}+\text{Red}} = \frac{\text{Band 8}-\text{Band 4}}{\text{Band 8}+\text{Band 4}}$$

Where NIR= near-infrared spectrum reflection

Red= visible infrared spectrum reflection of Red

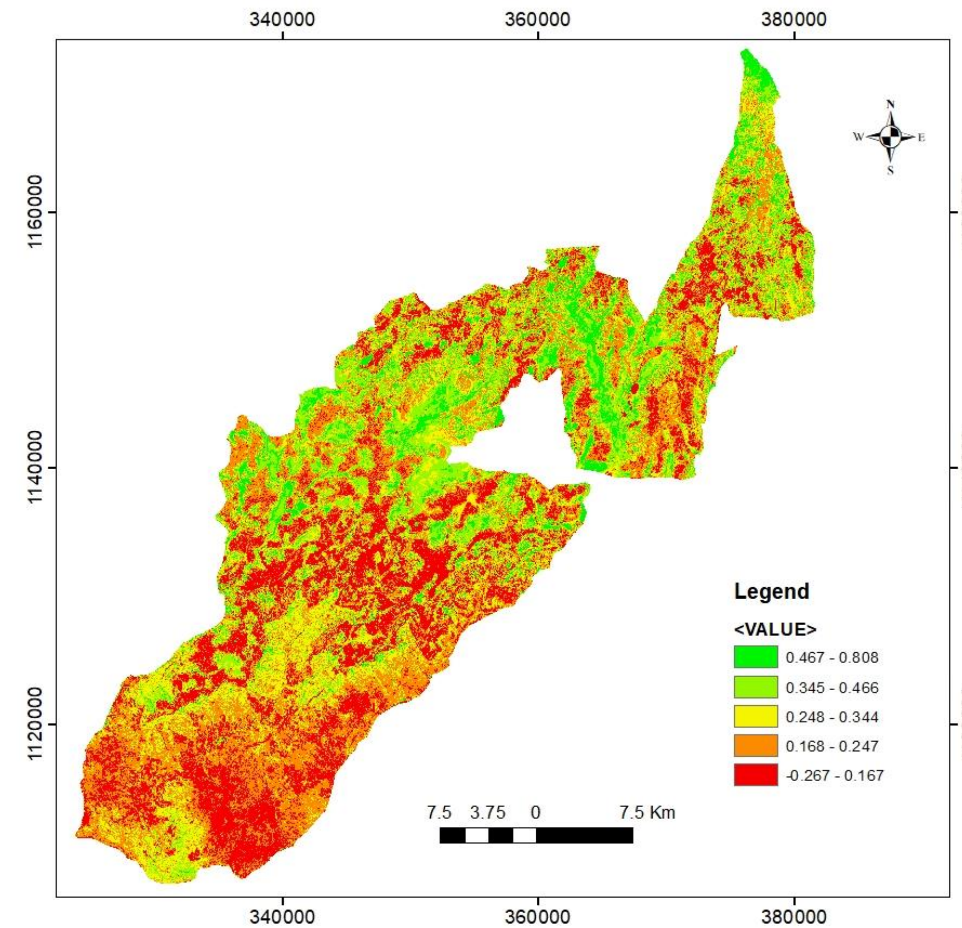

Figure 3.10: Normalized Difference Vegetation Index map

3.5.9. Mean Annual Precipitation

Precipitation is a triggering factor for landslide occurrences (Skilodimou et al., 2018). Rainfall distribution affects overland flow volume and soil moisture. In the present study, the recommended World Meteorological Organization's (WMO) reference climatic period was used. WMO's current climate reference period spans 30 years, from January 1, 1991, to December 31, 2020. However, it is also suggested that it is possible to adapt the reference period to following a "rolling" set of 30 years, updated every 10 years depending on the best available datasets (WHO, 1983; Psomiadis et al., 2020). Precipitation was spatially distributed based on its mean annual values. Mean annual precipitation was reclassified based on the rainfall amount into five classes 1040–1123 mm as 1, 1124–1221 mm as 2, 1222–1288 mm as 3, 1289–1322 mm as 4, and 1323-1492 mm as 5 ArcGIS environment (Figure 3.11).

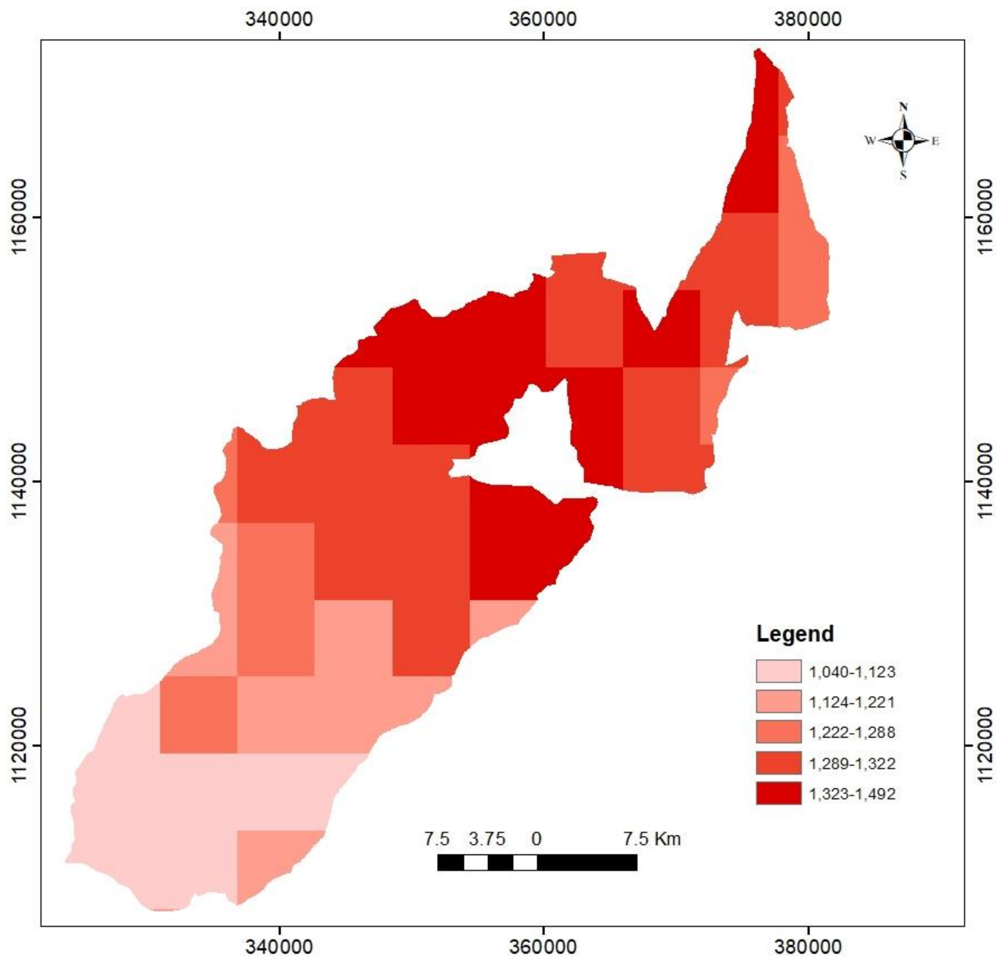

Figure 3.11: Mean annual rainfall (1991-2020), source:- CHIRPS data

3.5.10. Soil

Soil type is an important parameter in landslide analysis because the type of soil determines the tendency of soil particles to resist sliding across each other. The nature of the movement is, controlled by the earth materials involved (Peter, 1970; Hewison & Kuras, 2005). Soil types with large particles such as sandy soils are the most cohesive while clayey soils with fine particles are almost cohesive. Friction forces are dependent on the load placed on the soil surface. The greater the load the greater likelihood the force of friction will overcome. This results in the movement of soil particles within the soil layer and the potential for slope failure (Ramakrishnan et al., 2013). Four different soil types exist in the study area. Although, the presence of different soil type in the area determine the nature of mass movement and slope failure. A soil type map was constructed from the data obtained from the Ministry of Agriculture of Ethiopia and four soil types (chromic luvisols, Eutric vertisols, Humic nitisols, and Rendzic leptosols) are seen in the Gozamin district (Figure 3.12).

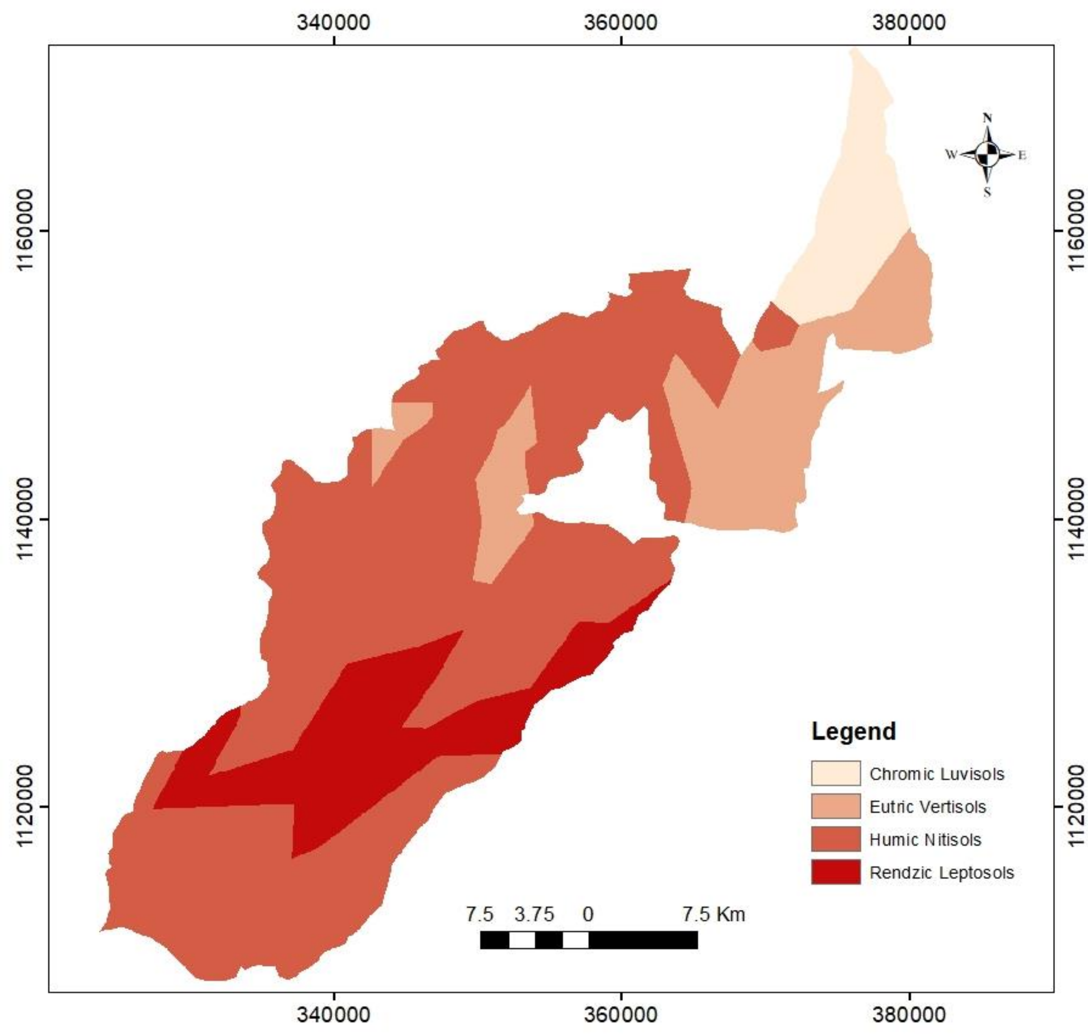

Figure 3.12: Soil type map

3.6. Slope Instability Analysis

3.6.1. InSAR Processing Dataset

Differential Synthetic Aperture Radar Interferometry (DInSAR) is a remote sensing technique that uses complicated satellite radar image datasets to measure surface deformation on the ground (Arroyo, 2020; Crosetto et al., 2016). To monitor the slope instability of Gozamin district, 13 Sentinel-1A C-Band SLC images were acquired for the study area from 2017 to 2020 by the EO satellite from the European Space Agency and were used for the analysis. Sentinel 1A image of 08 August 2018 is chosen as the master image based on minimizing the perpendicular baseline. SAR satellites orbit the Earth at an altitude of about 700 km and revisit every location on Earth after a specific time. The period between two successive visits the repeat cycle is called Temporal Baseline. However, the satellite may not be in the same location again during the acquisition of the next radar image due to limitations in orbit control. The distance between two acquisition spots perpendicular to the satellite viewing direction is known as Perpendicular Baseline (Crosetto et al., 2016; Milone & Scepi, 2011; Hooper et al., 2007). The dataset is presented in Table 3.3 along with the perpendicular baseline length with respect to the master image. The data were processed using the time-series approach of Persistent Scattered and finally done the time-series analysis to derive a two-dimensional Line-of-Sight (LOS) time-series and displacement map of surface deformation on the slope. Persistent scatterer interferometry is a powerful remote sensing technique able to measure and monitor displacements of the Earth's surface over time (Crosetto et al., 2016).

To date, Sentinel-1 has been able to collect SAR images in four (4) different modes: Strip map (SM), Interferometric Wide swath (IW), Extra-Wide swath (EW), and Wave (WV). Interferometric wide-Swath (IW) is the basic operational mode over land that is suited for interferometric application through burst synchronization. The data in this mode covers a 250km swath with a spectral resolution of 520m^2 in range and azimuth direction, and the data products are available in (HH (Horizontal Transmit and Horizontal Receive)/VV (Vertical transmit and Vertical receive)) or (HH+VV/ VV+VH (Vertical transmit and Horizontal receive) polarization (Notti et al., 2015; Milone & Scepi, 2011; Nagler et al., 2015). The Terrain Observation with Progressive Scan (TOPS) operation is used to acquire SAR data in IW mode in order to achieve such a huge coverage from a single acquisition in space (De & Guarnieri, 2006). A TOPS SAR image is made up of three sub-swaths, each of which is made up of up to ten bursts, which are slightly overlapping subsets. Images for all bursts in all sub-swaths of an IW SLC product are re-sampled to a uniform pixel spacing grid in range and azimuth using the TOPS SAR deburst technique. After co-registration of Sentinel 1 SLC images pairs, we can generate the interferometric phase.

Table 3.3: SAR datasets with their details used in the Study

No.	Acquisition date	Master/ Slave	Polarization	Sensor mode	Product Type	Passes	Orbit	Bperpendicular (m)	Btemp (days)
1	08Aug2018	Master	VV	IW	SLC	Descending	23149	0	0
2	20Jul2017	Slave	VV	IW	SLC	Descending	17549	-38.95	384
3	01Aug2017	Slave	VV	IW	SLC	Descending	17724	41.81	372
4	13Aug2017	Slave	VV	IW	SLC	Descending	17899	28.75	360
5	25Aug2017	Slave	VV	IW	SLC	Descending	18074	17.44	348
6	30Sep2017	Slave	VV	IW	SLC	Descending	18599	42.88	312
7	20Aug2018	Slave	VV	IW	SLC	Descending	23324	-15.07	-12
8	01Sep2018	Slave	VV	IW	SLC	Descending	23499	50.39	-24
9	22Jul2019	Slave	VV	IW	SLC	Descending	28224	19.36	-348
10	03Aug2019	Slave	VV	IW	SLC	Descending	28399	-23.74	-360
11	27Aug2019	Slave	VV	IW	SLC	Descending	28749	24.71	-384
12	09Aug2020	Slave	VV	IW	SLC	Descending	33824	22.41	-732
13	21Aug2020	Slave	VV	IW	SLC	Descending	33899	-31.92	-744

3.6.2. Interferogram Generation

The interferogram generation for PS-InSAR processing was done using a single master image which involves co-registration, resampling, and complex multiplications of the master with all the slave images. The master SAR image is on August 08, 2018. The master image acquisition has been chosen based on stack coherence in SNAP Desktop software. The aim of the master selection using stack coherence is to minimize the total decorrelation of all the interferograms. Because it needs a high processor and the study area shapefile is wide first we made a subset of the area with the previous landslide was existed and around the high and very high susceptible area of the landslide hazard map.

Alongside, this approach can maximize the total correlation of the interferometric stack based on the perpendicular baseline, temporal baseline, and the mean Doppler centroid frequency difference (Hooper et al., 2007). The interferometric phase which is the phase difference between master and slave image is calculated as:

$$\Delta\varphi\text{interfrogram} = \Delta\varphi\text{Def} + \Delta\varphi\text{topo} + \Delta\varphi\text{Curv} + \Delta\varphi\text{atm} + \Delta\varphi\text{noise} \qquad (6)$$

Where Δφinterfrogram is the interferogram in the interferometric phase, ΔφDef is the phase component due to deformation, Δφtopo is associated with area topography, ΔφCurv is the phase component due to Earth curvature, Δφatm is atmospheric phase resulting from the different atmospheric delay at the different acquisition times, and Δφnoise is noise term primarily due to the decorrelation (Zebker and Goldstein, 1986). The interferogram phase is the sum of the contribution from several factors. To estimate the deformation, all other components have to be estimated and subtracted from the interferometric phase. DEM and precise orbit information are used to model and remove phase contributions due to earth curvature and topography.

3.6.3. StaMPS Approach Persistent Scattered Selection

Once the interferograms were generated, bursts are merged by Topsar deburst and the topographic phase was removed using DEM to convert the interferograms into differential interferograms which were suitable for PS processing, the phase stability test was applied to obtain a set of phase-stable pixels. In PS interferometry, the signal return from the dominant scattered in the resolution element. StaMPS use amplitude Dispersion value which is the ratio of the standard deviation and the mean of the amplitude value to select a subset of pixels that includes almost all of the PS pixels in the dataset. The pixels are selected based on amplitude stability, in which those pixels which have a value of the amplitude dispersion index with the threshold are selected as initial PS candidates (Hooper et al., 2007). The data input for PS-InSAR processing in StaMPS is a stack of differential interferograms coregistered to a selected master image. In this study, the parameter used for StaMPS based PS-InSAR processing is shown in (Table 3.4).

Table 3.4: Parameters used for PS candidate selection

No	Parameter	Value
1	Amplitude Dispersion threshold	0.41
2	Number of patches in a range	1
3	Number of patches in Azimuth	2
4	Overlapping pixels between patches in a range	50
5	Overlapping pixels between patches in azimuth	200

The first PS-InSAR observation is the double difference (both temporal and spatial) between master and slave for two nearby PS (Hanssen, 2004). This implies that StaMPS also requires a spatial and temporal reference one acquisition time i.e., master image and one reference Persistent Scattered. The PS-InSAR algorithm gives a temporal evolution of the landslide in Gozamin over 4 years using multiple SAR image acquisition. Setting the amplitude dispersion higher in the processing parameter can increase the number of initial PS candidates. The selected PS pixels are wrapped between $-\pi$ and $+\pi$ (Fig 3.13).

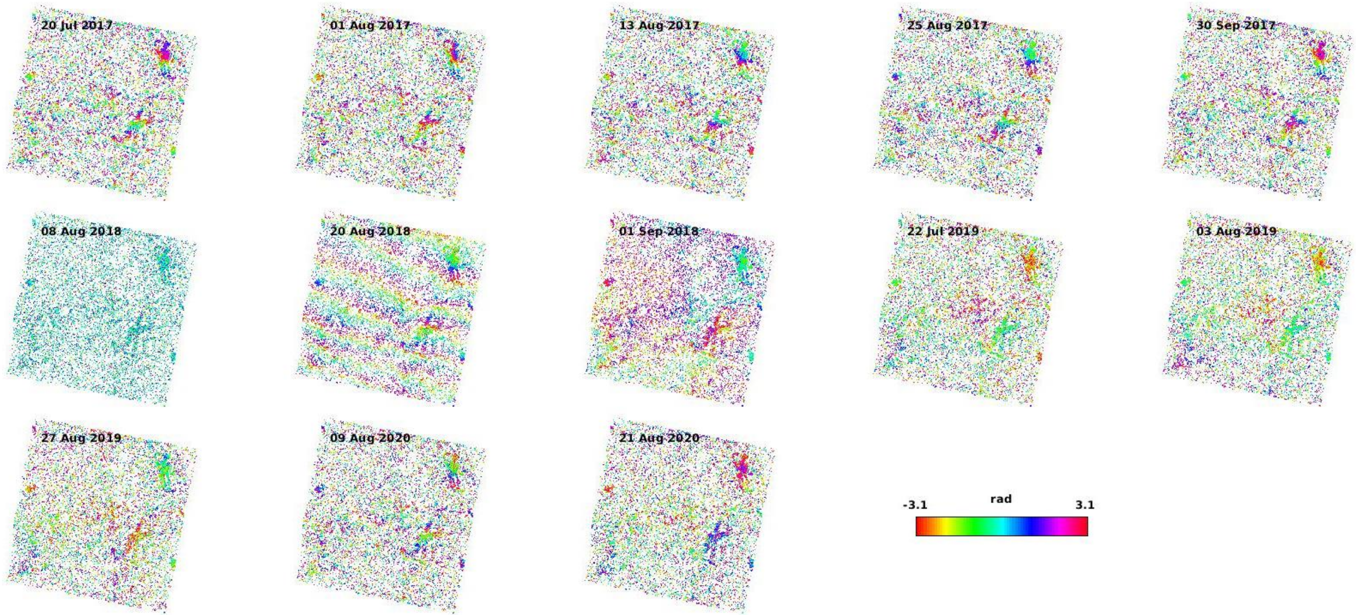

Figure 3.13: Wrapped interferogram with single master image 2017-2020

Phase unwrapping, therefore, is implemented in order to obtain a continuous deformation phase value. In this study, 3D phase unwrapping has been performed, two spatial and one temporal. The temporal phase difference for each PS pixel is calculated and then unwrapped spatially from reference PS pixels using an iterative least square method. PS pixel is also filtered using Goldstein phase filter before performing unwrapping (Fig. 3.14), high-pass filtering can be applied to the unwrapped data in order to remove the remaining look angle, atmosphere, and orbit errors (SCLA). By subtracting SCLA errors from PS pixels, it leaves only phase data due to deformation.

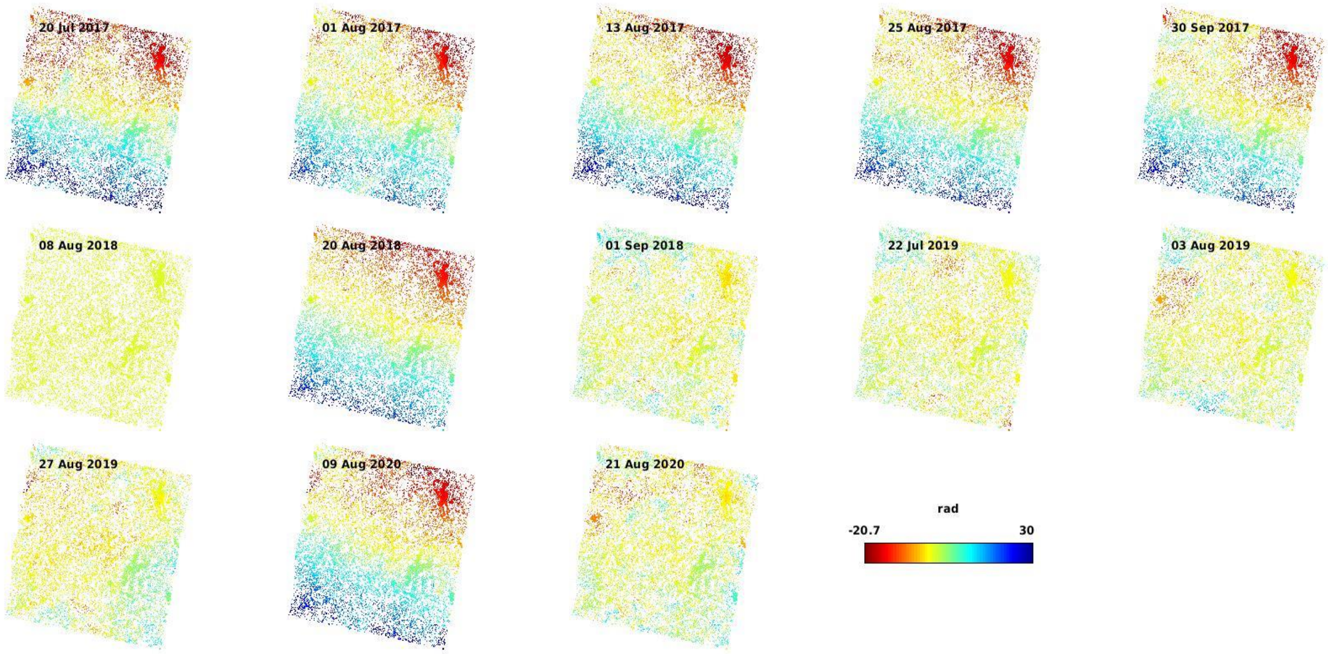

Figure 3.14: Unwrapped interferogram with single reference image 2017-2020

Chapter Four

Results and Discussions

4.1. Landslide hazard mapping

In this paper, one of the statistical methods was applied to map a landslide hazard which is the information value method. The influence of each causative factor class was defined by the combination of the landslide inventory map and each parameter. By the combination of following decision rules (addition, division, multiplication …etc.), the weight of each conditioning factor class was defined. Finally, the classification of landslide hazard maps is done using an ArcGIS environment.

4.1.1. Landslide Inventory Mapping

The landslide inventory map is the key and essential starting point for studying the relationship between landslides and conditioning factors (Raghuvanshi et al., 2015). In this study, a total of 58 landslide locations were identified using satellite images, Google Earth, field surveys, and reports of the district that are occurred from 2017 to 2020. From the total of 58 landslides identified and mapped in the study area, 49(84.48%) landslides are found in the eastern and central parts of the Gozamin district. A figure 4.1 illustrates the spatial distribution of landslide location in the Gozamin district, Ethiopia. The historical and recent landslides in the region were produced. Landslide frequency in a given location can be evaluated to provide reliable estimates of landslide likelihood over a region where landslides have caused considerable damage.

4.1.2. Elevation

Elevation is a factor frequently utilized in landslide hazard assessment (Raghuvanshi et al., 2014; Hamza and Raghuvanshi, 2017). According to the results (Table 4.1), 1940-2336m and 1458-1940m classes of elevation have 84.63% and 14.81% of historic landslide occurrence and these two elevation classes have the highest information value (IV) of 0.37 and 0.12, respectively. From these figures, it may be realized that the information value generally increases with the increase in elevation. In tropical mountainous environments mostly occur 1500 to 1800 m

(Nakileza & Nedala, 2020). In this study, there were no landslides in the highest and lowest parts of elevation values almost the same as the study by Nakileza & Nedala, 2020.

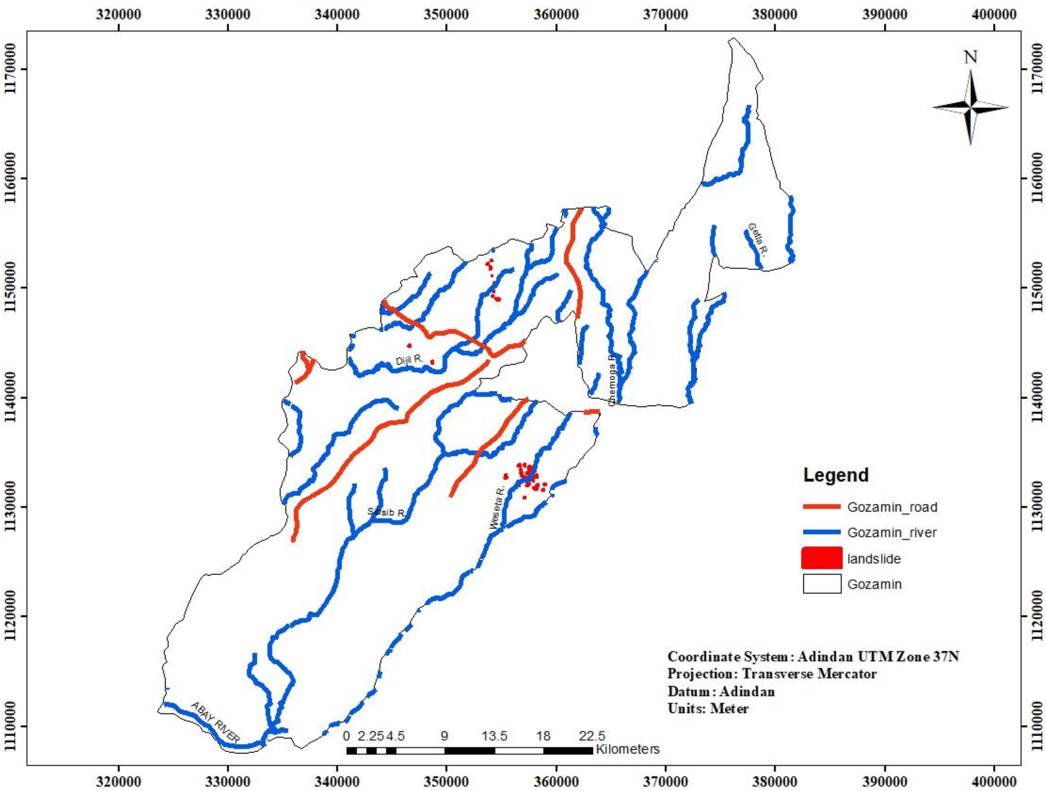

Figure 4.1: Landslide locations

Table 4.1: Landslide distribution related to elevation

ID	Factor Class(m)	No. of pixels	pixels %	Landslide Pixels within Factor class	Landslide %	conditional Probability	Prior probability	Weight of Factor class	Iv
1	859-1458	2463680	20.23	0	0	0	0.0024	0	0
2	1458-1940	1333010	10.95	4252	14.8086	0.003	0.0024	1.33	0.12
3	1940-2336	4348764	35.71	24302	84.6376	0.006	0.0024	2.33	0.37
4	2336-2807	3473157	28.52	159	0.5538	0.0001	0.0024	0.02	-1.72
5	2807-3809	559344	4.59	0	0	0	0.0024	0	0

4.1.3. Slope

During or after rainfall, the slope gradient also controls subsurface water distribution, surface runoff rate, and soil water content. Landslides are less likely to occur at low and near-vertical slope angles (Michael & Samanta, 2016; Guzzetti et al., 1999). The slope classes 0-5.9°, 6-12.1°, and 12.2-21.4° show low 'information value' (IV) of -0.94, -0.08, and -0.29, respectively, this indicates a low probability of landslide occurrence within these slope classes. However, the slope classes 21.5-35.3° and 35.4-79° show the highest probability of landslide occurrence with information values (IV) 0.96 and 0.34, respectively. The relation between landslide occurrence and slope angle shows that most of the landslides were observed with increasing slope angles (Table 4.2).

Table 4.2: Landslide distribution related to slope

ID	Factor Class	No. of pixels	pixels %	Landslide Pixels with in Factor class	Landslide %	conditional Probability	Prior probability	Weight of Factor class	Iv
1	0-5.9	5273302	43.30	1425	4.96	0.0003	0.0024	0.11	-0.94
2	6-12.1	4098870	33.66	8006	27.88	0.002	0.0024	0.83	-0.08
3	12.2-21.4	1848230	15.18	2254	7.85	0.0012	0.0024	0.52	-0.29
4	21.5-35.3	736790	6.05	15879	55.30	0.0216	0.0024	9.14	0.96
5	35.4-79	220761	1.81	1149	4	0.0052	0.0024	2.21	0.34

4.1.4. Aspect

According to the result the highest landslide occurrence in the slopes inclined towards Northwest, Northeast and, West show information values 0.14, 0.067, and 0.047, respectively. Further, from the landslide inventory data, it was observed that Northwest facing slopes covered the highest percentage of landslides (16.36%) followed by west-facing slopes (15.11%). A relatively smaller number of landslides occurred in other aspect classes. Less number of landslides was observed to occur in the flat aspect class in the study area (Table 4.3).

Table 4.3: Landslide distribution related to aspect

ID	Factor Class	No. of pixels	pixels %	Landslide Pixels within Factor class	Landslide %	conditional Probability	Prior probability	Weight of Factor class	Iv
1	Flat	196642	1.62	473	1.65	0.002	0.0024	1.02	0.009
2	North	912553	4.42	1862	6.49	0.004	0.0024	1.47	0.167
3	Northeast	976935	8.02	2686	9.36	0.003	0.0024	1.17	0.067
4	East	1493786	12.27	2537	8.84	0.002	0.0024	0.72	-0.143
5	Southeast	2114406	17.36	3466	12.07	0.002	0.0024	0.70	-0.158
6	South	1744460	14.33	3486	12.14	0.002	0.0024	0.85	-0.072
7	Southwest	1648191	13.53	4054	14.12	0.003	0.0024	1.04	0.018
8	West	1649384	13.54	4337	15.11	0.003	0.0024	1.12	0.047
9	Northwest	1441596	11.84	4698	16.36	0.003	0.0024	1.38	0.141

4.1.5. Lithology

In the study area, there were four lithological types Tertiary, Quaternary, Palaeozoic, and Mesozoic with 67.5%, 10.5%, 12.1%, and 9.9% coverage area respectively. Most landslides have occurred previously on the Tertiary followed by Quaternary with 98.1% and 1.9% of landslides. So, the highest information value is 0.15 on tertiary and the lowest is -0.75 on Quaternary lithology's as shown in (Table 4.4).

Table 4.4: Landslide distribution related to Lithology

ID	Factor Class	No. of pixels	pixels %	Landslide Pixels within Factor class	Landslide %	conditional Probability	Prior probability	Weight of Factor class	Iv
1	Mesozoic	1201268	9.86	0	0	0	0.0024	0	0
2	Paleozoic	1475314	12.12	0	0	0	0.0024	0	0
3	Quaternary	1277597	10.49	541	1.9	0.0004	0.0024	0.18	-0.75
4	Tertiary	8223175	67.53	28172	98.1	0.0034	0.0024	1.43	0.15

4.1.6. Distance from River

The distances from the streams play a great role in landslide occurrence. In this study, almost all previous landslides have occurred near a stream indicating it activates the most landslides in the district. The study classifies the distances from the river into five classes. Among these classifications, the first two classifications are the areas in which all previous landslides occurred. The maximum information value is in the first class (near to streams) which is 0.35 and the lowest value in the second class which is -0.19 and in other classes, there is no landslide in the previous years (Table 4.5).

Table 4.5: Landslide distribution related to distance from river

ID	Factor Class(m)	No. of pixels	pixels %	Landslide Pixels within Factor class	Landslide %	conditional Probability	Prior probability	Weight of Factor class	Iv
1	0-763	4324244	35.51	22575	78.62	0.005	0.0024	2.18	0.35
2	764-1,692	3964710	32.56	6138	21.38	0.002	0.0024	0.65	-0.19
3	1,693-2,854	2431591	19.97	0	0	0	0.0024	0	0
4	2,855-4,712	1096162	9.00	0	0	0	0.0024	0	0
5	4,713-8,461	361465	2.97	0	0	0	0.0024	0	0

4.1.7. Distance from Road

The distances from roads and other infrastructures play an important role in the occurrence of landslides. In this study, the distances from the main roads are classified into five groups. Even if the road distributions are few in the study area, the previous landslides occurred in the first three groups located near roads. The maximum information value is in the first class (0-2,870m) which is 0.38 and the minimum information value is in the third class (6,314-10,412) which is -1.31 (Table 4.6).

Table 4.6: Landslide distribution related to proximity to the road

ID	Factor Class(m)	No. of pixels	pixels %	Landslide Pixels within Factor class	Landslide %	conditional Probability	Prior probability	Weight of Factor class	Iv
1	0-2,870	3951563	32.45	22954	79.94	0.0058	0.0024	2.42	0.38
2	2,871-6,313	3315955	27.23	5538	19.29	0.0017	0.0024	0.70	-0.16
3	6,314-10,412	1869553	15.35	221	0.77	0.0001	0.0024	0.05	-1.31
4	10,413-14,758	1556794	12.78	0	0	0	0.0024	0	0
5	14,759-20,907	1484306	12.19	0	0	0	0.0024	0	0

4.1.8. Land Use Land Cover

The land use and land cover of the study area was classified as agricultural land, grazing land, settlement area, forest, and water body which cover 40.46%, 40.44%, 9.71%, 7.65%, and 1.74% of the total study area respectively. The overall accuracy of the classification is 90.8 percent, with a corresponding kappa coefficient of 88.5 percent, according to the findings. The categorization result was satisfactory because the kappa coefficient was above 0.85 (Haroun et al., 2013; Jensen, 2005). This study's LULC accuracy assessment was summarized in (appendix). The agricultural area and grazing land in the study area show the highest probability for landslide occurrence in the study area with the information values of 0.031 and 0.0005 respectively.

Moreover, settlement, Forest, and water body in the study area show the least probability for landslide occurrence as the information values for these classes are -0.1223, -0.062, and -0.73, respectively (Table 4.7).

Table 4.7: Landslide distribution related to land use land cover

ID	Factor Class	No. of pixels	pixels %	Landslide Pixels within Factor class	Landslide %	conditional Probability	Prior probability	Weight of Factor class	Iv
1	Grazing Land	4924725	40.44	11834	41.21	0.0024	0.0024	1.001	0.0005
2	Forest	931327	7.65	1938	6.75	0.0021	0.0024	0.87	-0.062
3	Agriculture	4927788	40.47	12705	44.25	0.0026	0.0024	1.07	0.031
4	Settlement	1182792	9.71	2142	7.46	0.0018	0.0024	0.76	-0.12
5	Waterbody	211321	1.74	94	0.33	0.0004	0.0024	0.19	-0.73

4.1.9. Normalized Difference Vegetation Index (NDVI)

Vegetation in general improves the stability of the slope (Anbalagan & Singh, 1996; Raghuvanshi et al., 2014). The NDVI value indicates a proxy for measuring the status of the vegetation condition of the area. The result presented in Table 4.8 indicates that higher information values (IV) 0.0061 and 0.38 are distributed for the first two consecutive NDVI classes falling between -0.267 to 0.167 and 0.168-0.247 respectively which generally corresponds to the agricultural land, grazing land, and built-up area. As NDVI becomes higher, the probability of occurrence of landslide is lower (Tseng et al., 2015). From this, it can be realized that as the NDVI increases the Information value (IV) in general decreases.

The relation between landslide occurrence and NDVI clearly showed that most of the landslides occurred in the area where the NDVI values were low.

Table 4.8: Landslide distribution related to NDVI

ID	Factor Class	No. of pixels	pixels %	Landslide Pixels with in Factor class	Landslide %	conditional Probability	Prior probability	Weight of Factor class	Iv
1	-0.267-0.167	2917307	23.96	6975	24.29	0.0024	0.0024	1.014	0.0061
2	0.168-0.247	3660464	16.13	10994	38.29	0.0056	0.0024	2.37	0.38
3	0.248-0.344	2531679	20.79	4286	14.93	0.0017	0.0024	0.72	-0.14
4	0.345-0.466	3660464	30.06	4413	15.37	0.0012	0.0024	0.51	-0.29
5	0.467-0.808	1104541	9.07	2045	7.12	0.0019	0.0024	0.79	-0.11

4.1.10. Precipitation

The study area has had high rainfall in 30 years like the other parts of Ethiopia. The annual precipitation increased from year to year which means it facilitates landslide occurrence. In the study, the precipitation ranges from 1040 mm to 1492 mm and is classified into five groups. The annual precipitation that ranges from 1289-1322 mm has a higher information value (0.41) and 1323-1492 has a minimum information value (-1.45) (Table 4.9). This result indicated that there is a low landslide in high rainfall intensity areas this is because of the other triggering factors such as land use and NDVI.

Table 4.9: Landslide distribution related to rainfall

ID	Factor Class(mm)	No. of pixels	pixels %	Landslide Pixels with in Factor class	Landslide %	conditional Probability	Prior probability	Weight of Factor class	Iv
1	1,040-1,123	1951433	16.02	0	0.00	0.0000	0.0024	0.00	0.00
2	1,124-1,221	1696577	13.93	1226	4.27	0.0007	0.0024	0.30	-0.52
3	1,222-1,288	1604916	13.18	0	0.00	0.0000	0.0024	0.00	0.00
4	1,289-1,322	4370151	35.89	27267	94.96	0.0062	0.0024	2.60	0.41
5	1,323-1,492	2555094	20.98	220	0.77	0.0001	0.0024	0.04	-1.45

4.1.11. Soil

In the study area, there are four soil types chromic luvisols cover 6.72%, Eutric vertisols cover 16.14%, Humic nitisols cover 63%, and Rendzic leptosols covers 14.14% with the information values of 0, 0, 0.14, and -0.09 respectively for chromic luvisols, Eutric vertisols, Humic nitisols, and Rendzic leptosols from this the maximum information value is for Humic nitisols and it indicates this type of soil are more exposed to landslide (Table 4.10).

Table 4.10: Landslide distribution related to soil type

ID	Factor Class	No. of pixels	pixels %	Landslide Pixels within Factor class	Landslide %	conditional Probability	Prior probability	Weight of Factor class	Iv
1	Chromic Luvisols	814556	6.72	0	0.00	0.000	0.0024	0.00	0.00
2	Eutric Vertisols	1956146	16.14	0	0.00	0.000	0.0024	0.00	0.00
3	Humic Nitisols	7637612	63.00	25351	88.29	0.003	0.0024	1.38	0.14
4	Rendzic Leptosols	1714368	14.14	3362	11.71	0.002	0.0024	0.82	-0.09

4.2. Highly Contributing Classes from Causative Factors

In this study 10 causative factors namely land use land cover, NDVI, soil type, lithology, elevation, slope, aspect, rainfall, distance from main roads, distance from streams(rivers), and these factors are classified in 53 classes. From the 53-factor classes agriculture has an information value of 0.031, NDVI class ranges from 0.167-0.247 has information value of 0.37, distance from rivers ranges from 0-763 has the maximum information value of 0.35, distance from roads (0-2,870) has the maximum information value of 0.38, the elevation of 1940-2336 has the maximum information value of 0.37, the slope that ranges between 21.062-34.998 has the maximum information value of 0.96, aspect facing towards the northwest has the maximum information value of 0.14, rainfall (1,289-1,322mm) has the maximum information value 0.41, lithology of Tertiary has the maximum information value 0.15, soil type Humic Nitisols has the maximum information value of 0.14 (Table 4.11). So, the above classes of the conditioning factors play a great role in the occurrence of previous landslides, and by the statement of the future occurs like the past these factors will have a great influence on the occurrence of future landslides.

Table 4.11: Highest information value classes

Causative factor	Class	Information value
Elevation	1940-2336	0.37
Slope	21.062-34.998	0.96
Aspect	Northwest	0.14
Lithology	Tertiary	0.15
LULC	Agriculture	0.031
NDVI	0.167-0.247	0.37
Distance from river	0-763	0.35
Distance from road	0-2,870	0.38
Soil	Humic Nitisols	0.14
Rainfall	1,289-1,322	0.41

4.3. Landslide Hazard Evaluation and Zonation

The information value method was used to map landslide hazard zones in this study. The combination of each parameter and the landslide inventory map determined the weight of each causative factors class. The weight of each conditioning factor class was determined using a variety of decision rules (multiplication, addition, division, etc.).The causative factor classes were combined with a landslide inventory map and information values of each factor were calculated in excel. After that, each factor map was joined with its information value table and do a lookup in the ArcGIS environment to get a landslide hazard map and classified into groups. There are five groups very high hazard, high hazard, moderately hazard, low hazard, and very low hazard zones with 6.61%, 14.69%, 38.20%, 15.53%, and 24.97% of the study area respectively (Figure 4.2).

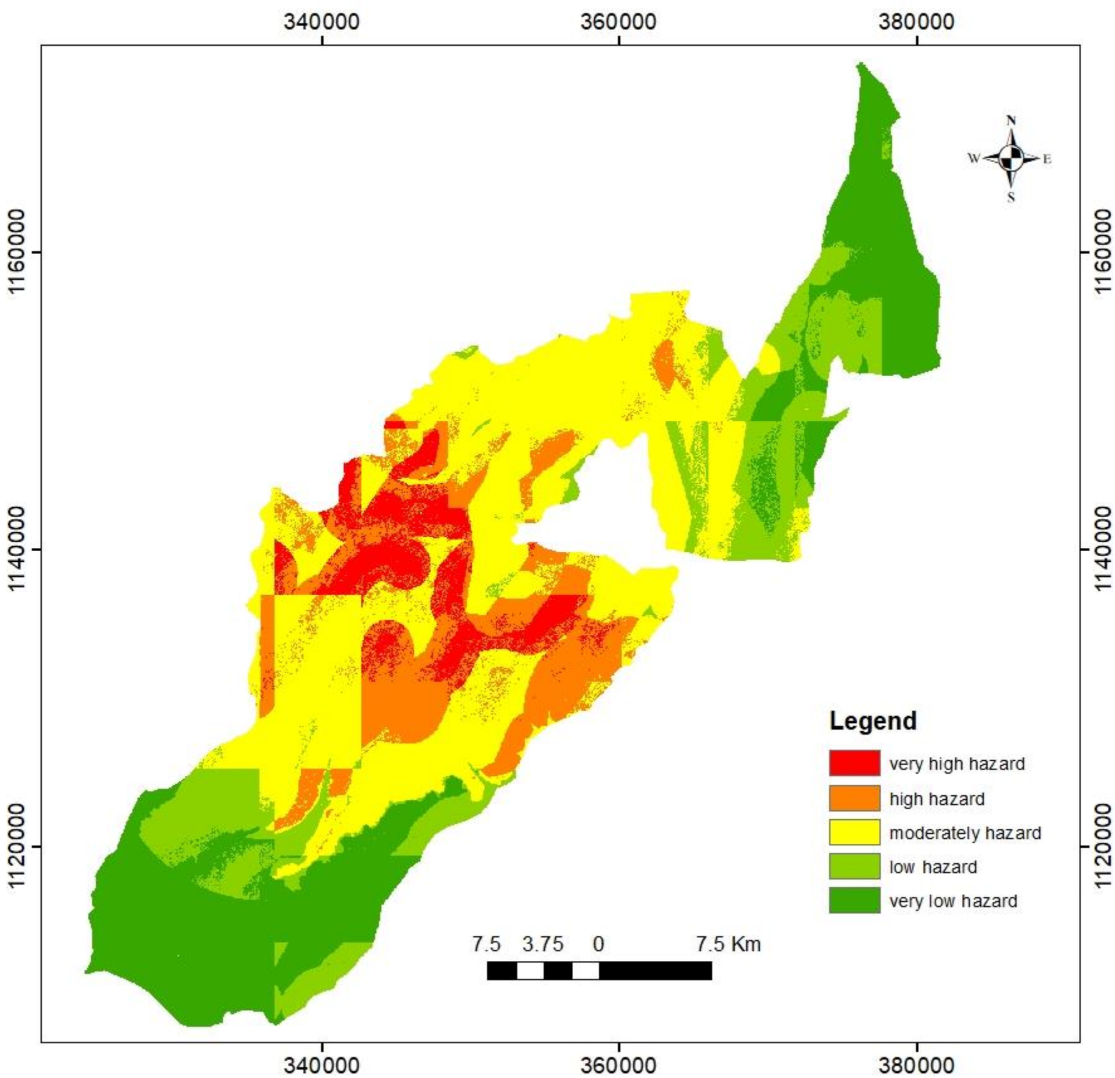

Figure4.2: Landslide hazard zones of the study area

4.4. Validation

The validation samples of landslide pixels were overlaid on the landslide hazard zonation map to know how much the landslide hazard zonation was correct. These establish that among the total of previously identified 58 landslides 17(29.31%) of landslide lies under a very highly susceptible region followed by 29(50%) in high, 12(20.69%) of the landslides were in moderate, and there were no landslides that occurred in previous low and very low hazard zones.

4.5. Vulnerability and Risk Mapping

4.5.1. Mapping Landslide Vulnerability

To enable a landslide event in a GIS setting, the weighted linear combination (WLC) approach, which involves many parameters, is utilized to determine the relative importance and degree of influence of the specified parameters (Mahini and Gholamalifard 2006; Ladas et al., 2007). According to Ladas et al., 2007 there is no standard number of parameters or type of parameter to choose from when using the WLC approach; instead, it is dependent on expert and local knowledge. According to the classes bearing on landslides, each parameter was classified into classes and assigned ratings ranging from very low to very high, 1 (very low) to 5 (very high). Each parameter is given weight against the other parameters, with a total weight of 14 distributed among the ten parameters. To generate vulnerability output maps, the classes within each parameter are multiplied by the weight and added using the spatial analysis tool. The result showed that 4.64% of the area is very high vulnerable, 16.26% is highly vulnerable, 41.87% is moderately vulnerable, 15.02% is low vulnerable, and 22.21% is very low vulnerable (Figure 4.3).

Table4.12: Classed table with assigned ranks and weights

Parameters	Class	Rank	Weight	Comments
	859-1458	1		The ranks are given by their LD in the study
	1458-1940	3		
Elevation	1940-2336	5	1	
	2336-2807	4		
	2807-3809	2		
	0-5.575	1		Here the rank increased through increasing the slope angle
	5.576-11.769	2		
Slope	11.77-21.061	3	3	

	21.062-34.998	5		
	34.999-78.976	4		
Aspect	Flat	1	1	The ranking is by their LD
	North	5		
	Northeast	4		
	East	2		
	Southeast	2		
	South	1		
	Southwest	4		
	West	4		
	Northwest	5		
	North	5		
Lithology	Mesozoic	1	1	The ranking is by their LD
	Paleozoic	1		
	Quaternary	3		
	Tertiary	4		
Distance from road	0-2,870	5	1	The ranking is by their LD
	2,871-6,313	4		
	6,314-10,412	3		
	10,413-14,758	2		
	14,759-20,907	1		
	0-763	5		The ranking is by their

Distance from River	764-1,692	4	2	LD
	1,693-2,854	3		
	2,855-4,712	2		
	4,713-8,461	1		
Land Use Land Cover	Agriculture	4	1	The ranking is by their LD
	Grazing Land	4		
	Settlement	5		
	Forest	2		
	Water Body	1		
Rainfall	1,040-1,123	1	2	The ranking is by their value
	1,124-1,221	2		
	1,222-1,288	3		
	1,289-1,322	4		
	1,323-1,492	5		
Soil	Humic Nitisols	4	1	
	Rendzic Leptosols	3		
	Chromic Luvisols	2		
	Eutric Vertisols	1		
NDVI	-0.267-0.167	5	1	The ranking is by their LD
	0.167-0.247	4		
	0.247-0.344	3		
	0.344-0.466	2		
	0.466-0.807	1		

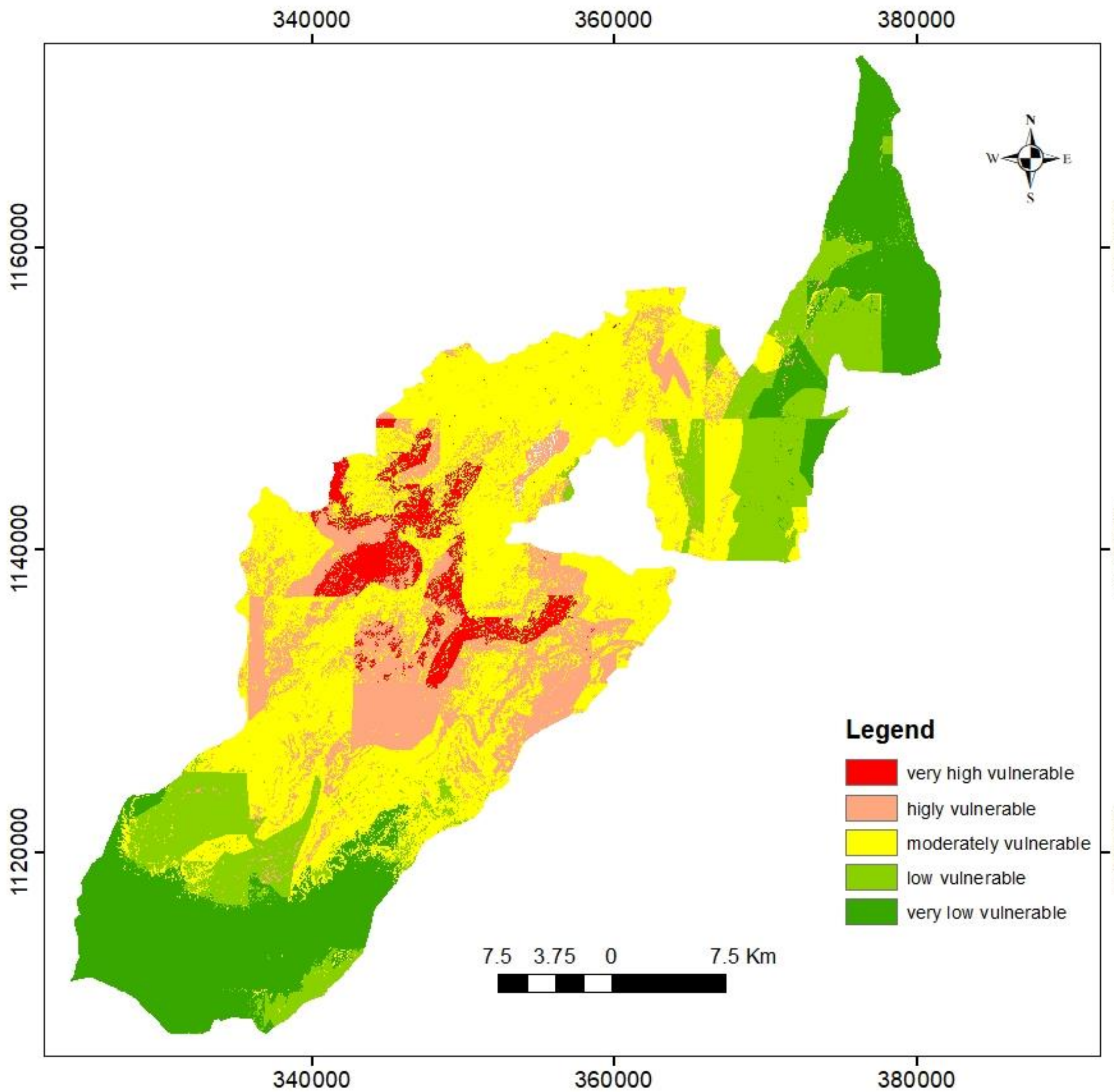

Figure4.3: Landslide vulnerability

4.5.2. Mapping Risk of Landslide

Risk assessment refers to an estimation of the extent of damage likely to result if the landslide occurs. Damage can occur on the same slope aspect where the hazard is present, or it can spread to adjacent facets. Since risk is a function of hazard probability and damage potential, the damage potential area should be mapped first.

The risk map was prepared by the product of hazard and vulnerability so it also uses 10 causative factors of landslide and the result is grouped into five from very low to very high-risk zones.

According to the result, the very high-risk zone covers 6.33%, high-risk covers 8.44%, moderately risk covers 22.02%, low-risk covers 17.17%, and very low-risk zone cover 46.04% of the area under the study.

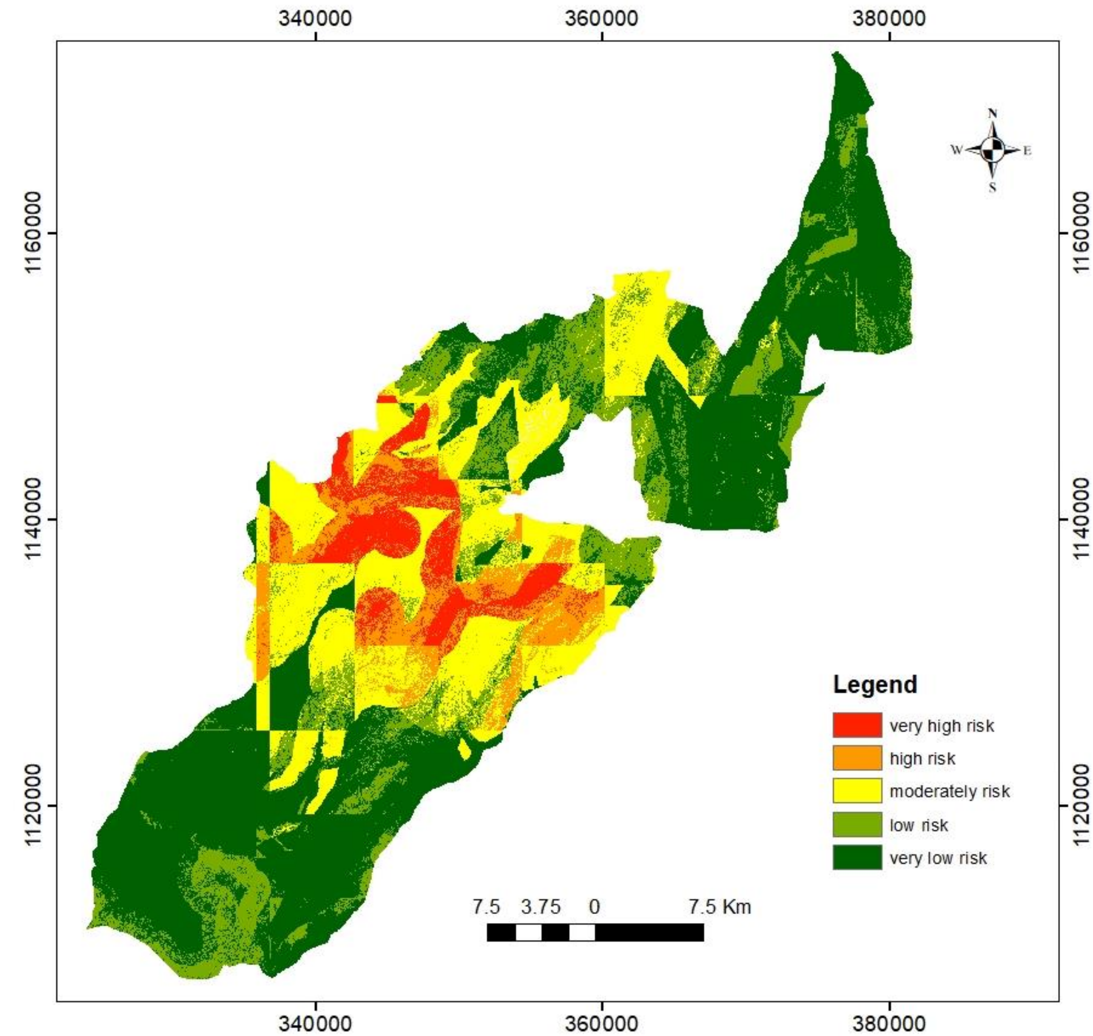

Figure4.4: Landslide risk map

4.6. Slope Instability Assessment

4.6.1 Displacement Map and Time Series Analysis

This study utilized the time series of InSAR data from sentinel 1A SLC images for the period between 2017 and 2020. The mean deformation velocity of PS-InSAR was utilized to assess landslide deformations in Gozamin district. These techniques can be used to notice displacement in the study area, particularly in areas with very high hazards and high hazard zones in the landslide hazard zonation map. PS-InSAR techniques were used to do time series analysis. PSInSAR processing of 12 single master interferograms revealed that the Dispersion Amplitude index value identified a total of 688, 998 PS candidates. The displacement in the study area ranges from 16.9 mm/yr to -12.2 mm/yr, as seen in the graph (Figure 4.5). The surface displacement in the satellite's line of sight (LOS) is measured by the displacement phase calculated from interferograms.

The findings of this study are expressed in terms of vertical displacement, which is defined as the vertical projection of LOS displacement onto the vertical axis. The negative sign implies that the land surface is continuously moving away from the satellite LOS, while the positive sign shows that the area is continuously moving toward LOS.

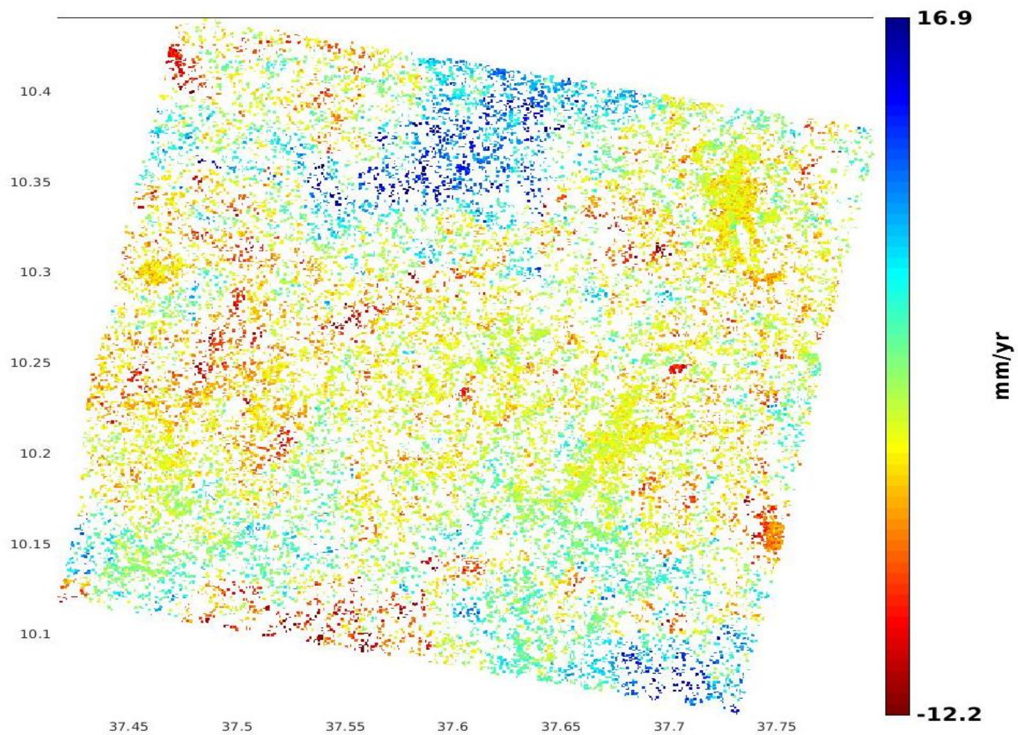

Figure 4.5: Mean line of site displacement

Four sites were chosen and their time series were presented to better demonstrate the time evolution of surface displacement (Figure 4.7). These points are found in the sliding surface's eastern, southern, and central parts of the research area. These locations were chosen using the landslide inventory map. The dynamics of the observed movement vary depending on whatever section of the landslide region you're looking at. The area affected by the Gozamin landslide grew over the four-year study. To study the displacement rates, we plotted the time series in Figure 4.7. The stack of images averaging the time series for all the distant scatterers in the places where line of sight displacements appear to be typical for landslide slope.

The purpose of this research is to determine whether or not the process of surface displacement in the area is still ongoing. Furthermore, in all points of the time series analysis, the direction of movement is opposite to the line of sight.

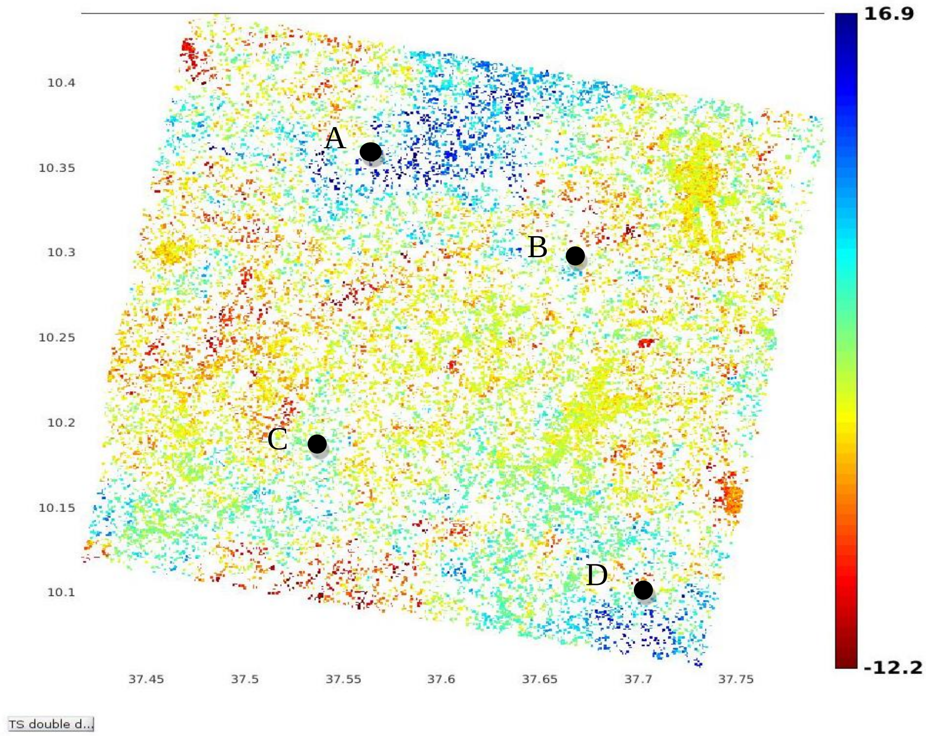

Figure 4.6: Distribution of selected PS points A-D

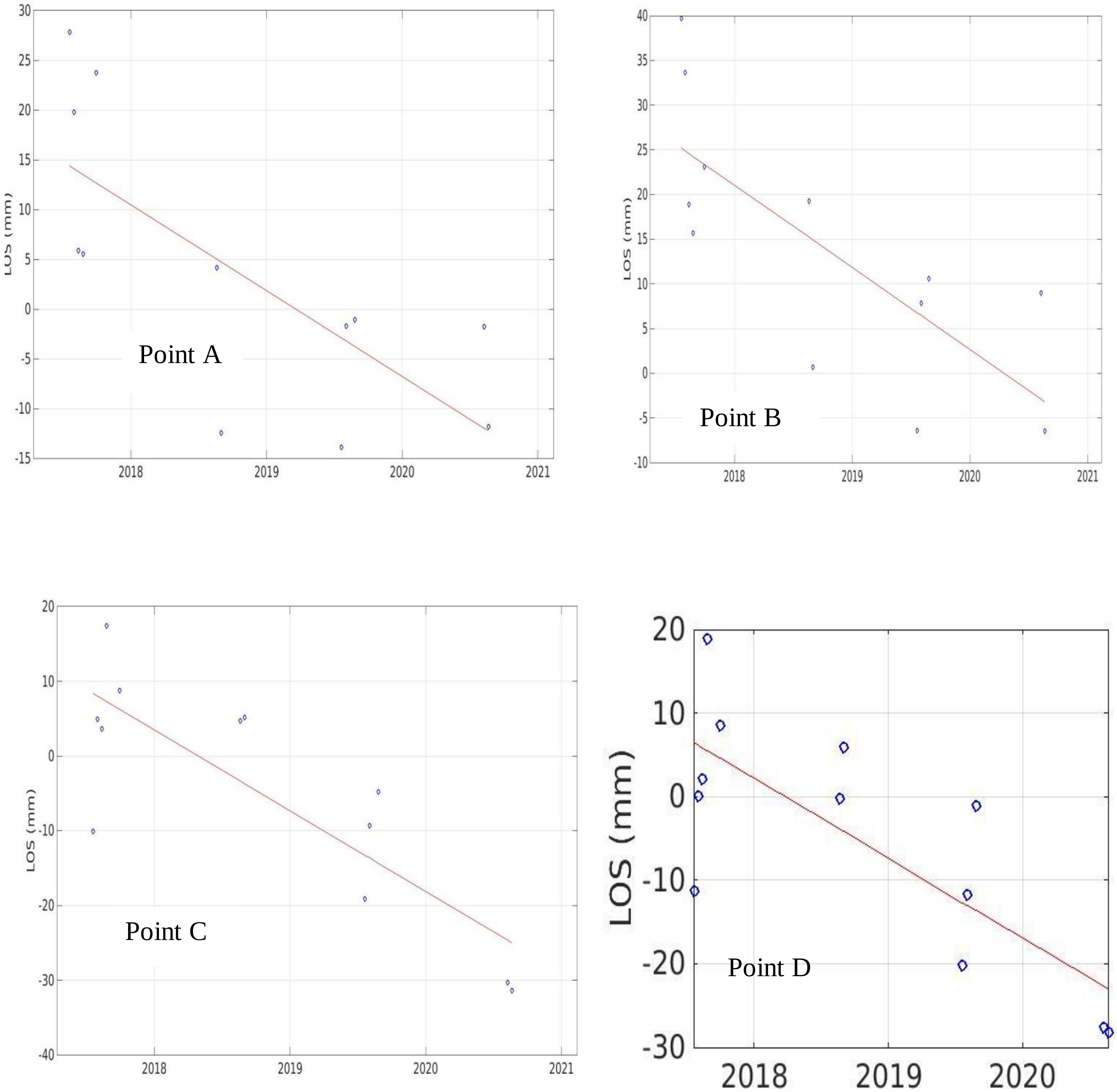

Figure 4.7: LOS displacement time series of the selected points (A, B, C, D)

To trace the deformation pattern of a single point, information like that shown in Figure (4.7) can be derived. Figure (4.8), on the other hand, depicts the standard deviation of mean LOS displacement. Because the displacement rates in multiple interferograms were low or almost identical, the standard deviation was minimal. Due to differences in the displacement rate in different interferograms, the other locations had a standard deviation of 9.7mm/yr.

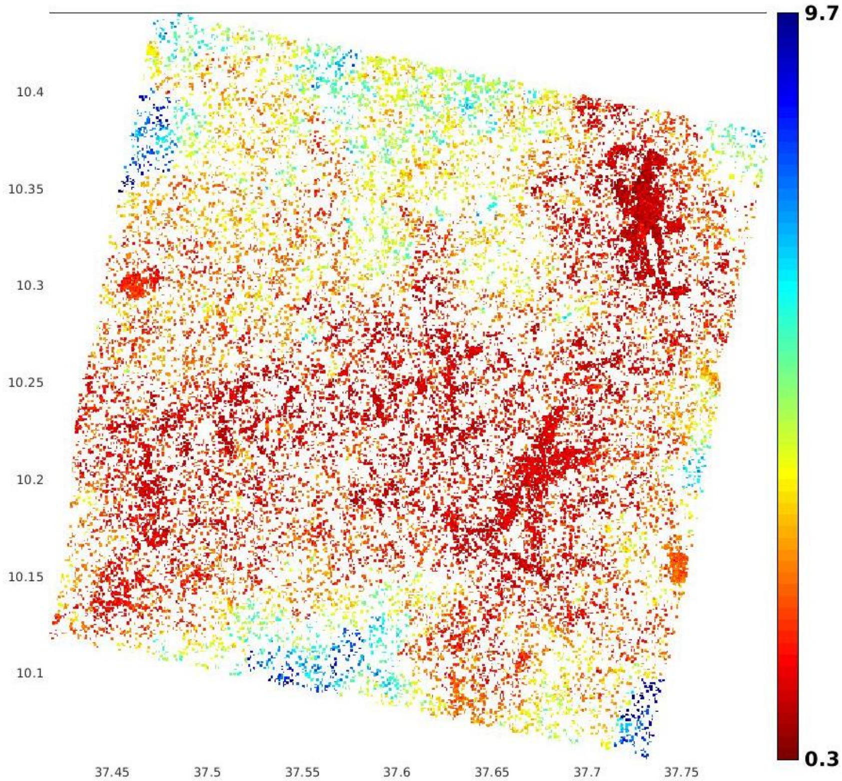

Figure 4.8: Standard deviation of mean LOS displacement

4.6.2 Stamps Visualizer

The output extracted in MATLAB when processing persistent scatterer is difficult to interpret, and specific time series can rarely be linked to a PS pixel. Stamps-Visualizer is a program that is used to solve this problem. The reliability of the interpretation of interferometric data can be increased by an appropriated 3D-visualization of the data. The result from StaMPS analysis consists on discrete ground measurement points, each of which has a temporal displacement. Data can be presented as single points on a background map or as interpolated points creating, for instance, a 3D perspective visualization of the deformation surfaces. The program is designed to improve the investigation and display of data, allowing the user to browse and compare PS pixels and time series straightforwardly. In this study the high and very high hazard zone was extracted and processed using Mat lab. The objects formed in MATLAB during StaMPS/MTI processing are tallied first to achieve this. The table's several columns contain information about each PS pixel's coordinates, deformation, and mean velocity. These are then saved as a.csv file and imported into the StaMPS-Visualizer shiny app (Höser, 2018).

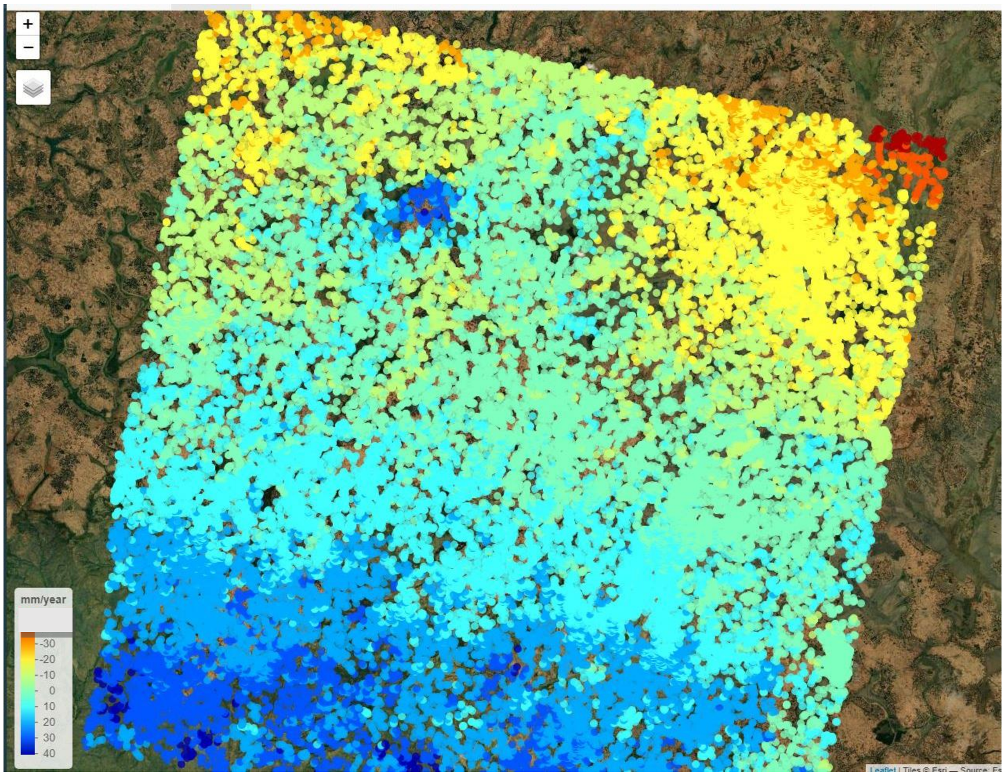

Figure 4.9: Stamps visualization showing landslide distribution

4.7. Discussion

Landslides are the most common and destructive of the different natural hazards. It destroys property with hundreds of billions of dollars each year, ruins transportation networks, buildings and structures, public works projects, and agricultural areas, and kills and injures thousands of people each year (Chimindi et al., 2017; Hamza and Raghuvanshi, 2017; Raghuvanshi et al., 2015). The investigation of the mix of causal elements that have led to previous landslides and the possibility of them occurring again in the region of interest is the primary assumption that is accompanied by most landslide studies, particularly those that employ quantitative methodologies (Shano et al., 2020). One of the quantitative methods information value method for landslide hazard zonation map was used in this study by combining the landslide inventory map with rainfall, slope, elevation, NDVI, land use land cover, lithology type, soil type, proximity to the road, aspect, and proximity to rivers (streams) as conditioning factors, the vulnerability map was created using the weighted linear combination (WLC) approach, the risk map was created by combining the vulnerability and hazard maps, and the surface displacement map caused by landslides were analyzed using time series PS-InSAR method.

The fundamental cause of slope instability is the slope angle, which is considered a significant element ((Totschnig et al., 2011; Raghuvanshi et al., 2015). Landslides are always triggered by the breakdown of slope stability (Guzzetti et al., 1999). The steepness of the slope is the most important terrain-related risk factor impacting slope stability. An increase in slope increased the landslide area and volume. But landslides mostly occur in the range of 15 º - 30º (Chen & Lee, 2003). According to the present data, the majority of historical landslides occurred in the slope class 21º - 35º with tertiary lithology. It is almost the same as the other researches. The mean of landslide area and mean of landslide volume on the northwest aspect was significantly more than that on other aspects. Landslides are most common in rainy seasons in hilly tropical climates, when soil saturation increases, resulting in a loss in cohesiveness and increased pore pressure (Hosseini et al., 2011) similar to the result in this paper landslides in the study area usually occur during the rainy seasons. The major triggering factors for the breakdown of slope stability in the Gozamin area are intense rainstorms that cause over-saturation of the slope materials as well as human impact which causes changes and modifications that influence natural processes such as agricultural activities across the high slope.

The research area's landslide hazard map is divided into five classification schemes: very low, low, moderate, high, and very high susceptibility. The accuracy of the final map was confirmed by overlaying the hazard map over the landslide inventory map (Oh et al., 2009). In this study, the areas with high and very high susceptibility classes are found on steep slopes with humic nitisol soil types, closer to streams, and agricultural and grazing land on a steep slope, while highland landscapes have a moderate susceptibility class. Low to extremely low susceptibility was discovered in low plain landscapes the same result as of conducted by (Oh et al., 2009). The majority of the study area (78.7%) falls between moderate, low, and very low hazard zones, according to the landslide hazard zonation map created during the current study. The research area's southern and northern regions are characterized by zones with very low hazards (24.97 percent). The Low Hazard zone, which represents 15.53 percent of the study area, is concentrated in the east and south, with a dispersed distribution in the northeast, center, and north. Furthermore, a very high hazard zone dominates the western and central regions of the research area, accounting for 6.61 percent of the total area. High hazard and moderate hazard zones cover 14.69 percent and 38.20 percent of the region, respectively, distributed in the central, western, and eastern parts of the area.

According to a study conducted by (Filagot et al., 2018) elevation has a significant impact on the occurrence of landslides. According to the findings of this study, historical landslides in the area were more prevalent in the elevation class 1940-2336m. A key explanation for the domination of landslides in this elevation range, aside from the influence of other causative factors, is that much of the slopes in this elevation range are occupied by agricultural land. The current study's findings also revealed that agricultural land has the largest number of historical landslides in the area. Displacements occur when the bodies of shallow landslides suffer abrupt changes in the pore pressure regime, which is chiefly triggered by heavy rainfall in combination with the high slope cut during anthropogenic activities like plowing and digging for agricultural activities as indicated in the study conducted by (Kirche *et al*., 2000). The massive landslide in the study area is a result of unplanned slope cuttings during anthropogenic activities like plowing and digging for agricultural activities. Agricultural works and water saturation leads to an increase in slope instability. The result of PS-InSAR analysis shows the presence of displacement ranging from +16.9 mm/yr. to -12.2 mm/yr. The PS-InSAR results showed that the process of surface displacement in the area is still active. The area is highly populated, thus the landslides pose a major threat to human life and animals, especially Aba Libanos and Dess Anessie villages are partly surrounded by potentially dangerous landslides, which can affect the infrastructure, agricultural land and may cause primarily material damage. The current instability of the Gozamin landslide might result from a combination of slope, agricultural works, precipitation rate, and high elevation difference. Thus, the PS-InSAR and GIS-based methodology for the integration of various topographic, geological, structural, land-use/land-cover, and other datasets is quite suitable for developing a landslide hazard zonation map and slope instability assessment.

Chapter Five
Conclusion and Recommendation

5.1. Conclusion

Landslides are natural phenomena that are often difficult to predict; in this study, the information value method was used for landslide hazard assessment. Pixel-based information value model was found useful in handling variables of all causative factor maps using the same pixel size, calculating quantitative information values for all variables to obtain hazard classes, and performing matrix and overlay analysis for combining information values for all variables to obtain final landslide hazard map. In the study, landslide hazard mapping was obtained using the combination of spatial distribution maps of ten (10) different causative factors with a landslide inventory map. This study classified the landslide into very low(24.97%), low(15.53%), moderate(38.20%), high(14.69%) and very high(6.61%)hazard zones.

The change in water levels due to heavy rainfall in the main river and trunk streams might decrease the stability of slopes which resulted in a higher number of landslides near water bodies. The current sliding movements generally occur in the years of usually high rainfall. The agricultural activities of lands at steep slopes increase the occurrences of landslides. Rainfall intensity, slope, distances from the main river (streams) & road, and elevation were identified to be the causal elements with the greatest effect on landslide occurrence in this study. In this study, landslides occur more frequently in barren and sparsely vegetated areas (agricultural and grazing land) than in heavily and moderately planted areas.

In the study, landslide vulnerability was mapped using the weighted linear combination method, and risk was mapped by the product of hazard and vulnerability with five classes from very low to very high. Finally, the surface displacement map due to landslide was mapped using persistent scatterer interferometry (PS-INSAR) and it shows +16.9 mm/yr to -12.2 mm/yr. The results showed that the process of surface displacement in the area is still active. The area is highly populated, thus the landslides pose a major threat to human life and animals, especially Aba Libanos and Dess Anessie villages are partly surrounded by potentially dangerous landslides, which can affect the infrastructure, agricultural land and may cause primarily material damage.

5.2. Recommendation

- Landslides in the study area destruct houses and agricultural areas of the living community so the governmental organizations should provide preventive methods for future land utilization.
- Future researchers should work on social vulnerability, physical vulnerability, and economic vulnerability by using social, physical, and economic aspects.
- A risk management program can be planned to avoid a possible risk to the human population, land, and properties including engineering structures.
- The high and very high-risk areas are given top priority for remedial/control measures. Immediate short-term measures such as grading of slopes, proper drainage, as well as long-term measures such as adequate drainage (rerouting springs and rainwater) out of the slopes.
- Future researchers should work the displacement map by using differential GPS to do it more accurately.

References

(ADPC), A. D. P. C. (2000). *CONCEPTS OF HAZARDS, DISASTERS AND HAZARD ASSESSMENT* (pp. 1–14).

Abebe, B., Dramis, F., Fubelli, G., Umer, M., & Asrat, A. (2010). Landslides in the Ethiopian highlands and the Rift margins. *Journal of African Earth Sciences*, *56*(4–5), 131–138. https://doi.org/10.1016/j.jafrearsci.2009.06.006

Akbar, T. A., & Ha, S. R. (2011). Landslide hazard zoning along Himalayan Kaghan Valley of Pakistan-by integration of GPS, GIS, and remote sensing technology. *Landslides*, *8*(4), 527–540. https://doi.org/10.1007/s10346-011-0260-1

Aleotti, P., & Chowdhury, R. (1999). Landslide hazard assessment: Summary review and new perspectives. *Bulletin of Engineering Geology and the Environment*, *58*(1), 21–44. https://doi.org/10.1007/s100640050066

Anbalagan, R., & Singh, B. (1996). Landslide hazard and risk assessment mapping of mountainous terrains - A case study from Kumaun Himalaya, India. *Engineering Geology*, *43*(4), 237–246. https://doi.org/10.1016/S0013-7952(96)00033-6

Arnous, M. O. (2011). Integrated remote sensing and GIS techniques for landslide hazard zonation: A case study Wadi Watier area, South Sinai, Egypt. *Journal of Coastal Conservation*, *15*(4), 477–497. https://doi.org/10.1007/s11852-010-0137-9

Arroyo, M. (2020). *The use of InSAR in landslide Monitoring Josep Raventós *, Marcos Arroyo †. May 2017*.

Ayalew, L. (1999). The effect of seasonal rainfall on landslides in the highlands of Ethiopia. *Bulletin of Engineering Geology and the Environment*, *58*(1), 9–19. https://doi.org/10.1007/s100640050065

Ayalew, Lulseged, & Yamagishi, H. (2004). Slope failures in the Blue Nile basin, as seen from landscape evolution perspective. *Geomorphology*, *57*(1–2), 95–116. https://doi.org/10.1016/S0169-555X(03)00085-0

Ayenew, T., & Barbieri, G. (2005). *Inventory of landslides and susceptibility mapping in the Dessie area , northern Ethiopia*. *77*, 1–15. https://doi.org/10.1016/j.enggeo.2004.07.002

Baum, R. L., Coe, J. A., Godt, J. W., Harp, E. L., Reid, M. E., Savage, W. Z., Schulz, W. H., Brien, D. L., Chleborad, A. F., McKenna, J. P., & Michael, J. A. (2005). Regional landslide-hazard assessment for Seattle, Washington, USA. *Landslides*, *2*(4), 266–279. https://doi.org/10.1007/s10346-005-0023-y

Berardino, P., Fornaro, G., Lanari, R., & Sansosti, E. (2002). A new algorithm for surface deformation monitoring based on small baseline differential SAR interferograms. *IEEE Transactions on Geoscience and Remote Sensing*, *40*(11), 2375–2383. https://doi.org/10.1109/TGRS.2002.803792

Berhanu Temesgen, Mohammed Umer, Asfawossen Asrat, Ogbaghebriel Berakhi, Abayneh Ayele, dramis francesco and M. D. (1999). *SINET*. 127–140.

Blahut, J., van Westen, C. J., & Sterlacchini, S. (2010). Analysis of landslide inventories for accurate prediction of debris-flow source areas. *Geomorphology*, *119*(1–2), 36–51. https://doi.org/10.1016/j.geomorph.2010.02.017

Bolstad, P. V., & Lillesand, T. M. (1991). Rapid maximum likelihood classification. *Photogrammetric*

Engineering & Remote Sensing, *57*(1), 67–74.

Bourenane, H., Bouhadad, Y., Guettouche, M. S., & Braham, M. (2015). GIS-based landslide susceptibility zonation using bivariate statistical and expert approaches in the city of Constantine (Northeast Algeria). *Bulletin of Engineering Geology and the Environment*, *74*(2), 337–355. https://doi.org/10.1007/s10064-014-0616-6

Buckle, P., Mars, G., & Smale, R. S. (2000). New approaches to assessing vulnerability and resilience. *Australian Journal of Emergency Management*, *15*(2), 8–15.

Carrara, A., Cardinali, M., Detti, R., Guzzetti, F., Pasqui, V., & Reichenbach, P. (1991). GIS techniques and statistical models in evaluating landslide hazard. *Earth Surface Processes and Landforms*, *16*(5), 427–445. https://doi.org/10.1002/esp.3290160505

Carrara, A., Guzzetti, F., Cardinali, M., & Reichenbach, P. (1999). Use of GIS technology in the prediction and monitoring of landslide hazard. *Natural Hazards*, *20*(2–3), 117–135. https://doi.org/10.1023/A:1008097111310

Carrara, Alberto. (1983). *Multivariate Models for Landslide Hazard Evaluation I*. *15*(3).

Catani, F., Casagli, N., Ermini, L., Righini, G., & Menduni, G. (2005). Landslide hazard and risk mapping at catchment scale in the Arno River basin. *Landslides*, *2*(4), 329–342. https://doi.org/10.1007/s10346-005-0021-0

Chau, K. T., Sze, Y. L., Fung, M. K., Wong, W. Y., Fong, E. L., & Chan, L. C. P. (2004). *Landslide hazard analysis for Hong Kong using landslide inventory and GIS*. *30*, 429–443. https://doi.org/10.1016/j.cageo.2003.08.013

Chimidi, G., Raghuvanshi, T. K., & Suryabhagavan, K. V. (2017). Landslide hazard evaluation and zonation in and around Gimbi town, western Ethiopia—a GIS-based statistical approach. *Applied Geomatics*, *9*(4), 219–236. https://doi.org/10.1007/s12518-017-0195-x

Clémence, G.-G. (2016). *Vulnerability Assessment and Landslide Risk Analysis . Application to the Instituto de Geografia e Ordenamento do Território Vulnerability Assessment and Landslide Risk Analysis . Application to the Loures Municipality , Portugal Clémence Guillard-Gonçalv*. *January*. https://doi.org/10.13140/RG.2.1.3309.4648

Colesanti, C., Ferretti, A., Prati, C., & Rocca, F. (2003). Monitoring landslides and tectonic motions with the Permanent Scatterers Technique. *Engineering Geology*, *68*(1–2), 3–14. https://doi.org/10.1016/S0013-7952(02)00195-3

Costantini, M., Falco, S., Malvarosa, F., Mammone, C., Minati, F., Trillo, F., Vecchioli, F., & Paglia, L. (2000). *Persistent Scatterer Pair (Psp) Interferometry and Surface Reconstruction Techniques for Urban Dsm From High Resolution*.

Crosetto, M., Monserrat, O., Cuevas-González, M., Devanthéry, N., & Crippa, B. (2016). Persistent Scatterer Interferometry: A review. *ISPRS Journal of Photogrammetry and Remote Sensing*, *115*, 78–89. https://doi.org/10.1016/j.isprsjprs.2015.10.011

Crozier, M. J., & Glade, T. (2012). Landslide Hazard and Risk: Issues, Concepts and Approach. In *Landslide Hazard and Risk*. https://doi.org/10.1002/9780470012659.ch1

Cruden, D. M. (1991). A simple definition of a landslide. *Bulletin of the International Association of Engineering Geology - Bulletin de l'Association Internationale de Géologie de l'Ingénieur*, *43*(1), 27–29. https://doi.org/10.1007/BF02590167

Cruden, D. M., & Varnes, D. . (1996). *Landslide types and Processes*.

Dai, F., & Lee, C. (2001). *Terrain-based mapping of landslide susceptibility using a geographical information system: A case study*. *38*(5), 911–923.

De Zan, F., & Guarnieri, A. M. (2006). TOPSAR: Terrain observation by progressive scans. *IEEE Transactions on Geoscience and Remote Sensing*, *44*(9), 2352–2360. https://doi.org/10.1109/TGRS.2006.873853

Devanthéry, N., Crosetto, M., Monserrat, O., Cuevas-González, M., & Crippa, B. (2018). Deformation Monitoring Using Sentinel-1 SAR Data. *Proceedings*, *2*(7), 344. https://doi.org/10.3390/ecrs-2-05157

Dietz and Kruse. (1996). *AN APPROACH TOWARDS DETERMINISTIC LANDSLIDE HAZARD ANALYSIS IN GIs . A CASE STUDY FROM MANIZALES*. *21*, 853–868.

Dikshit, A., Sarkar, R., Pradhan, B., Acharya, S., & Alamri, A. M. (2020). Spatial landslide risk assessment at Phuentsholing, Bhutan. *Geosciences (Switzerland)*, *10*(4), 1–16. https://doi.org/10.3390/geosciences10040131

Eidsvig, U. M. K., McLean, A., Vangelsten, B. V., Kalsnes, B., Ciurean, R. L., Argyroudis, S., Winter, M. G., Mavrouli, O. C., Fotopoulou, S., Pitilakis, K., Baills, A., Malet, J. P., & Kaiser, G. (2014). Assessment of socioeconomic vulnerability to landslides using an indicator-based approach: Methodology and case studies. *Bulletin of Engineering Geology and the Environment*, *73*(2), 307–324. https://doi.org/10.1007/s10064-014-0571-2

Ercanoglu, M., Gokceoglu, C., & Van Asch, T. W. J. (2004). Landslide susceptibility zoning north of Yenice (NW Turkey) by multivariate statistical techniques. *Natural Hazards*, *32*(1), 1–23. https://doi.org/10.1023/B:NHAZ.0000026786.85589.4a

Esa. (2010). *INTERFEROMETRIC SYNTHETIC APERTURE RADAR An Introduction for Users of InSAR Data*.

Ethiopia Central Statistical Agency. (2013). *Federal Demographic Republic of Population Projection of Ethiopia from 2014 – 2017*. *August 2013*, 1–118.

Fall, M., Azzam, R., & Noubactep, C. (2006). *A multi-method approach to study the stability of natural slopes and landslide susceptibility mapping*. *82*, 241–263. https://doi.org/10.1016/j.enggeo.2005.11.007

Fell, R., Corominas, J., Bonnard, C., Cascini, L., Leroi, E., & Savage, W. Z. (2008). Guidelines for landslide susceptibility, hazard and risk zoning for land use planning. *Engineering Geology*, *102*(3–4), 85–98. https://doi.org/10.1016/j.enggeo.2008.03.022

Ferretti, A., Prati, C., & Rocca, F. (2000). Nonlinear subsidence rate estimation using permanent scatterers in differential SAR interferometry. *IEEE Transactions on Geoscience and Remote Sensing*, *38*(5 I), 2202–2212. https://doi.org/10.1109/36.868878

Ferretti, A., Prati, C., & Rocca, F. (2001). Permanent scatterers in SAR interferometry. *IEEE Transactions on Geoscience and Remote Sensing*, *39*(1), 8–20. https://doi.org/10.1109/36.898661

Filagot, M. (2018). Advisor: Dr. K.V. Suryabhagavan. *Landslide Hazard Zonation and Slope Instability Assessment by Using Optical and InSAR Reote Sensing: The Case of Arbaminch-Gidole Road,Southern Ethiopia*.

Fleming, R. W., & Taylor, F. A. (1980). Estimating the Costs of Landslide Damage in the United States.

Geological Survey Circular (United States), *832*. https://doi.org/10.3133/cir832

Fotopoulou, S. D., & Pitilakis, K. D. (2013). Vulnerability assessment of reinforced concrete buildings subjected to seismically triggered slow-moving earth slides. *Landslides*, *10*(5), 563–582. https://doi.org/10.1007/s10346-012-0345-5

Franco Mantovani, Robert Soeters, C. J. V. W. (1996). Remote Sensing techniques for landslide studies and hazard zonation in Europe. *ELSEVIER*, *15*.

Gabriel, A. K., Goldstein, R. M., & Zebker, H. A. (1989). Mapping small elevation changes over large areas: differential radar interferometry. *Journal of Geophysical Research*, *94*(B7), 9183–9191. https://doi.org/10.1029/JB094iB07p09183

Galli, M., & Guzzetti, F. (2007). Landslide vulnerability criteria: A case study from Umbria, central Italy. *Environmental Management*, *40*(4), 649–664. https://doi.org/10.1007/s00267-006-0325-4

Ganapathy, G. P., & Rajawat, A. S. (2015). Use of hazard and vulnerability maps for landslide planning scenarios: a case study of the Nilgiris, India. *Natural Hazards*, *77*(1), 305–316. https://doi.org/10.1007/s11069-015-1587-z

Gashe, A and Kassa, A. (2017). Feed Resources Gozamen District, East Gojjam Zone, Amhara Region. *Journal of Environmental & Analytical Toxicology*, *07*(02). https://doi.org/10.4172/2161-0525.1000437

Gheorghe, M., & Armaş, I. (2016). Comparison of Multi-Temporal Differential Interferometry Techniques Applied to the Measurement of Bucharest City Subsidence. *Procedia Environmental Sciences*, *32*, 221–229. https://doi.org/10.1016/j.proenv.2016.03.027

Glade, T. (2003). Vulnerability assessment in landslide risk analysis. *Erde*, *134*(2), 123–146.

Gupta, R. ., & Josh, B. . (1990). *Landslide Hazard Zoning Using the GIS Approach A Case Study from the Ramganga Catchment , Himalayas*. *28*, 119–131.

Guzzetti, F., Carrara, A., Cardinali, M., & Reichenbach, P. (1999). Landslide hazard evaluation: A review of current techniques and their application in a multi-scale study, Central Italy. *Geomorphology*, *31*(1–4), 181–216. https://doi.org/10.1016/S0169-555X(99)00078-1

Hailemariam, S. N., Soromessa, T., & Teketay, D. (2016). Land use and land cover change in the bale mountain eco-region of Ethiopia during 1985 to 2015. *Land*, *5*(4). https://doi.org/10.3390/land5040041

Hamza, T., & Raghuvanshi, T. K. (2017). GIS based landslide hazard evaluation and zonation – A case from Jeldu District, Central Ethiopia, GIS based landslide hazard evaluation and zonation. *Journal of King Saud University - Science*, *29*(2), 151–165. https://doi.org/10.1016/j.jksus.2016.05.002

Hanssen, R. F. (2004). Stochastic modeling of time series radar interferometry. *International Geoscience and Remote Sensing Symposium (IGARSS)*, *4*(C), 2607–2610. https://doi.org/10.1109/igarss.2004.1369832

Hewison, D., & Kuras, M. (2005). Book reviews: Book reviews. *Journal of Analytical Psychology*, *50*(3), 395–403. https://doi.org/10.1111/j.0021-8774.2005.00541.x

Highland, L. M., & Bobrowsky, P. (2008). *The Landslide Handbook — A Guide to Understanding Landslides*. U.S. Geological Survey Circular 1325,.

Hooper, A., Segall, P., & Zebker, H. (2007). Persistent scatterer interferometric synthetic aperture radar for crustal deformation analysis, with application to Volcán Alcedo, Galápagos. *Journal of*

Geophysical Research: Solid Earth, *112*(7). https://doi.org/10.1029/2006JB004763

Höser, T. (2018). Analysing the Capabilities and Limitations of InSAR using Sentinel-1 data for Landslide Detection and Monitoring. *University of Bonn*, *July*, 104.

Hosseini, S. A., Lotfi, R., Lotfalian, M., Kavian, A., & Aidin, P. (2011). The effect of terrain factors on landslide features along forest road. *African Journal of Biotechnology*, *10*(64), 14108–14115. https://doi.org/10.5897/ajb11.856

Irigaray, C., & Hamdouni, R. El. (2006). *Engineering geology maps : Landslides and geographical information systems Engineering geology maps : landslides and geographical information systems*. *May 2014*. https://doi.org/10.1007/s10064-006-0064-z

Jensen, J R. Introductory digital image processing: A remote sensing perspective. United States.

Kanungo, D. ., Arora, M. ., Sarkar, S., & Gupta, R. . (2006). A comparative study of conventional, ANN black box, fuzzy and combined neural and fuzzy weighting procedures for landslide susceptibility zonation in Darjeeling Himalayas. *Engineering Geology*, *85*, 347–366.

Lan, H. X., Zhou, C. H., Wang, L. J., Zhang, H. Y., & Li, R. H. (2004). Landslide hazard spatial analysis and prediction using GIS in the Xiaojiang watershed, Yunnan, China. *Engineering Geology*, *76*(1–2), 109–128. https://doi.org/10.1016/j.enggeo.2004.06.009

Lanari, R., Mora, O., Manunta, M., Mallorquí, J. J., Berardino, P., & Sansosti, E. (2004). A small-baseline approach for investigating deformations on full-resolution differential SAR interferograms. *IEEE Transactions on Geoscience and Remote Sensing*, *42*(7), 1377–1386. https://doi.org/10.1109/TGRS.2004.828196

Lee, S. (2005). Application of logistic regression model and its validation for landslide susceptibility mapping using GIS and remote sensing data. *International Journal of Remote Sensing*, *26*(7), 1477–1491. https://doi.org/10.1080/01431160412331331012

Lee, S. and, & Min, K. (2001). *Statistical analysis of landslide susceptibility at Yongin , Korea*. 1095–1113.

Lee, S., & Pradhan, B. (2006). Probabilistic landslide hazards and risk mapping on Penang Island, Malaysia. *Journal of Earth System Science*, *115*(6), 661–672. https://doi.org/10.1007/s12040-006-0004-0

Lee, S., & Pradhan, B. (2007). Landslide hazard mapping at Selangor, Malaysia using frequency ratio and logistic regression models. *Landslides*, *4*(1), 33–41. https://doi.org/10.1007/s10346-006-0047-y

Li, Z., Nadim, F., Huang, H., Uzielli, M., & Lacasse, S. (2010). Quantitative vulnerability estimation for scenario-based landslide hazards. *Landslides*, *7*(2), 125–134. https://doi.org/10.1007/s10346-009-0190-3

Lillesand, T. M., Kiefer, R. W., & Chipman, J. W. (2004). *Remote Sensing and Image Interpretation* (Fifth Edit). John Wiley & Sons, Inc.

Lu, D., & Weng, Q. (2007). A survey of image classification methods and techniques for improving classification performance. *International Journal of Remote Sensing*, *28*(5), 823–870. https://doi.org/10.1080/01431160600746456

Mandanici, E., & Bitelli, G. (2016). Preliminary comparison of sentinel-2 and landsat 8 imagery for a combined use. *Remote Sensing*, *8*(12). https://doi.org/10.3390/rs8121014

Marangoz, A. M., Sekertekin, A., & Akçin, H. (2017). Analysis of land use land cover classification results derived from sentinel-2 image. *International Multidisciplinary Scientific GeoConference Surveying Geology and Mining Ecology Management, SGEM*, *17*(23), 25–32. https://doi.org/10.5593/sgem2017/23/S10.004

Martha, T. R., & Vinod Kumar, K. (2013). September, 2012 landslide events in Okhimath, India-an assessment of landslide consequences using very high resolution satellite data. *Landslides*, *10*(4), 469–479. https://doi.org/10.1007/s10346-013-0420-6

Massonnet, D., & Feigl, K. L. (1998). Radar interferometry and its application to changes in the earth's surface. *Reviews of Geophysics*, *36*(4), 441–500. https://doi.org/10.1029/97RG03139

Mavrouli, O., Giannopoulos, P. G., Carbonell, J. M., & Syrmakezis, C. (2017). Damage analysis of masonry structures subjected to rockfalls. *Landslides*, *14*(3), 891–904. https://doi.org/10.1007/s10346-016-0765-8

Meten, M., PrakashBhandary, N., & Yatabe, R. (2015). Effect of Landslide Factor Combinations on the Prediction Accuracy of Landslide Susceptibility Maps in the Blue Nile Gorge of Central Ethiopia. *Geoenvironmental Disasters*, *2*(1). https://doi.org/10.1186/s40677-015-0016-7

Michael, E. A., & Samanta, S. (2016). Landslide vulnerability mapping (LVM) using weighted linear combination (WLC) model through remote sensing and GIS techniques. *Modeling Earth Systems and Environment*, *2*(2), 1–15. https://doi.org/10.1007/s40808-016-0141-7

Milone, G., & Scepi, G. (2011). A clustering approach for studying ground deformation trends in Campania Region through PS-InSAR^{TM} time series analysis. In *Journal of Applied Sciences* (Vol. 11, Issue 4, pp. 610–620). https://doi.org/10.3923/jas.2011.610.620

Mokadem, S. (2018). *Landslide susceptibility*. *04*, 1865–1867.

Mora, O., Lanari, R., Mallorquí, J. J., Berardino, P., & Sansosti, E. (2002). A new algorithm for monitoring localized deformation phenomena based on small baseline differential SAR interferograms. *International Geoscience and Remote Sensing Symposium (IGARSS)*, *2*(11), 1237–1239. https://doi.org/10.1109/igarss.2002.1025900

Murillo-García, F. G., Rossi, M., Ardizzone, F., Fiorucci, F., & Alcántara-Ayala, I. (2017). Hazard and population vulnerability analysis: a step towards landslide risk assessment. *Journal of Mountain Science*, *14*(7), 1241–1261. https://doi.org/10.1007/s11629-016-4179-9

Nagler, T., Rott, H., Hetzenecker, M., Wuite, J., & Potin, P. (2015). The Sentinel-1 mission: New opportunities for ice sheet observations. *Remote Sensing*, *7*(7), 9371–9389. https://doi.org/10.3390/rs70709371

Nakileza, B. R., & Nedala, S. (2020). Topographic influence on landslides characteristics and implication for risk management in upper Manafwa catchment, Mt Elgon Uganda. *Geoenvironmental Disasters*, *7*(1). https://doi.org/10.1186/s40677-020-00160-0

Nelson, S. A. (2013). *Slope Stability , Triggering Events , Mass Movement Hazards*. 1–17.

Nguyen, H. T. T., Doan, T. M., Tomppo, E., & McRoberts, R. E. (2020). Land Use / Land Cover Mapping Using Multitemporal Sentinel-2 Imagery and Four Classification. *Remote Sens*, *12*, 1–27. www.mdpi.com/journal/remotesensing

Notti, D., Calò, F., Cigna, F., Manunta, M., Herrera, G., Berti, M., Meisina, C., Tapete, D., & Zucca, F. (2015). A User-Oriented Methodology for DInSAR Time Series Analysis and Interpretation: Landslides and Subsidence Case Studies. *Pure and Applied Geophysics*, *172*(11), 3081–3105. https://doi.org/10.1007/s00024-015-1071-4

Papathoma-Köhle, M., Kappes, M., Keiler, M., & Glade, T. (2011). Physical vulnerability assessment for alpine hazards: State of the art and future needs. In *Natural Hazards* (Vol. 58, Issue 2). https://doi.org/10.1007/s11069-010-9632-4

Pathak, R. U., Srinivasan, A., & Mishra, R. K. (2014). Genome-wide mapping of matrix attachment regions in Drosophila melanogaster. *BMC Genomics*, *15*(1), 1–10. https://doi.org/10.1186/1471-2164-15-1022

Pradhan, B. (2013). A comparative study on the predictive ability of the decision tree, support vector machine and neuro-fuzzy models in landslide susceptibility mapping using GIS. *Computers and Geosciences*, *51*(January 2012), 350–365. https://doi.org/10.1016/j.cageo.2012.08.023

Psomiadis, E., Papazachariou, A., Soulis, K. X., Alexiou, D. S., & Charalampopoulos, I. (2020). Landslide mapping and susceptibility assessment using geospatial analysis and earth observation data. *Land*, *9*(5). https://doi.org/10.3390/LAND9050133

Raghuvanshi, T. K., Ibrahim, J., & Ayalew, D. (2014). Slope stability susceptibility evaluation parameter (SSEP) rating scheme - An approach for landslide hazard zonation. *Journal of African Earth Sciences*, *99*(PA2), 595–612. https://doi.org/10.1016/j.jafrearsci.2014.05.004

Raghuvanshi, T. K., Negassa, L., & Kala, P. M. (2015). GIS based Grid overlay method versus modeling approach - A comparative study for landslide hazard zonation (LHZ) in Meta Robi District of West Showa Zone in Ethiopia. *Egyptian Journal of Remote Sensing and Space Science*, *18*(2), 235–250. https://doi.org/10.1016/j.ejrs.2015.08.001

Ramakrishnan, D., Singh, T. N., Verma, A. K., Gulati, A., & Tiwari, K. C. (2013). Soft computing and GIS for landslide susceptibility assessment in Tawaghat area, Kumaon Himalaya, India. *Natural Hazards*, *65*(1), 315–330. https://doi.org/10.1007/s11069-012-0365-4

Remondo, J., Bonachea, J., & Cendrero, A. (2005). A statistical approach to landslide risk modelling at basin scale: From landslide susceptibility to quantitative risk assessment. *Landslides*, *2*(4), 321–328. https://doi.org/10.1007/s10346-005-0016-x

Sarkar, S., Kanungo, D. P., & Mehrotra, G. S. (1995). *Landslide Hazard Zonation : A Case Study in Garhwal Himalaya , India Author (s): S . Sarkar , D . P . Kanungo and G . S . Mehrotra Published by : International Mountain Society Stable URL : https://www.jstor.org/stable/3673806 REFERENCES Linked referenc*. *15*(4), 301–309.

Schuster, R. L., & Highland, L. M. (2001). *Socioeconomic and Environmental Impacts of Landslides in the Western Hemisphere*. *August*.

Shano, L., Raghuvanshi, T. K., & Meten, M. (2020). Landslide susceptibility evaluation and hazard zonation techniques – a review. *Geoenvironmental Disasters*, *7*(1). https://doi.org/10.1186/s40677-020-00152-0

Sharma, L. P., Patel, N., Ghose, M. K., & Debnath, P. (2011). Landslide vulnerability assessment and zonation through ranking of causative parameters based on landslide density-derived statistical indicators. *Geocarto International*, *26*(6), 491–504. https://doi.org/10.1080/10106049.2011.598951

Sheila, N. (2006). *Predictive Modelling of Rainfall Induced Landslides in a Tropical Environment Predictive Modelling of Rainfall Induced Landslides in a Tropical Environment* . Internationa Institute for Geo-Information Science and Earth Observation ENSCHEDE, The Netherlands.

Silva, M., & Pereira, S. (2014). Assessment of physical vulnerability and potential losses of buildings due to shallow slides. *Natural Hazards*, *72*(2), 1029–1050. https://doi.org/10.1007/s11069-014-1052-4

Skilodimou, H. D., Bathrellos, G. D., Koskeridou, E., Soukis, K., & Rozos, D. (2018). Physical and anthropogenic factors related to landslide activity in the northern Peloponnese, Greece. *Land*, *7*(3). https://doi.org/10.3390/land7030085

Soeters, R., & Westen, V. A. N. (1996). Slope instability recognition, analysis and zonation. In *Landslides, investigation and mitigation, Transportation Research Board, National Research Council* (pp. 129–177).

Suman, S. (2014). *SLOPE STABILITY ANALYSIS USING NUMERICAL MODELLING*. NATIONAL INSTITUTE OF TECHNOLOGY ROURKELA.

Süzen, M. L., & Doyuran, V. (2004). Data driven bivariate landslide susceptibility assessment using geographical information systems: A method and application to Asarsuyu catchment, Turkey. *Engineering Geology*, *71*(3–4), 303–321. https://doi.org/10.1016/S0013-7952(03)00143-1

Tehrany, M. S., Lee, M. J., Pradhan, B., Jebur, M. N., & Lee, S. (2014). Flood susceptibility mapping using integrated bivariate and multivariate statistical models. *Environmental Earth Sciences*, *72*(10), 4001–4015. https://doi.org/10.1007/s12665-014-3289-3

Tehrany, M. S., Pradhan, B., & Jebur, M. N. (2014). Flood susceptibility mapping using a novel ensemble weights-of-evidence and support vector machine models in GIS. *Journal of Hydrology*, *512*, 332–343. https://doi.org/10.1016/j.jhydrol.2014.03.008

Totschnig, R., & Fuchs, S. (2013). Mountain torrents: Quantifying vulnerability and assessing uncertainties. *Engineering Geology*, *155*, 31–44. https://doi.org/10.1016/j.enggeo.2012.12.019

Totschnig, R., Sedlacek, W., & Fuchs, S. (2011). A quantitative vulnerability function for fluvial sediment transport. *Natural Hazards*, *58*(2), 681–703. https://doi.org/10.1007/s11069-010-9623-5

Tsegaw, T. (2007). *Assessment of Land use/Land cover Dynamics and Soil Erosion Estimation for Sustainable Management of Land Resources, A Case study in Gozamin Woreda, Amhara Region, North Central Ethiopia. July.*

Tseng, C. M., Lin, C. W., & Hsieh, W. D. (2015). Landslide susceptibility analysis by means of event-based multi-temporal landslide inventories. *Natural Hazards and Earth System Sciences Discussions*, *3*(2), 1137–1173. https://doi.org/10.5194/nhessd-3-1137-2015

van Westen, C. J., Rengers, N., Terlien, M. T. J., & Soeters, R. (1997). *Soeters and van Westen 1997*. *86*, 404–414.

Van Westen, C. J., & Terlien, M. T. J. (1996). An approach towards deterministic landslide hazard analysis in GIS. A case study from Manizales (Colombia). *Earth Surface Processes and Landforms*, *21*(9), 853–868. https://doi.org/10.1002/(SICI)1096-9837(199609)21:9<853::AID-ESP676>3.0.CO;2-C

van Westen, C. J., van Asch, T. W. J., & Soeters, R. (2006). Landslide hazard and risk zonation - Why is it still so difficult? *Bulletin of Engineering Geology and the Environment*, *65*(2), 167–184. https://doi.org/10.1007/s10064-005-0023-0

Varnes, D.J. (1978). *.ANDSLIDES Analysis and Control*.

Varnes, David J. (1984). *Landslide hazard zonation: a review of principles and Practice*. United Nations Educational,Scientific and Cultural Organization 7 place de Fontenoy.

Vision, M. (1993). *Image pre-processing*. 56–57.

Wachal, D. J., & Hudak, P. F. (2000). *Mapping landslide susceptibility in Travis County , Texas , USA*

Author (s): David J . Wachal and Paul F . Hudak Published by : Springer Stable URL : https://www.jstor.org/stable/41147516 REFERENCES Linked references are available on JSTOR for this artic. *51*(3), 245–253.

WHO. (1983). *Guide to meteorological instruments and methods of observation.* (Issue 8).

Woldearegay, K. (2013). Review of the occurrences and influencing factors of landslides in the highlands of Ethiopia: With implications for infrastructural development. *Momona Ethiopian Journal of Science*, *5*(1), 3. https://doi.org/10.4314/mejs.v5i1.85329

Xie, P., Wen, H., Ma, C., Baise, L. G., & Zhang, J. (2018). Application and comparison of logistic regression model and neural network model in earthquake-induced landslides susceptibility mapping at mountainous region, China. *Geomatics, Natural Hazards and Risk*, *9*(1), 501–523. https://doi.org/10.1080/19475705.2018.1451399

Yesilnacar, E., & Topal, T. (2005). Landslide susceptibility mapping: A comparison of logistic regression and neural networks methods in a medium scale study, Hendek region (Turkey). *Engineering Geology*, *79*(3–4), 251–266. https://doi.org/10.1016/j.enggeo.2005.02.002

Yin K.L., and Yan T.Z., 1988. Statistical prediction model for slope instability of metamorphosed rocks. In: Proceedings of 5th Int Symp on Landslides, Lausanne, Switzerland 2:1269-1272.

ZEBKER, HOWARD A. AND GOLDSTEIN, R. M. (1986). h = p sin (cos _ O). *Journal of Geophysical Research*, *91*(B5), 4993–4999. http://adsabs.harvard.edu/abs/1986JGR....91.4993Z%5Cnhttp://doi.wiley.com/10.1029/JB091iB05p04993

Zhang, T., Su, J., Liu, C., Chen, W. H., Liu, H., & Liu, G. (2017). Band selection in sentinel-2 satellite for agriculture applications. *ICAC 2017 - 2017 23rd IEEE International Conference on Automation and Computing: Addressing Global Challenges through Automation and Computing*, *August*. https://doi.org/10.23919/IConAC.2017.8081990

Zimmer, W. (2011). Classification methods. *Passive Acoustic Monitoring of Cetaceans*, 164–197. https://doi.org/10.1017/cbo9780511977107.008

Appendices

Appendix 1

Table 7.1: Points used for land use land cover classification

No.	Easting	North	No.	Easting	North	No.	Easting	North
1	355490	1137168	21	344094	1140479	41	345580	1142297
2	357280	1136890	22	344053	1139690	42	346562	1141426
3	353107	1139546	23	343296	1139454	43	345359	1144778
4	351254	1140283	24	343231	1138559	44	342410	1142610
5	350058	1137017	25	342386	1140425	45	342760	1141559
6	343389	1123054	26	342537	1139974	46	335639	1106193
7	326968	1110768	27	340566	1140379	47	330150	1107715
8	322732	1111649	28	340005	1139951	48	329574	1111312
9	333223	1108210	29	337928	1126620	49	328596	1109192
10	342444	1105486	30	338179	1123546	50	329119	1115859
11	334544	1116526	31	360191	1150815	51	332899	1113164
12	348430	1130133	32	355366	1152475	52	331983	1113996
13	339208	1131280	33	357006	1148741	53	331292	1114353
14	347543	1144987	34	355165	1145777	54	331142	1113660
15	347481	1144751	35	353314	1148629	55	330610	1114544
16	347326	1144584	36	342610	1115535	56	334470	1115821
17	347188	1145197	37	342532	1144807	57	336083	1119506
18	347494	1143830	38	342529	1143784	58	334925	1118707
19	347921	1143977	39	344012	1145091	59	339173	1121289
20	343476	1141145	40	344452	1142728	60	339173	1121289

Table 7.2: Point Coordinates used for accuracy Assessment

No	Easting	North	No	Easting	North	No	Easting	North
1	351563	1142014	41	342297	1140140	81	357133	1139442

2	351563	1142014	42	342297	1140140	82	357133	1139442
3	351563	1142014	43	341922	1134242	83	357133	1139442
4	351563	1142014	44	341922	1134242	84	356393	1138304
5	344352	1141164	45	347143	1137638	85	352790	1134612
6	344352	1141164	46	347143	1137638	86	352792	1134592
7	344352	1141164	47	347143	1137638	87	352806	1134491
8	341979	1143250	48	349011	1137234	88	352806	1134491
9	341979	1143250	49	349011	1137234	89	352839	1134503
10	341979	1143250	50	349011	1137234	90	352754	1134821
11	341979	1143250	51	348980	1138242	91	352754	1134821
12	351046	1144497	52	348980	1138242	92	352754	1134821
13	351046	1144497	53	348033	1138320	93	352754	1134821
14	349832	1143427	54	347597	1138923	94	353607	1143074
15	351119	1137548	55	344966	1141587	95	349819	1141165
16	351119	1137548	56	344575	1141688	96	349819	1141165
17	351119	1137548	57	344587	1141697	97	343061	1136132
18	352394	1135429	58	344839	1141492	98	343061	1136132
19	352394	1135429	59	347964	1145095	99	343061	1136132
20	345784	1138856	60	348018	1145373	100	343061	1136132
21	345784	1138856	61	348018	1145373	101	342201	1135672
22	345784	1138856	62	348018	1145373	102	342170	1135670
23	342873	1138094	63	348133	1145543	103	342333	1136545
24	342873	1138094	64	348133	1145543	104	342333	1136545
25	342873	1138094	65	348133	1145543	105	342237	1137620
26	354170	1142709	66	348090	1145564	106	342237	1137620
27	354170	1142709	67	348104	1145684	107	341711	1138723
28	355313	1143852	68	348311	1145681	108	342901	1138605
29	355313	1143852	69	354234	1143707	109	342901	1138605
30	355313	1143852	70	354366	1143861	110	344619	1138165
31	355313	1143852	71	355500	1144636	111	344675	1138624
32	355525	1139308	72	355851	1144672	112	359245	1132826
33	354373	1136841	73	355851	1144672	113	359245	1132826

34	354413	1134779	74	356135	1144747	114	357440	1133719
35	354413	1134779	75	356135	1144747	115	357440	1133719
36	353650	1133692	76	356400	1144829	116	357321	1134331
37	342297	1140140	77	356715	1144940	117	356219	1134783
38	342297	1140140	78	356715	1144940	118	356219	1134783
39	342297	1140140	79	357150	1145165	119	354558	1136453
40	342297	1140140	80	357133	1139442	120	355496	1138408
No	Easting	North	No	Easting	North	No	Easting	North
121	356166	1140801	161	343537	1141156	201	333901	1117748
122	354431	1141553	162	343363	1141167	202	346678	1119286
123	355096	1145159	163	356754	1144619	203	346234	1118826
124	346411	1137099	164	343363	1141167	204	345191	1117709
125	346391	1137158	165	346838	1140912	205	344990	1117423
126	347003	1139267	166	346838	1140912	206	344540	1116720
127	346988	1139550	167	347536	1144706	207	343398	1113328
128	347412	1141259	168	347536	1144706	208	343216	1113271
129	344496	1142388	169	347536	1144706	209	342968	1113006
130	344496	1142388	170	347135	1144539	210	342151	1112069
131	344496	1142388	171	344975	1141389	211	341860	1111763
132	347145	1144040	172	344910	1141368	212	341643	1111569
133	347145	1144040	173	344910	1141368	213	341420	1111476
134	347920	1135501	174	344910	1141368	214	341279	1111218
135	346996	1135318	175	344910	1141368	215	341193	1111098
136	347178	1135891	176	344910	1141368	216	340904	1110599
137	347435	1136458	177	344422	1141830	217	340695	1110588
138	347435	1136458	178	344422	1141830	218	340001	1110461
139	346877	1136983	179	344317	1141719	219	339649	1110333
140	355843	1133090	180	345863	1136423	220	339623	1110133
141	355631	1133561	181	345975	1136438	221	339438	1109975
142	355631	1133561	182	345975	1136438	222	339250	1109790
143	355631	1133561	183	345975	1136438	223	339065	1109817

144	355503	1133613	184	347234	1134813	224	338952	1109405
145	355323	1133586	185	347234	1134813	225	338717	1109383
146	355398	1133926	186	350254	1135522	226	338464	1109161
147	355398	1133926	187	350254	1135522	227	338433	1109018
148	355398	1133926	188	350254	1135522	228	337725	1108602
149	355235	1133942	189	350995	1134604	229	337475	1108396
150	355235	1133942	190	350995	1134604	230	337202	1108162
151	358771	1141447	191	350995	1134604	231	336996	1108180
152	358771	1141447	192	353168	1134271	232	336488	1108383
153	358771	1141447	193	353168	1134271	233	336209	1108955
154	356843	1143743	194	353168	1134271	234	335948	1109031
155	356843	1143743	195	353168	1134271	235	335199	1109194
156	356843	1143743	196	353280	1134104	236	335015	1109271
157	348282	1145251	197	353280	1134104	237	334886	1109075
158	348282	1145251	198	353480	1134329	238	334413	1108993
159	348334	1145198	199	353746	1134550	239	333759	1109209
160	343537	1141156	200	353989	1134612	240	333584	1109026

No	Easting	North
241	333561	1108885
242	333380	1108582
243	332597	1107935
244	331410	1107675
245	330711	1107713
246	329528	1108094
247	329997	1107843
248	327911	1109777
249	325961	1110799
250	325098	1111377

Table 7.3: Accuracy Assessment result

	Grazing Land	Forest	Agriculture	Settlement	water body	Total (user)
Grazing Land	48	0	2	0	0	50
Forest	1	44	5	0	0	50
Agriculture	1	3	46	0	0	50
Settlement	0	1	7	42	0	50
Water body	0	0	3	0	47	50
Total (producer)	50	48	63	42	47	250

Appendix 2

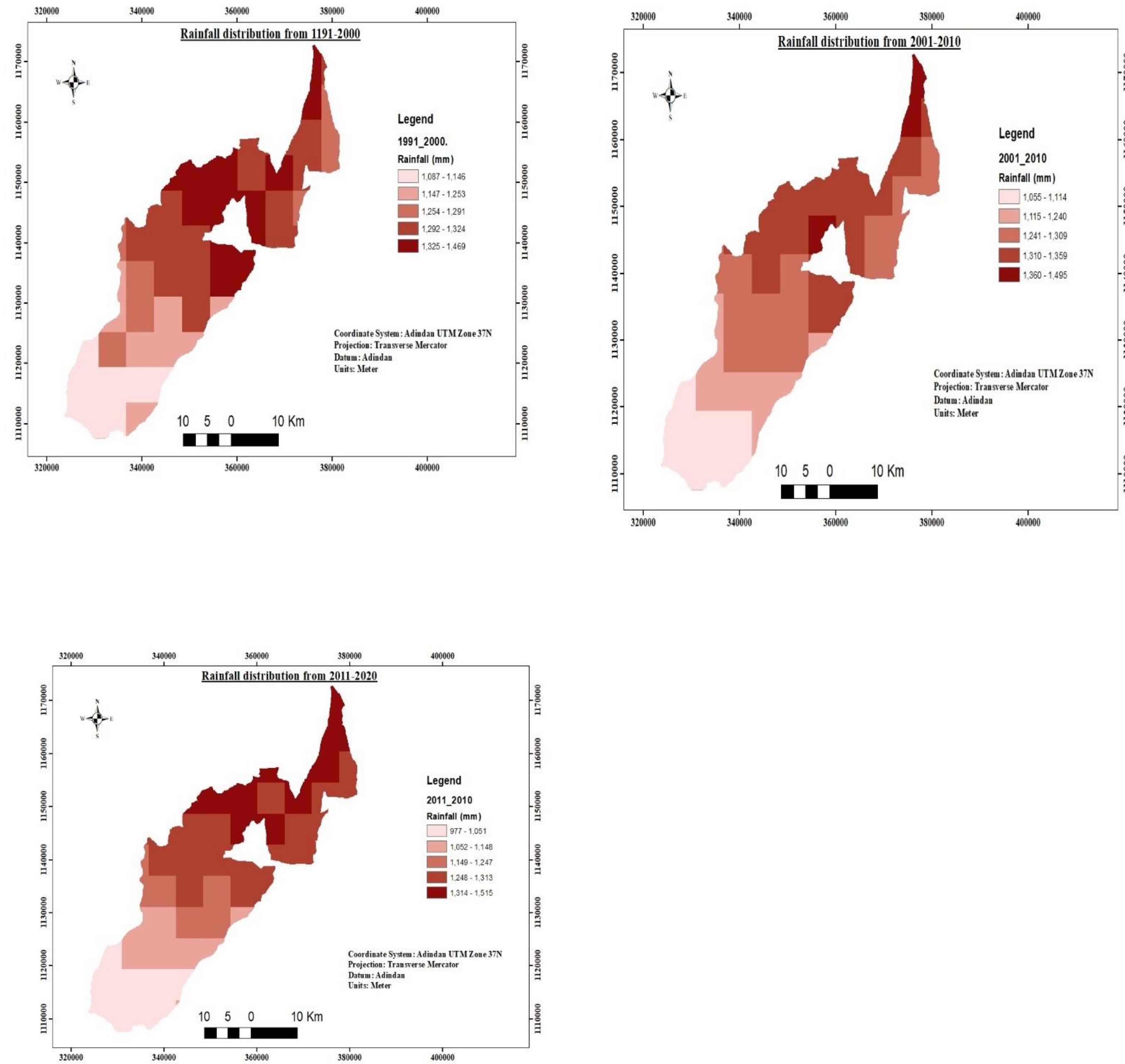

Figure 7.1: Rainfall distribution in a range of ten years from 1991 to 2020

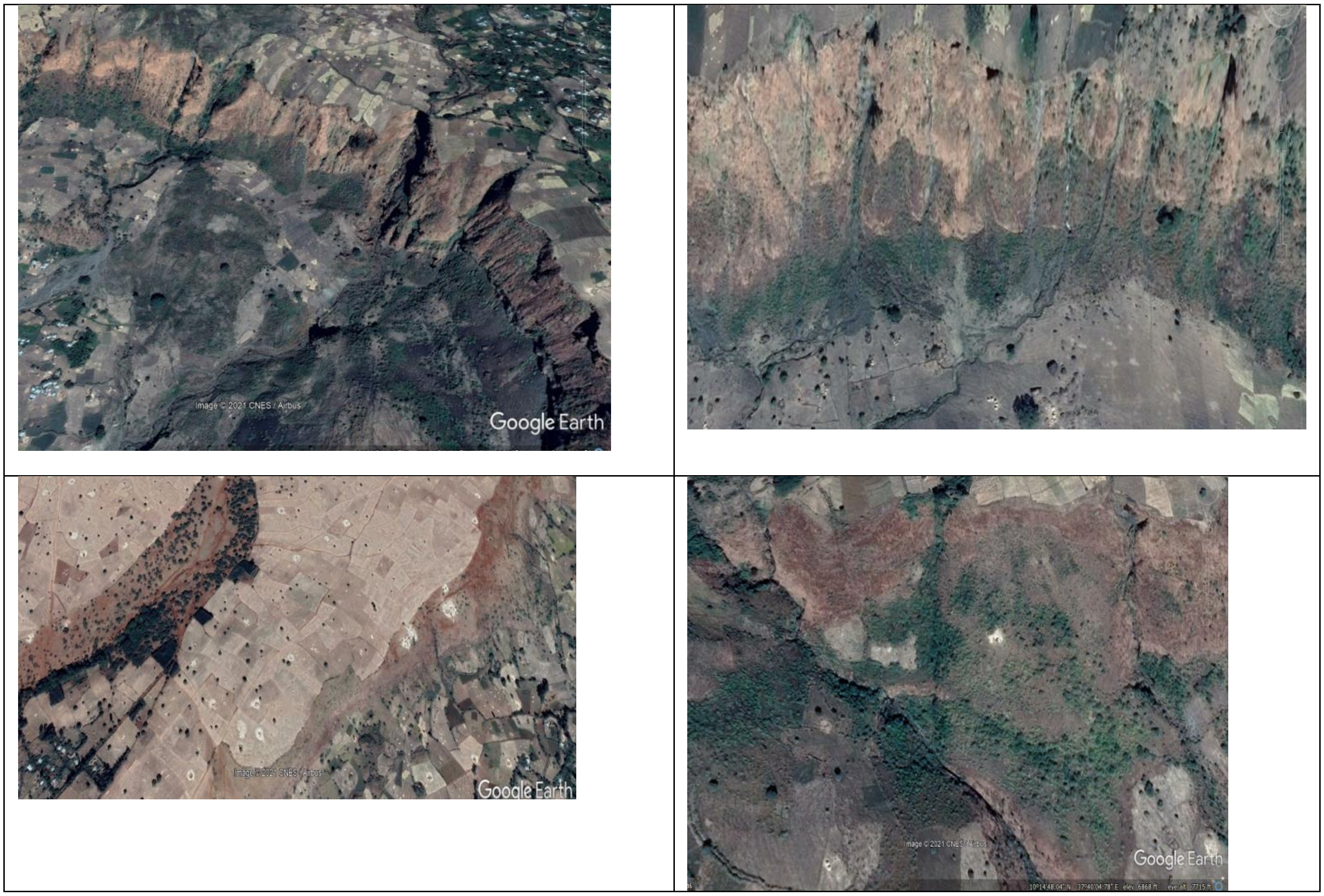

Figure 7.2: Sample Google earth image of the study area